Characterization of Nanoparticle-DNA Conjugate and Control of DNA Conformation on Particle Surface

by

Sunho Park

B.S. Mechanical Engineering
Seoul National University, 1998

M.S. Mechanical Engineering
Massachusetts Institute of Technology, 2004

SUBMITTED TO THE DEPARTMENT OF MECHANICAL ENGINEERING IN PARTIAL FULFILLMENT OF THE REQUIREMENTS FOR THE DEGREE OF

DOCTOR OF PHILOSOPHY IN MECHANICAL ENGINEERING
AT THE
MASSACHUSETTS INSTITUTE OF TECHNOLOGY

Feburary 2009

Signature of Author: _____
Department of Mechanical Engineering
December 12th, 2008

Certified by: _____
Kimberly Hamad-Schifferli
Assistant Professor of Mechanical Engineering
Thesis Supervisor

Accepted by: _____
David E. Hardt
Chairman, Department Committee on Graduate Students

Characterization of Nanoparticle-DNA Conjugate and Control of DNA Conformation on Particle Surface

by

Sunho Park

Submitted to the Department of Mechanical Engineering
on December 12th, 2008 in Partial Fulfillment of the
Requirements for the Degree of Doctor of Philosophy in
Mechanical Engineering

Abstract

Nano-science has exploited the hybridization and de-hybridization phenomena of DNA which are one of its fundamental functions. In particular, conjugates of gold nanoparticles and DNA (Au NP-DNA) have been extensively explored for their potential in biological applications such as DNA delivery for gene therapy and disease detection. However, DNA strands are known to adsorb onto the Au NP surface, which can severely limit the hybridization ability of Au NP-DNA conjugates. Therefore, methods of chemical modification of Au NP surfaces and evaluating DNA conformation via Ferguson analysis of gel electrophoresis are proposed in the thesis. Conjugates of DNA with Au NP of different sizes and coverages are evaluated with Ferguson analysis to characterize important parameters such as hydrodynamic size and zeta-potential. Surface modified Au NP exhibits enhanced stability and hybridization specificity in the system, which infers the effectiveness of those methods towards biological systems where non-specific adsorption is problematic. To confirm the validity of the concept, Au NP-antisense DNA experiments for gene silencing are performed in the work. Antisense DNA is designed to inhibit ribosomal activity on mRNAs and cooperatively works with Au NPs to enhance physical blocking mechanisms. However, the result shows that Au NP-DNA conjugates can enhance *in vitro* gene expression depending on DNA sequence and coverage of the conjugates. Suggestions are made for further investigation on proof and improvement of the translation enhancer concept.

Thesis Supervisor: Kimberly Hamad-Schifferli
Title: Assistant Professor of Mechanical Engineering

Acknowledgements

Most of all, I thank God for my entire life here at M.I.T. and in Cambridge. I could finish my Ph.D. program through his guidance and meet many good people through the school and the church under his love.

I thank my wife Hyejin for her love and patience. She had delayed her Ph.D. study until I finished mine, and had a really hard time starting new program in Maryland and bringing up our lovely son, Joshua Seojin, by herself during my last semester. It has been almost ten years since we met, and she has been very consistent to live in God and support other people. I thank God again for letting us be a couple.

I should thank my advisor, Professor Kimberly Hamad-Schifferli for her support for my entire graduate study. I realize that she is a very ideal academic advisor in that she has managed the research group at very reasonable level and has always been very nice to her students. I have learned a lot of Chemistry and Biology from her and got very many helps on experiments and writing papers. I admit that there was a period of time when I had been away from active research for some issues. However, she had shown great endurance and I really thank her again at this time.

I thank Professor Roger Kamm and Professor Jongyoon Han for their help on my research and thesis writing as a thesis committee member. They are always busy but willingly shared their time to meet me individually or in committee meetings.

지금까지 저를 키워 주시고 오랜 학업기간 동안 항상 아낌없는 사랑과 지원을 아끼지 않으신 부모님께 감사드립니다. 예기치 않게 편찮으실 때 큰 힘이 되어 드리지 못한 것이 못내 가슴아프지만, 부모님께 받은 사랑을 조금이나마 돌려 드리려 애쓰겠습니다. 항상 건강하세요.
저의 아내가 된 혜진을 잘 키워주시고, 결혼한 이후에도 너무나 많은 기도와 도움으로 저희들을 보살펴 주신 장인어른, 그리고 장모님께 감사드립니다. 공부가 길어져 아직 어른 구실을 제대로 하지 못함에도 변함없이 사랑해주셔서 너무나 감사드립니다. 항상 건강하시길 기도합니다.
사랑하는 큰형과 작은형, 그리고 새로이 가족이 된 형수님과 처형, 처남 그리고 동서. 항상 변함없이 서로를 아끼며 존중하며 살 수 있기를 기도합니다.

Sunho Park

January 27, 2009

Table of Contents

Chapter 1. Introduction

1.1 Introduction to nanoparticle and biomolecule conjugates study

Nanoparticles have attracted many interests due to their unique electronic, optical and catalytic properties.[1, 2] Those properties are strongly dependent on the materials and structures constructing the particles. For example, quantum dots (QDs) are made of metal/semi-conducting metal, and sized/structured to have specific energy bands such that they have desired wavelength of absorbance or fluorescence emission and are utilized in bio-imaging and target-molecule sensing.[3-6] Noble metals such as gold and silver are also popularly used. Especially gold nanoparticles (Au NPs) have been extensively explored and utilized recently owing to their relatively low reactivity in random environment while maintaining versatility in surface modification and conjugation to a variety of biomolecules.[1, 2] Magnetic particles are also frequently used in that they are responsive to external magnetic field so that they are easily directed and collected in solutions.[7-10] Hyperthermia is an interesting area concerning about using alternating magnetic field to generate thermal energy in localized spots like human tumors.[11, 12] Not only metal based nanoparticles but also polymeric micro/nanoparticles have long history and well established synthesis techniques[13]. In addition, metal-polymer composite particles are recently being developed by various methods such as polymer swelling–metal particle uptake[14-16], block co-polymer polymerization[17, 18] and direct synthesis from raw materials.[19]

Due to their size range similar to that of biomolecules (a few nanometer to some hundred nanometers) nanoparticles have been utilized in self-assembly, gene delivery, bio-

molecular target sensing, and control.[1, 20-28] Functionalized biomolecules are attached to nanoparticles directly or via linkers depending on the type of particles and biomolecules.[1] For example, short single stranded DNA (ssDNA) modified with C-6 thiol group at 5' end makes a strong covalent bond with a gold atom (Au-S) on the surface of Au NPs.[29] The ability to hybridize with its complementary strand, which is the primary functionality of DNA, together with the inertness of Au NPs makes Au NP-DNA conjugates widely used in bio-applications. One or more types of Au NPs can be modified with ssDNA and/or its complementary DNA such that those particles are connected to each other by forming double stranded DNA (dsDNA).[29-33] Once aggregates of Au NPs are formed the peak of extinction spectra, which is normally at ~520nm, shifts to higher wavelength[34] and the color of bulk solution changes. DNA strands on Au NPs can be designed to detect a certain target biomolecules such that aggregated Au NPs are re-dissolved and each Au NP-DNA conjugate binds to the target so that the change in color indicates the presence of the targets.[21] Other techniques including using chips or evaluating size change are also available for Au NP-DNA based sensing.[26-28] Au NP-DNA Nanoparticles have been tested as vectors of drug/DNA delivery[35] and it has been shown that DNA is transferred better into cells by being conjugated with Au NPs.[24]

However, it is known that DNA strands are non-specifically adsorbed on Au NPs' surface depending on nucleotide content, DNA length, and coverage (# DNA strands / NP).[36, 37] These phenomena should be controlled since non-specific adsorption can significantly limit the capacity of DNA to hybridize to its target and ruin the functionality of designed Au NP-DNA for real applications. In most of the previous research performed with Au NP-DNA systems this issue has not been recognized or addressed, and it is believed that the hybridization efficiency of the Au NP-DNA systems used has been limited. In addition,

conjugation of biomolecules and nanoparticles results in significant change in charge distribution so that conjugated DNA or biomolecules may function differently. Charge interaction becomes even more complicated when real biological systems are involved since ionic conditions in physiological systems vary significantly.

Therefore, conformation and charge status of designed Au NP-DNA conjugates should be evaluated before utilized. Furthermore, DNA conformation on Au NPs must be controlled to make DNA strands easily hybridize with target complementary strands. The primary goal of this thesis is to propose fundamental tools of evaluating and controlling nanoparticle-biomolecule conjugates to make the molecules behave in a predicted way and to achieve better efficiency and stability in real biological applications.

1.2 Topics in the thesis

In Chapter 2, Ferguson analysis is introduced as a method of particle sizing and free mobility measurements. Ferguson analysis is based on gel electrophoresis at different polymer concentrations and varying running buffer concentrations. Electrophoresis and Ferguson analysis theories are intensively reviewed and summarized. Actual Au NPs (5-20nm) are tested with Ferguson analysis and the effectiveness of the method is proven. Zeta-potential is an important parameter of particles and is a function of particle size, buffer condition and surface charge state. Zeta-potential is calculated from the Ferguson analysis data by use of some conventional theories such as Henry's solutions and Ohshima's solutions.

In Chapter 3, Au NP-DNA conjugates are subjected to Ferguson analysis and it is shown that Ferguson analysis is more reliable and repeatable method for Au NP-DNA

conjugates compared with commercial dynamic light scattering or zeta-potential measurement devices. Au NP-DNA conjugation techniques are described and quantification of conjugated DNA is done by fluorescence measurement of dye-functionalized DNA. Once Au NP-DNA system to be used is synthesized, non-specific adsorption between Au NP and DNA should be eliminated. This is performed by surface modification of Au NP-DNA with 6-mercapto-1-hexanol. Ferguson analysis and fluorescence test confirms that DNA hybridization to complementary strands is improved, which means that most of the non-specific adsorption sites are eliminated.

In Chapter 4, *in vitro* antisense regulation of enhanced green fluorescent protein (eGFP) expression is discussed as a biological application of Au NP-DNA conjugate. Antisense DNA is hybridized to a specific sequence of messenger ribonucleic acid (mRNA) and sterically blocks ribosomal activity so that translation into protein is limited. It is proposed that Au NPs are attached to antisense DNA to enhance mechanical blocking efficiency in that antisense DNA strand alone is not enough to limit very active ribosomal functionality. Characteristics of Au NP-antisense DNA conjugates such as coverage and size are evaluated by fluorescence measurement and Ferguson analysis. However, the result shows that Au NP-antisense DNA conjugates actually enhance eGFP expression depending on DNA sequence design and coverage of the conjugates. The phenomena may be due to Au NP-DNA's recruiting of translation molecules to mRNA. Suggestions will be made for further investigation on proof and optimization of the concept.

1.3 Reference

(1) Niemeyer, C. M. *Angew. Chem., Int. Ed. Engl.* **2001,** 40, 4128-4158.
(2) Katz, E.; Willner, I. *Angew. Chem., Int. Ed. Engl.* **2004,** 43, 6042-6108.
(3) Chan, W. C. W.; Maxwell, D. J.; Gao, X.; Bailey, R. E.; Han, M.; Nie, S. *Curr. Opin. Biotech.* **2002,** 13, 40-46.
(4) Chan, W. C. W.; Nie, S. *Science* **1998,** 281, 2016-2018.
(5) Crut, A.; Geron-Landre, B.; Bonnet, I.; Bonneau, S.; Desbiolles, P.; Escude, C. *Nucleic Acids Res.* **2005,** 33, e98.
(6) Michalet, X.; Pinaud, F. F.; Bentolila, L. A.; Tsay, J. M.; Doose, S.; Li, J. J.; Sundaresan, G.; Wu, A. M.; Gambhir, S. S.; Weiss, S. *Science* **2005,** 307, 538-544.
(7) Brückl, H.; Panhorst, M.; Schotter, J.; Kamp, B.; Becker, A. *IEE Proc.-Nanobiotechnol.* **2005,** 152, 41-46.
(8) Pankhurst, Q. A.; Connolly, J.; Jones, S. K.; Dobson, J. *J. Phys. D: Appl. Phys.* **2003,** 36, R167-R181.
(9) Robinson, D. B.; Persson, H. H. J.; Zeng, H.; Li, G.; Pourmand, N.; Sun, S.; Wang, S. X. *Langmuir* **2005,** 21, 3096-3103.
(10) Sun, S.; Zeng, H.; Robinson, D. B.; Raoux, S.; Rice, P. M.; Wang, S. X.; Li, G. *J. Am. Chem. Soc.* **2004,** 126, 273-279.
(11) Hergt, R.; Andra, W.; d'Ambly, C. G.; Hilger, I.; Kaiser, W. A.; Richter, U.; Schimidt, H.-G. *IEEE Trans. Magn.* **1998,** 34, 3745-3754.
(12) Jordan, A.; Scholz, R.; Maier-Hauff, K.; Johannsen, M.; Wust, P.; Nadobny, J.; Schirra, H.; Schmidt, H.; Deger, S.; Loening, S.; Lanksch, W.; Felix, R. *J. Magn. Magn. Mater.* **2001,** 225, 118-126.
(13) Antonietti, M.; Landfester, K. *Prog. Polym. Sci.* **2002,** 27, 689-757.
(14) Bradley, M.; Bruno, N.; Vincent, B. *Langmuir* **2005,** 21, 2750-2753.
(15) Menager, C.; Sandre, O.; Mangili, J.; Cabuil, V. *Polymer* **2004,** 45, 2475-2481.
(16) Pich, A.; Hain, J.; Lu, Y.; Boyko, V.; Prots, Y.; Adler, H.-J. *Macromolecules* **2005,** 38, 6610-6619.
(17) Kim, B.-S.; Qiu, J.-M.; Wang, J.-P.; Taton, T. A. *Nano Lett.* **2005,** 5, 1987-1991.
(18) Kang, Y.; Taton, T. A. *Macromolecules* **2005,** 38, 6115-6121.
(19) Csetneki, I.; Faix, M. K.; Szilagyi, A.; Kovacs, L.; Nemeth, Z.; Zrinyi, M. *J. Polym. Sci. Part A: Polym. Chem.* **2004,** 42, 4802-4808.
(20) Alivisatos, P. *Nat. Biotechnol.* **2004,** 22, 47-52.
(21) Fischer, N. O.; Tarasow, T. M.; Tok, J. B.-H. *Curr. Opin. Chem. Biol.* **2007,** 11, 316-328.
(22) Taton, T. A.; Mirkin, C. A.; Letsinger, R. L. *Science* **2000,** 289, 1757-1760.
(23) Hamad-Schifferli, K.; Schwartz, J. J.; Santos, A. T.; Zhang, S.; Jacobson, J. M. *Nature* **2002,** 415, 152-155.
(24) Thomas, M.; Klibanov, A. M. *Proc. Natl. Acad. Sci. USA* **2003,** 100, 9138-9143.
(25) Loweth, C. J.; Caldwell, W. B.; Peng, X.; Alivisatos, A. P.; Schultz, P. G. *Angew. Chem., Int. Ed. Engl.* **1999,** 38, 1808-1812.
(26) Qin, W. J.; Yung, L. Y. L. *Nucleic Acids Res.* **2007,** 35, e111.
(27) Shiddiky, M. J. A.; Shim, Y.-B. *Anal. Chem.* **2007,** 79, 3724-3733.
(28) Hazarika, P.; Ceyhan, B.; Niemeyer, C. M. *Small* **2005,** 1, 844-848.
(29) Mirkin, C. A.; Letsinger, R. L.; Mucic, R. C.; Storhoff, J. J. *Nature* **1996,** 382, 607-609.

(30) Maye, M. M.; Nykypanchuk, D.; Lelie, D. v. d.; Gang, O. *J. Am. Chem. Soc.* **2006,** 128, 14020-14021.
(31) Cardenas, M.; Barauskas, J.; Schillen, K.; Brennan, J. L.; Brust, M.; Nylander, T. *Langmuir* **2006,** 22, 3294-3299.
(32) Goodrich, G. P.; Helfrich, M. R.; Overberg, J. J.; Keating, C. D. *Langmuir* **2004,** 20, 10246-10251.
(33) Park, S.-J.; Lazarides, A. A.; Storhoff, J. J.; Pesce, L.; Mirkin, C. A. *J. Phys. Chem. B* **2004,** 108, 12375-12380.
(34) Noyong, M.; Ceyhan, B.; Niemeyer, C. M.; Simon, U. *Colloid Polym. Sci.* **2006,** 284, 1265-1273.
(35) Patil, S. D.; Rhodes, D. G.; Burgess, D. J. *AAPSJ* **2005,** 7, Article 9.
(36) Parak, W. J.; Pellegrino, T.; Micheel, C. M.; Gerion, D.; Williams, S. C.; Alivisatos, A. P. *Nano Lett.* **2003,** 3, 33-36.
(37) Storhoff, J. J.; Elghanian, R.; Mirkin, C. A.; Letsinger, R. L. *Langmuir* **2002,** 18, 6666-6670.

Chapter 2. Ferguson analysis: Particle sizing and ζ-potential measurement.

2.1 Introduction

Gel electrophoresis has been found to be highly effective for separating Au NPs and Au NP-DNAs based on their mobility difference in gels.[1-3] The mobility of a species is a function of both size and charge of the particles, type and concentrations of the running buffer, and gel concentrations.[4] However, recent research has focused primarily on using electrophoresis for separation of NP-bio-polymers as a function of size since electrophoresis is intensively utilized for separations of uniformly charged bio-polymers at a small range of gel and buffer concentrations. For example, there is a simple correlation between the mobility of a DNA strand and its number of base pairs. In the case of highly surface-modified Au NPs and Au NP-DNA conjugates, the effect of charge and buffer concentration can significantly affect mobility, and band separations in the gel are a function of both size and charge.

In this chapter, it is proposed that Ferguson analysis is an integrated gel electrophoresis technique that can relate the mobility of Au NP-based molecules to both their size and surface charge. We use Ferguson analysis to evaluate Au NPs (D~ 5 to 20 *nm*) as a function of size and surface functionalization. It is shown that certain ranges of electrokinetic formulas are necessary for NPs of this size range. In Chapter 3 and 4, developed techniques of Ferguson analysis are utilized to evaluate Au NP-DNA conjugates to obtain information on the DNA behavior on the NP surface.

2.2 Theories of nanoparticle characterization

2.2.1 Ferguson analysis theories

The behavior of molecules in gel electrophoresis can be predicted by some models for random meshwork or cylindrical hollow pore.[5-7] Due to some researchers' early work, the below relationship had been established.[6]

$$\frac{V_e - V_o}{V_T - V_o} = f = \frac{M}{M_o} \tag{2.1}$$

f is the fraction of available volume to molecules V_e to total volume of gel V_T, and it is assumed to be the same as the ratio of mobility M to free mobility M_0. Void volume V_0 is identically subtracted from both the volumes. Mobility is defined as migration velocity divided by electric field strength. f is expressed in different forms, depending on the assumptions made on geometry of molecules and gel material, which are highly associated with the collision behavior between them.[6] For spherical molecules, Ogston model[8] had been established and expressed as:

$$f = \exp\left(-s\overline{L}\right) \quad : \text{2-D gel structure} \tag{2.2}$$

$$f = \exp\left(-lS/4\right) \quad : \text{1-D gel structure} \tag{2.3}$$

$$f = \exp\left(-n_0 V\right) \quad : \text{0-D gel structure} \tag{2.4}$$

A gel with random planes is called a 2-D structure and 1-D gel denotes a fibrous structure. If the volume of each gel fiber is very small compared to the molecules running in gel, it is called a 0-D gel. s is the surface area of the planes per unit volume of 2-D gel, and $\overline{L}$ is the

mean length of the molecule. For 1-D gel, l is the total length of fibers per unit volume and S is coupled surface area of molecules and fibers considering collisions between them. n_0 and V of 0-D gel means the number of gel fibers per unit volume and coupled volume of molecules and fibers respectively. S and V are given below.

$$S = 4\pi(R+r)^2 \qquad \text{: Coupled surface area in 1-D gel} \qquad (2.5)$$

$$V = \frac{4}{3}\pi(R+r)^3 \qquad \text{: Coupled volume in 0-D gel} \qquad (2.6)$$

R is the radius of molecule and r is that of gel fiber.

Equation 2.7 shows the combined effect of gel pieces in different dimensions.

$$f = \exp\left\{-(s\bar{L} + lS + n_0 V)\right\} \qquad (2.7)$$

In reality, 1-D elements dominate in gel structure.[6, 7] Equation 2.1, 2.3 and 2.5 thus can be combined as

$$\frac{M}{M_0} = \exp\left(-\pi(R+r)^2 l\right) \qquad (2.8)$$

Note that l is in $[cm/ml]$ and M is in $[cm^2/V\cdot s]$. By taking logarithm,

$$\begin{aligned} \log_{10} M &= \log_{10} M_0 - \left(\log_{10} e\right)\cdot \pi l(R+r)^2 \\ &= \log_{10} M_0 - \left(\log_{10} e\right)\cdot \frac{1}{100}\pi L(R+r)^2 \cdot T \\ &= \log_{10} M_0 - K_R \cdot T \end{aligned} \qquad (2.9)$$

where T is gel percentage (%, $[g/100ml]$) and $L = l/T$ ($[cm/g]$) is the total length of fibers per unit mass of gel material. From equation 2.9, we can see that retardation coefficient K_R, which is given by $\left(\log_{10} e\right)\cdot(1/100)\pi L(R+r)^2$, is the slope of linear equation between the

logarithm of the mobility and gel percentage. Note that the fitting extrapolated to T=0 will give free mobility M_0. In addition, if we take a square root of the K_R,

$$\begin{aligned}\sqrt{K_R} &= \frac{1}{10}\sqrt{\log_{10} e}\left(\sqrt{\pi L}\cdot R + \sqrt{\pi L}\cdot r\right) \\ &= \left\{\frac{1}{10}\sqrt{(\log_{10} e)\pi L}\right\}\cdot R + \left\{\frac{1}{10}\sqrt{\log_{10} e}\cdot\sqrt{V_{fiber}}\right\}\end{aligned} \tag{2.10}$$

where V_{fiber} is the volume of fiber per unit mass, given as $\pi r^2 L([cm^3/g])$. Because this value is an intrinsic property of gel material that is constant, $\sqrt{K_R}$ is linearly fitted as a function of R. According to equation 2.10, larger particle gives bigger slope of Ferguson plot. This means that large molecules experience much more retardation in gel due to frequent collision with gel structure. Figure 2.1 shows pictures of 0.5% and 4.5% agarose gel in 0.5xTBE with 5.5-20*nm* gold particles. They clearly show the relation between slopes and size.

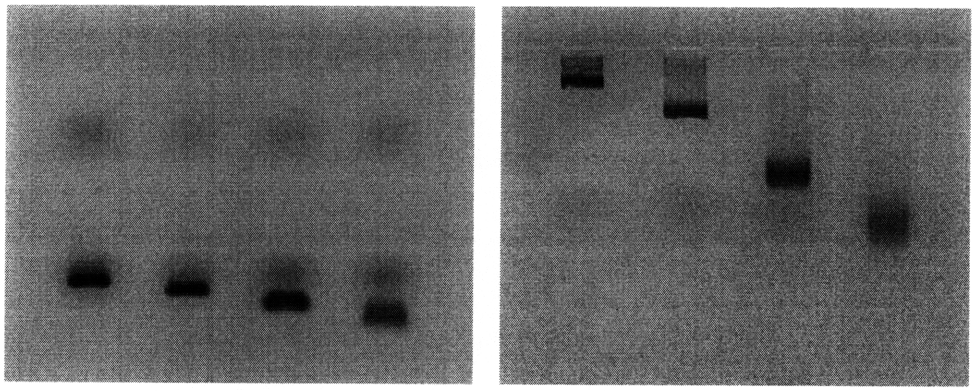

(a) (b)

Figure 2.1 Pictures of agarose gel with gold particles. D=5.5, 9.4, 15 and 20*nm* from the left. Electric field strength is about 4 *V/cm*. Gel percentage is (a) 0.5%, (b) 4.5%

Unfortunately, the actual fitting of $\log_{10} M$ and T is generally convex or concave depending on type of molecules. Random coiled DNA experiences reptation, which results in

much less change of mobility at high gel percentage range.[9-11] On the contrary, spherical molecules experience more collisions than expected at high gel percentage, therefore the mobility rapidly decreases as T becomes high.[7, 10] Figure 2.2 shows a Ferguson plot with agarose gel and ligand modified gold particles of $20nm$ diameter (i.e., $10nm$ in radius). Running buffer used is 0.5×TBE.

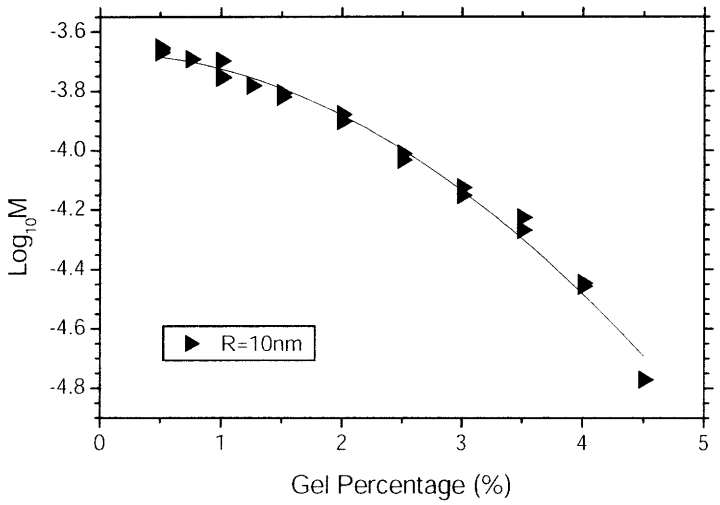

Figure 2.2 Ferguson plot with agarose gel and gold particles in 20nm diameter. Gel percentage is from 0.5% to 4.5%.

At low gel concentrations, the slope of the plot decreases, which means the particles hardly experience collisions below a certain level of gel concentration and shows very little change of mobility. To explain this convex behavior, a modified form of equation 2.9 was suggested.[7]

$$\begin{aligned} \log_{10} M &= \log_{10} M_0 - a \cdot T^b \\ &= \log_{10} M_0 - K_R' \cdot T \end{aligned} \qquad (2.11)$$

Note $K_R' = a \cdot T^{b-1}$. In this case, $\sqrt{K_R'}$ and R is fitted to the sigmoidal function rather than linear relation.

$$\sqrt{K_R'} = \frac{(A_1 - A_2)}{1 + (R/R_0)^p} + A_2 \qquad (2.12)$$

A_1, A_2, p and R_0 are determined by fitting the data. R_0 is an inflection point of the sigmoidal curve. From the experience, however, it was found that it is hard to get consistent K_R' from the fitting because it contains T^{b-1} term whose exponent is very close to zero. A significant error arises from equation 2.12, too.

To utilize equation 2.9, we need to limit the range of gel concentration.[5] For example, gold particles in 5.5 - 20*nm* diameter give linear Ferguson plots when agarose gel percentages are below ~3.5% (Figure 2.3).

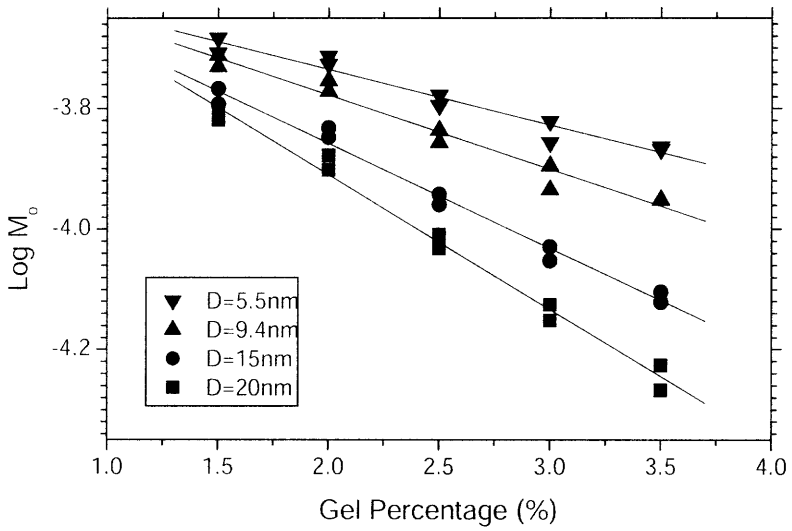

Figure 2.3 Ferguson plot with agarose gel and gold particles in 5.5-20*nm* diameter. Gel percentage is from 1.5% to 3.5%

$\sqrt{K_R}$ can be calculated from the square root of the slopes in Figure 2.3. These values are fitted again as a function of R (see equation 2.10). Very nice linear fitting has been achieved in Figure 2.4. The fitted equation is shown in the graph and will be utilized to calculate effective size from $\sqrt{K_R}$ of samples of unknown size.

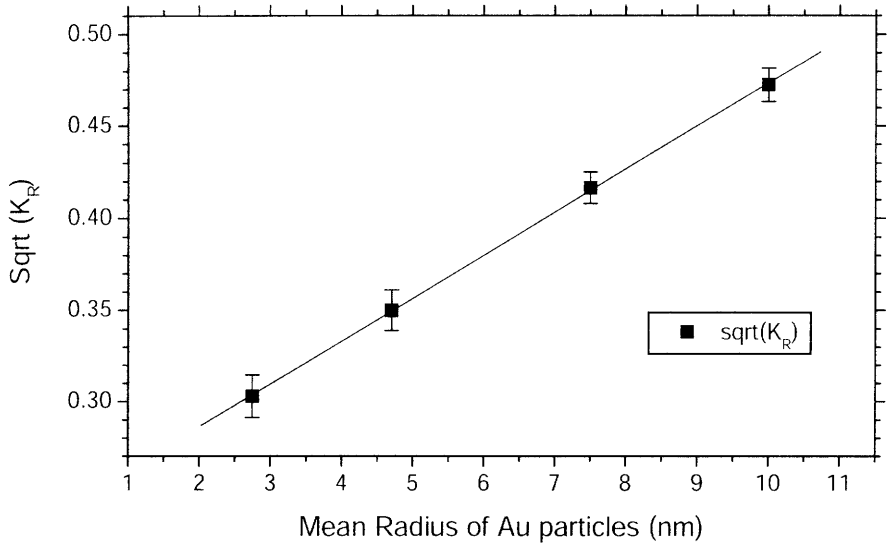

$$\sqrt{K_R} = 0.23935 + 0.02345 \cdot R$$

Figure 2.4 $\sqrt{K_R}$ vs. R of Ferguson plots of gold particles in 5.5-20nm diameter. Agarose gel percentage is from 1.5% to 3.5%

2.2.2 Mobility of DNA in gel

Gel electrophoresis is widely used for separating DNA fragments. The mobility of DNA is strongly related with its chain length. The polymer chain sufficiently longer than its persistence length composes globular random coil (see Chapter 3). It behaves like a spherical molecule if gel concentration is low. At high gel concentration, however, the pore size may be smaller than the random coil. Under the external electric field, a part of their strand is unraveled and sneaks through the gel pores.[11] This is called reptation. To explain this phenomenon, the gel structure is treated as a porous material, rather than a matrix of fibers described in the previous section.

Classical models of mobility in porous gel structure are given below.[5, 12]

$$\frac{M}{M_0} = 1 - \frac{R}{P_E} \tag{2.13}$$

$$\frac{M}{M_0} = \left(1 - \frac{R}{P_E}\right)^2 \tag{2.14}$$

$$\frac{M}{M_0} = 1 - 2.104\left(\frac{R}{P_E}\right) + 2.09\left(\frac{R}{P_E}\right)^3 - 0.95\left(\frac{R}{P_E}\right)^5 \tag{2.15}$$

$$\frac{M}{M_0} = \left(1 - \frac{R}{P_E}\right)^2\left[1 - 2.104\left(\frac{R}{P_E}\right) + 2.09\left(\frac{R}{P_E}\right)^3 - 0.95\left(\frac{R}{P_E}\right)^5\right] \tag{2.16}$$

P_E is effective gel pore size, empirically determind by standard molecules with known size. It decreases as gel concentration increases. But equation 2.13-16 are still based on the assumption of spherical molecules, thus they cannot be used for reptating DNA strands.

As far as DNA strands are concerned, the size of molecule is usually given as the number of bases in the strand N_0, rather than the average end-to-end length.[9-11] For reptating DNA, the following formula known as vWBR is often used.[9, 11]

$$M = \frac{1}{b + a\left(1 - e^{-N_0/N_c}\right)} \tag{2.17}$$

a, b and N_c are experimentally determined. N_c is a critical number of DNA bases that is a function of gel percentage. If N_0 is replaced with zero, equation 2.17 gives $M(N_0=0)=1/b \equiv M_s$, which means the asymptotic mobility of very small DNA fragment. From the other extreme, $M(N_0 \rightarrow \infty)$ gives $1/(b+a) \equiv M_\infty$, the mobility of infinitely long DNA chain. Equation 2.17 then can be rewritten as[9, 11]

$$\frac{1}{M} = \frac{1}{M_\infty} - \left(\frac{1}{M_\infty} - \frac{1}{M_s}\right)e^{-N_0/N_c} \tag{2.18}$$

or

$$\frac{\frac{1}{M}-\frac{1}{M_\infty}}{\frac{1}{M_s}-\frac{1}{M_\infty}}=e^{-N_0/N_c} \tag{2.19}$$

The equation looks like equation 2.8, but N_0 is used as the size parameter instead of R. Note that the information on gel percentage is contained in N_c.

2.2.3 Free mobility and zeta-potential

As mentioned in the previous section, M_0 extrapolated to T=0% is an estimator of the free mobility of a given sample. M_0 is a function of the particle's zeta-potential, ζ, which is determined by the surface charge density of the particle and the Debye-length of the salt media. Debye-length of ionic media varies with ionic strength of the solution. I, Ionic strength, is given by equation 2.20.

$$I=\frac{1}{2}\sum_i C_i\cdot Z_i^2 \tag{2.20}$$

where C_i is concentration and Z_i is charge valance of ionic species i. For N×TBE, which is a very popular buffer used for gel electrophoresis, is expressed by

$$I=\frac{1}{2}C(\alpha+\beta)\sim\frac{1}{2}N(89mol/m^3)(\alpha+\beta) \tag{2.21}$$

Note that 0.5×TBE is composed of 45mM tris, 45mM boric acid, and 1mM EDTA. Dissociation factor α and β are given as

$$\alpha=\frac{10^{-(pKa(acid)-pH)}}{\left(1+10^{-(pKa(acid)-pH)}\right)} \tag{2.22a}$$

$$\beta = \frac{10^{-(pH-pKa(base))}}{\left(1+10^{-(pH-pKa(base))}\right)} \tag{2.22b}$$

Then Debye-length is calculated by

$$\frac{1}{\kappa} = \sqrt{\frac{\varepsilon k_B T_A}{N_A e^2 I}} \tag{2.23}$$

where ε is the permittivity of the media, k_B is the Boltzmann constant, T_A the absolute temperature, N_A Avogadro's number, e= -1.602×10^{-19}C.

Ionic strength of TBE is calculated by using literature values of the *pKa* of tris base (~8.15) and boric acid (~9.14), and experimentally measured *pH* (8.4 - 8.6) at room temperature. Based on the calculation, Debye length of TBE is shown in Figure 2.5.

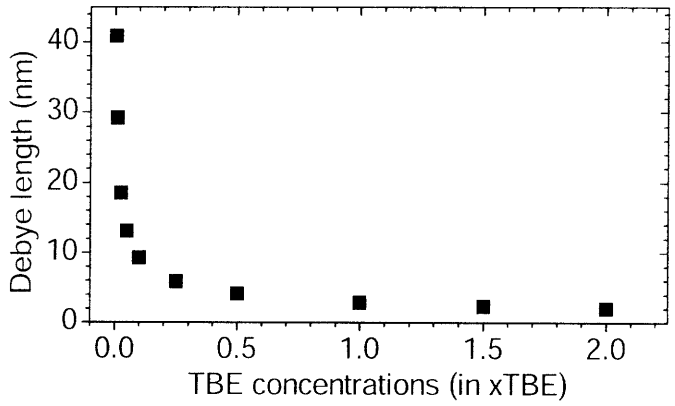

Figure 2.5 Debye length of *N*×TBE

From the given particle size and measured M_0, ζ can be calculated by conventional theories. When Debye length is much larger than the particle size ($\frac{1}{\kappa} >> R$), the particle behaves like a point charge in the medium (Hückel's solutions). On the contrary, charged ions are distributed very nearly to the particle surface when Debye length is much smaller than the

particle size ($\frac{1}{\kappa} << R$). Electrophoresis of the particle is very similar to electroosmosis at flat walls in the case (Smoluchowski's solutions).

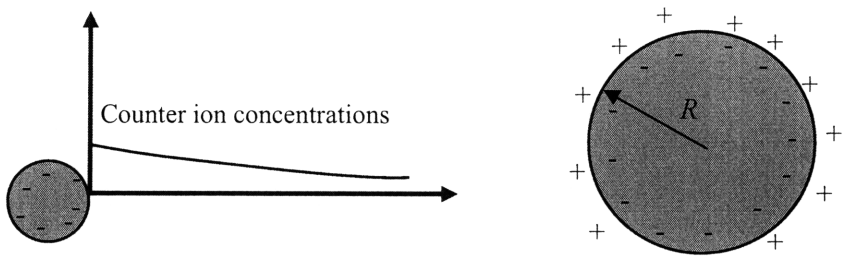

$\kappa R << 1$ $\kappa R >> 1$

Figure 2.6 Two extreme cases of relative magnitude between Debye length and particle size

From Hückel's solutions, zeta-potential and mobility are given as

$$\zeta = \frac{Q}{4\pi R\varepsilon} \tag{2.24}$$

$$M_0 = \frac{U_0}{E} = \frac{2}{3}\frac{\varepsilon\zeta}{\eta} \tag{2.25}$$

where Q is total charge of particle, U_0 is free migration velocity of the particle, E is electric field strength, and η is viscosity of the media. Results of Smoluchowski's solutions are also expressed by

$$\zeta = \frac{\sigma_s}{\varepsilon}\frac{1}{\kappa} \tag{2.26}$$

$$M_0 = \frac{\varepsilon\zeta}{\eta} \tag{2.27}$$

where σ_s is surface charge density of the particle. It can be noted that mobility of a particle differs by factor of 2/3 in the two solutions by comparing equation 2.25 and 2.27 when given zeta potential is the same.

The two solutions explained above deal only with extreme cases of κR. By solving governing equations of electrophoresis, Henry's solutions are approximated as[13]

$$M_0 = \frac{2}{3}\left(1+\frac{1}{2}\left(1+\frac{\delta}{\kappa R}\right)^{-1}\right)\frac{\varepsilon}{\eta}\zeta = f(\kappa R)\cdot\frac{\varepsilon}{\eta}\zeta \qquad (2.28)$$

where δ~2.5. $f(\kappa R)$ is shown in Figure 2.7.

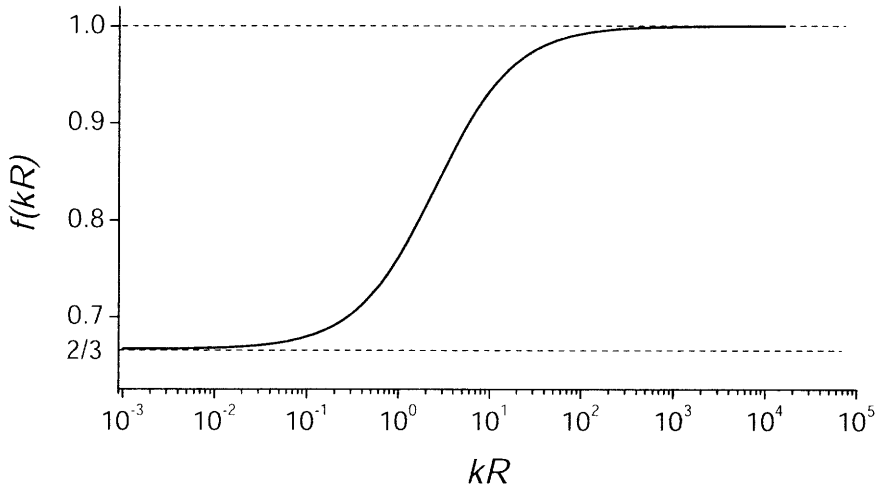

Figure 2.7 $f(\kappa R)$ is drawn in κR range of $(0,\infty)$

Once ζ is calculated from a measured M_0, surface charge density is obtained from:

$$\zeta = \frac{R\sigma_s}{\varepsilon(1+\kappa R)} \qquad (2.29)$$

and the effective total charge is given as $4\pi R^2 \sigma_s$.

Henry's solutions become less precise when the ionic species surrounding the particles are retarded relative to the particles as they migrate through the gel. This occurs when the ionic mobility is low or ζ of the particle is high, resulting in a distorted velocity field and electric field of media around the particle,[14] and consequently decreasing particle mobility. TBE is a widely used gel running buffer but it possesses a very low ionic mobility (Tris: $2.7\times10^{-4}cm^2/Vs$, Borate: $3.3\times10^{-4}cm^2/Vs$ at 25°C)[15] that is even comparable to typical measured mobility of the Au NPs in ~$10nm$ diameter. A suggested asymptotic formula with the correction of charge retardation is:[13]

$$M_0 = \frac{\varepsilon\zeta}{\eta}\left[f(\kappa R) - \frac{2}{3}\left(\frac{ze\zeta}{k_B T_A}\right)^2 \left\{ f_3(\kappa R) + \left(\frac{m_+ + m_-}{2}\right) f_4(\kappa R) \right\} \right] \quad (2.30)$$

$$m_\pm = \frac{2\varepsilon k_B T_A}{3\eta |z_\pm| \mu_\pm e} \quad (2.31)$$

$m_\pm$ is non-dimensional ionic drag coefficient that is inversely proportional to free mobility ($\mu_\pm$) and valence ($z_\pm$) of positive or negative ionic species. The first term in the square brackets is the same as $f(\kappa R)$ in Henry's solutions and the rest are correction terms.

$$f_3(\kappa R) = \frac{\kappa R\{\kappa R + 1.3\exp(-0.18\kappa R) + 2.5\}}{2\{\kappa R + 1.2\exp(-7.4\kappa R) + 4.8\}^3} \quad (2.32)$$

$$f_4(\kappa R) = \frac{9\kappa R\{\kappa R + 5.2\exp(-3.9\kappa R) + 5.6\}}{8\{\kappa R - 1.55\exp(-0.32\kappa R) + 6.02\}^3} \quad (2.33)$$

$f_3(\kappa R)$ and $f_4(\kappa R)$ have maxima around $O(\kappa R)$~1, but vanish as κR approach to zero or infinite.

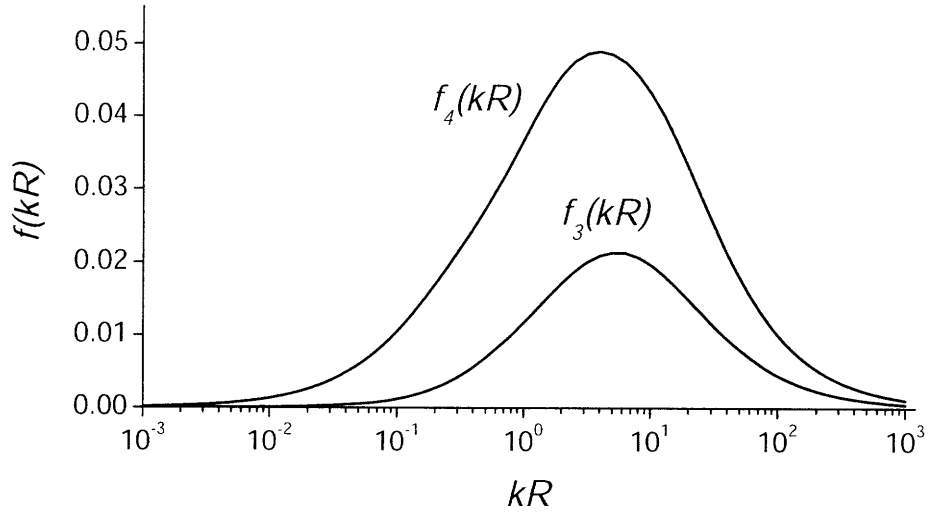

Figure 2.8 $f_3(\kappa R)$ and $f_4(\kappa R)$ is drawn in κR range of $(0,\infty)$

2.3 Gold nanoparticle synthesis

Theories of particle characterization are summarized in the previous section. Before proceed to the discussion in detail, general procedure of Au NP synthesis and Au NP DNA conjugations are described.

Au NPs were synthesized by reduction of $HAuCl_4$ according to literature methods.[16] For the synthesis, 1% $HAuCl_4 \cdot xH_2O$, 1% Sodium Citrate, 1% Tannic acid and 0.265% Sodium Carbonate solutions are prepared. Tannic acid is used to nucleate small Au seeds in the solution and additional Au ions being reduced are adsorbed on the seeds, therefore Au NPs grow. By changing the amount of Tannic acid or the other chemicals in the solution, size distribution of synthesized particles can be tuned.

$100ml$ of ~$11nm$ Au NPs are synthesized by following protocol. In mixture A, 79ml of water and $1ml$ of 1% $HAuCl_4 \cdot xH_2O$ are mixed and heated on bench-top hot plate. In mixture B, 16.8 ml of water, 3 ml of 1% Sodium Citrate, $100\mu l$ of 1% Tannic acid, and 100 μl of 0.265% Sodium Carbonate are mixed and heated, too. When the temperature of the mixtures reaches 60^oC, they are mixed quickly and stirred for 10min. at the same temperature. At the beginning the color of the solution is purple but changes into red as reaction goes on. After the time is elapsed, the solution is removed from the hot plated and cooled down in room temperature. A few hours later the temperature of the solution should not be much different from the room temperature. Then small amount of BPS (bis(p-sulfonatophenyl) phenylphosphine), negatively charged ligand (see Figure 2.9), is added and mildly stirred during overnight. Phosphorus atom of the molecules composes dipolar bonds with Au atoms of the particle surface and stabilizes the Au NPs electrostatically. Another popular ligand,

mPEG-SH (Methoxypolyethylene glycol thiol), is also shown in Figure 2.9. mPEG is neutral polymer and one end of the chains is modified with a thiol group which facilitates a covalent bond to an Au atom. Hydrophobic property of the mPEG is generally amplified as chain length gets larger.

Au NPs are generated; however, there still exist the agents used for synthesis in the solution. To separate the NPs from the original solutions, enough amount of sodium chloride is added into the solution such that Au NPs are aggregated due to charge screening caused by significant ionic strength. The solution is centrifuged to collect the sediment of aggregated Au NPs at the bottom of spin tubes. The Supernatent is discarded and the sediment is re-dispersed in small amount of pure water. For further purification, 1-1.5% agarose gel with 0.5×TBE is prepared. The particles are placed in gel and subject to 3-4V/cm of electric field. Once the band of particles migrates by a few centimeters, the band is cut out and placed into several milliliters of 0.5×TBE. After 1 or 2 days, most of the particles diffuse from the gel piece to TBE buffer. Collect the solution and centrifuge it again to achieve a layer of dark red Au NPs at the bottom of the spin tube. Collect the layer and finally filter it with 0.2μm spin columns to get rid of impurities.

After the synthesis is completed, transmission electron microscopy (TEM) pictures are taken to evaluate size distribution of the particles. Figure 2.9 shows a sample TEM picture of 10.8nm Au NPs. With the aid of image analysis software like ImageJ, particle boundaries are determined and the number of pixels within the boundaries are counted and then translated into size of the particles. From the distribution, average and standard deviation can be calculated.

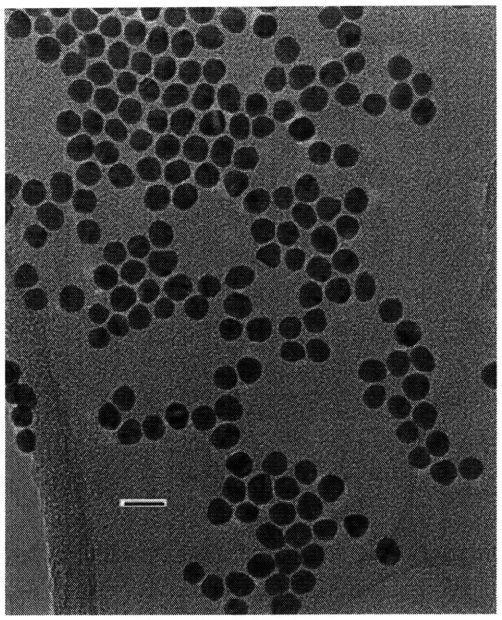

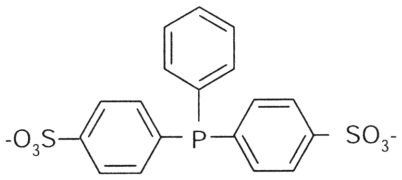

BPS (bis(p-sulfonatophenyl) phenylphosphine)

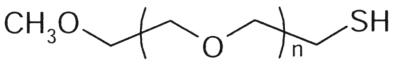

mPEG-SH (Methoxypolyethylene glycol thiol)

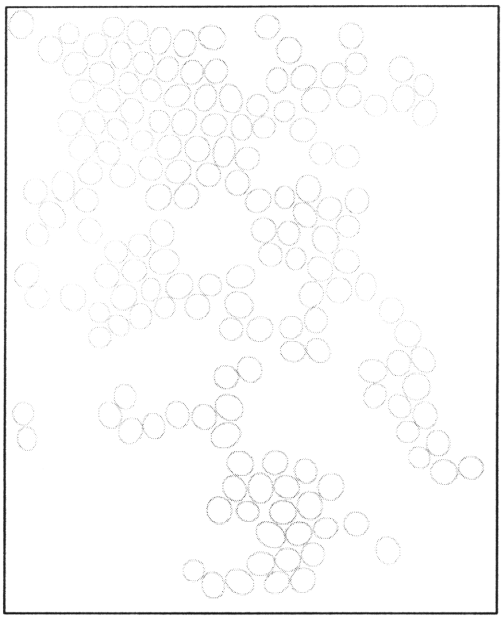

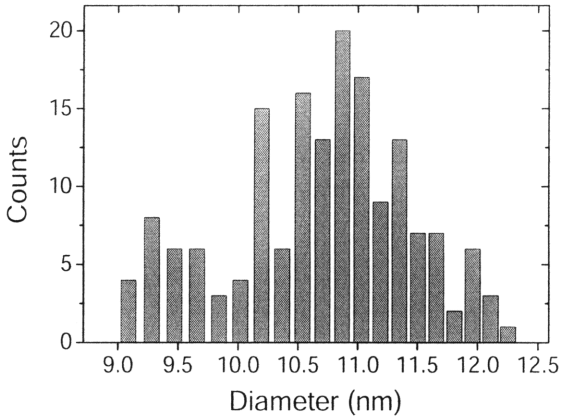

Figure 2.9 TEM (JEOL 2011, 200keV) picture of 10.8*nm* Au NP with size bar of 20*nm* in length. ImageJ drawing is generated and the numbers of pixels are counted. The bottom graph shows size distribution evaluated. Particles are modified with BPS ligand shown. Phosphorus atom is attached to Au NP via dipolar bond. mPEG thiol is neutral ligand and forms a covalent bond between gold and sulfur atoms.

Once size is determined, concentration of the Au NP solution is determined by absorption spectra measurement. Au NPs (~10*nm*) show absorption peak around 520nm (Figure 2.10) and follow Beer-Lambert law (equation 2.34).

$$A = \varepsilon_{abs} \cdot l \cdot C \tag{2.34}$$

where A is absorbance which is defined as logarithm of the ratio of light intensity ($Log_{10}\left(\frac{I_0}{I}\right)$), ε_{abs} $[cm^{-1}M^{-1}]$ is extinction coefficient of particle, l (cm) is path length of light and C $[M]$ is concentration of particles in the solution.

The absorbance at the wavelength that gives a peak of the spectra is a function of the number of gold atoms consisting of a particle (n). A correlation developed from lab experience is given as equation 2.35 and n is expressed as equation 2.36. Gold nanoparticles are assumed to have bulk structure of gold and the population of the atoms in unit volume ($\sim 5.9\times10^{28} m^{-3}$) is found elsewhere.[17]

$$Ln\,\varepsilon_{abs} = 1.1338 \cdot \ln n + 6.7429 \tag{2.35}$$

$$n = \frac{4}{3}\pi R^3 \cdot (5.9\times10^{28} m^{-3}) \tag{2.36}$$

For example, a 10.8*nm* Au NP is composed of approximately 38900 atoms and extinction coefficient is about 1.36×10^8 $cm^{-1}M^{-1}$. Concentration of a certain Au NP solution is then calculated by equation 2.37. Absorbance at 800nm is subtracted from the peak absorbance as a baseline value.

$$C = \frac{A(520nm) - A(800nm)}{\varepsilon_{abs}} \tag{2.37}$$

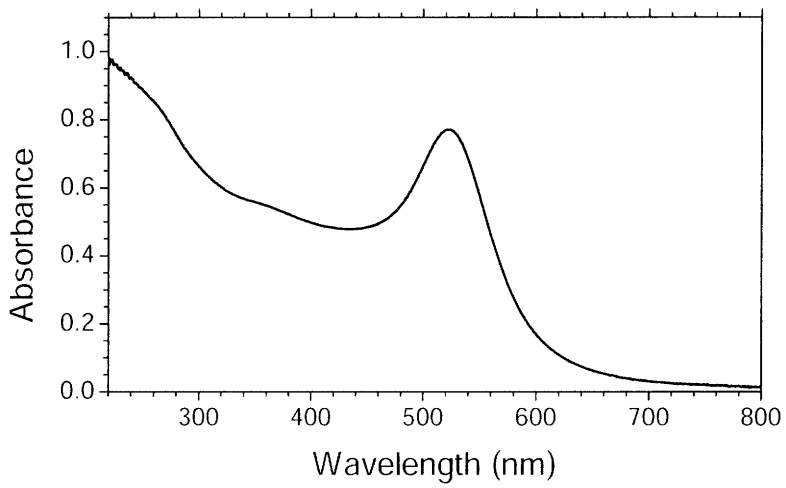

Figure 2.10 UV-VIS absorbance spectra of 10.8*nm* Au NP solution (~5.7*nM* in 0.5×TBE)

2.4 Ferguson analysis on Au NP

In this section, it is demonstrated that Ferguson analysis is a versatile method for simultaneously measuring size and zeta-potential of small (<~20*nm*) particles. Particles of different size and different surface charge density are tested to confirm the superiority of the methods.

Using Au NPs are synthesized or commercially obtained. Particles are functionalized with BPS as in section 2.3. Average sizes of the particles are 5.1, 7.5, 10.9, 12.5 and 18.2*nm*, obtained by analyzing TEM pictures (Figure 2.11). 10.9nm Au NPs with BPS were then incubated in mPEG-SH (n=6, MW = 356.5) bath for ~24hrs with different ratios of Au NP:mPEG-SH (1:200, 1:1000 and 1:2000, [Au NP] = $5 \times 10^{-7} M$) to allow thiol linkages between Au NP and mPEGs. Solutions are centrifuged and supernatant is discarded to get rid of free mPEG-SH molecules. Final Au NP-mPEG molecules are dispersed in 0.5×TBE. Thiol group is very common chemical residue that makes a covalent bond between gold and sulfur atom. This will be described further in Chapter 3.

Gel electrophoresis was done with the generated samples. Varying parameters are agarose gel percentage, T (0.5, 1, 1.5, 2, 2.5 and 3%) and TBE concentration (0.25, 0.5, 1 and 2×TBE). An example of gel pictures is shown in Figure 2.12. Applied electric field is 3.7-3.8 *V/cm* and running time is recorded (1.5-2 hrs). Digital images are taken immediately after the applied field is removed to minimize broadening of bands by diffusion. A ruler is placed right next to the gel to be a reference of length. The actual migration distances are measured by ImageJ, and then divided by elapsed time and electric field strength to achieve mobility, M.

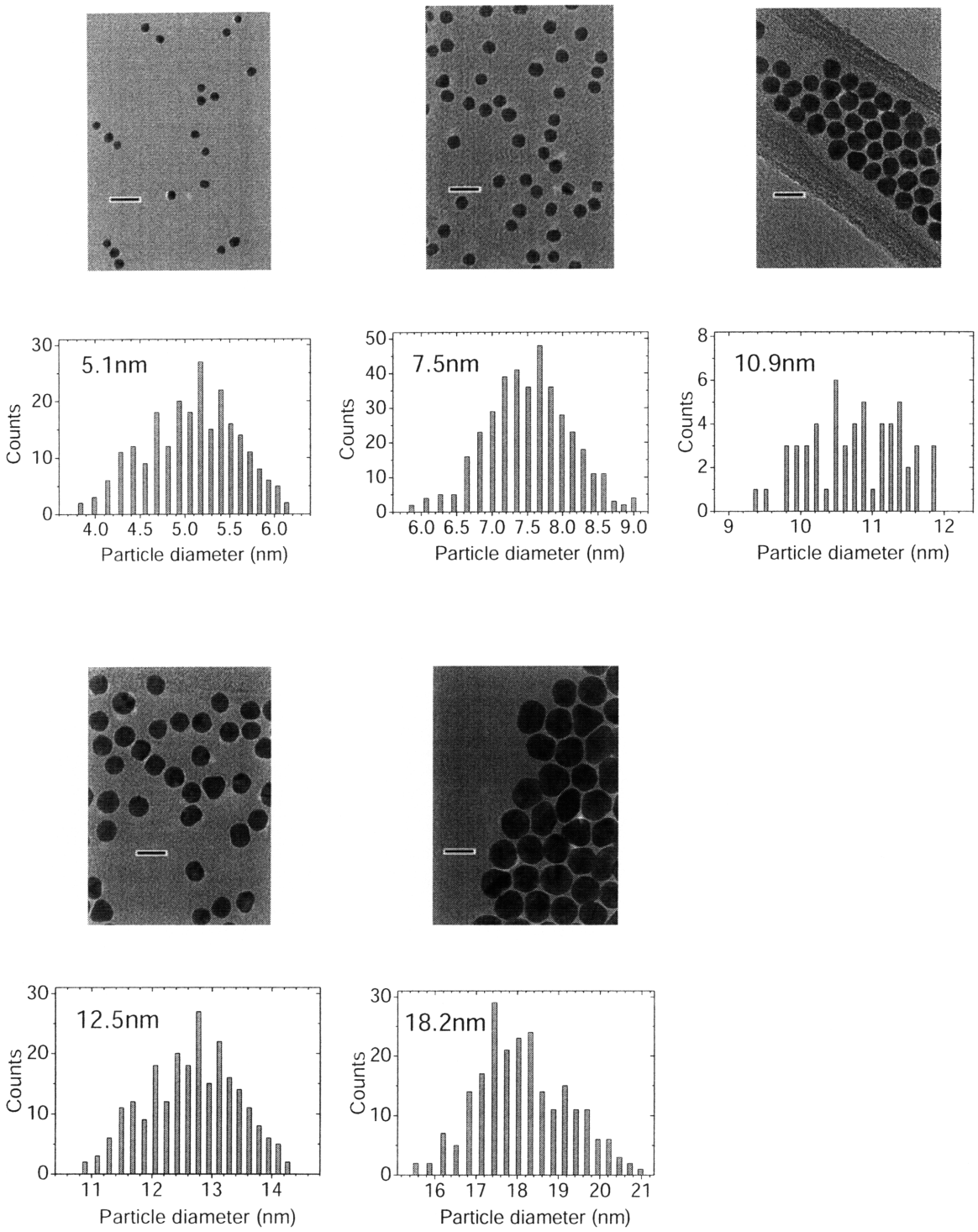

Figure 2.11 Size distributions of 5.1, 7.5, 10.9, 12.5 and 18.2*nm* Au NPs. Standard deviation of the particles are 0.51, 0.59, 1.0, 0.76 and 1.1*nm*, respectively.

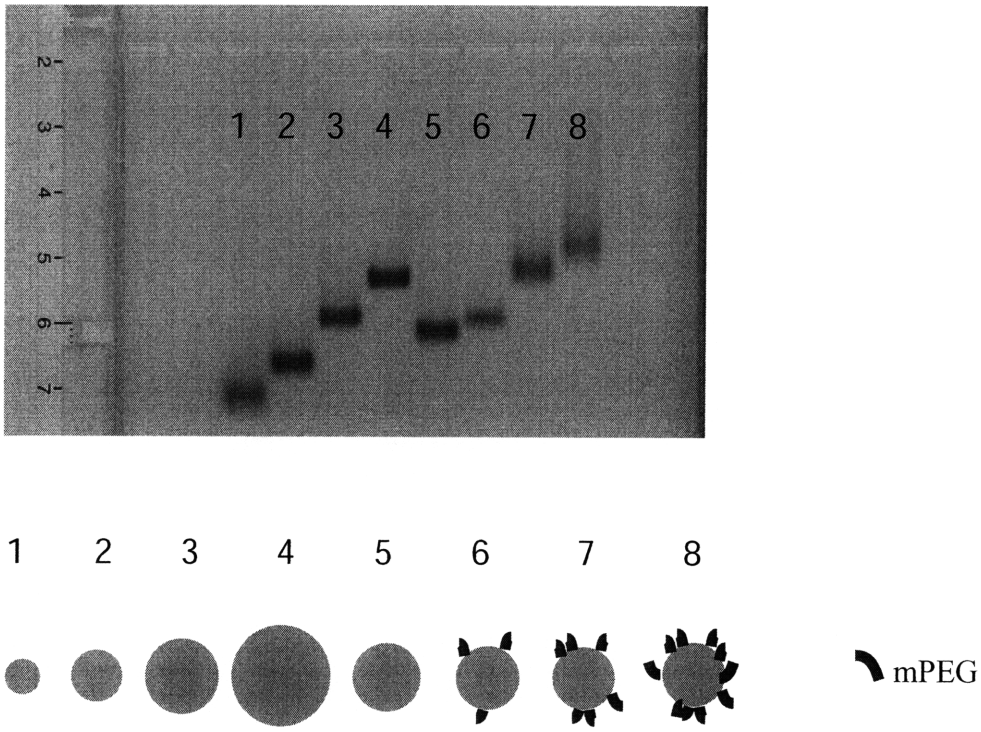

Figure 2.12 Example gel. 2% Agarose gel run for 2hrs in 0.5× TBE under 3.8*V/cm*. Lanes 1-4: 5.1, 7.5, 12.5, and 18.2*nm* Au NPs respectively. Lanes 5-8: 1:0, 1:200, 1:1000 and 1:2000 incubation of Au NP (10.9*nm*) : mPEG-SH for ~24hrs under the condition of [Au NP]=$5\times10^{-7}M$.

Ferguson plots of the samples are shown in figure 2.13. Mobility of the samples is generally smaller when buffer concentration is elevated. When buffer concentration is high (2×TBE) and gel percentage is low (0.5%), mobility difference among particles of different size almost vanishes. This implies that low percentage agarose gel in high running buffer concentration may not be suitable for size comparison between nanoparticles because particles experience much less collisions with gel fiber - size effect on retardation mechanism thus very small - and surface charge cannot alter mobility much due to charge screening by counter-ions.

(a) 0.25×TBE

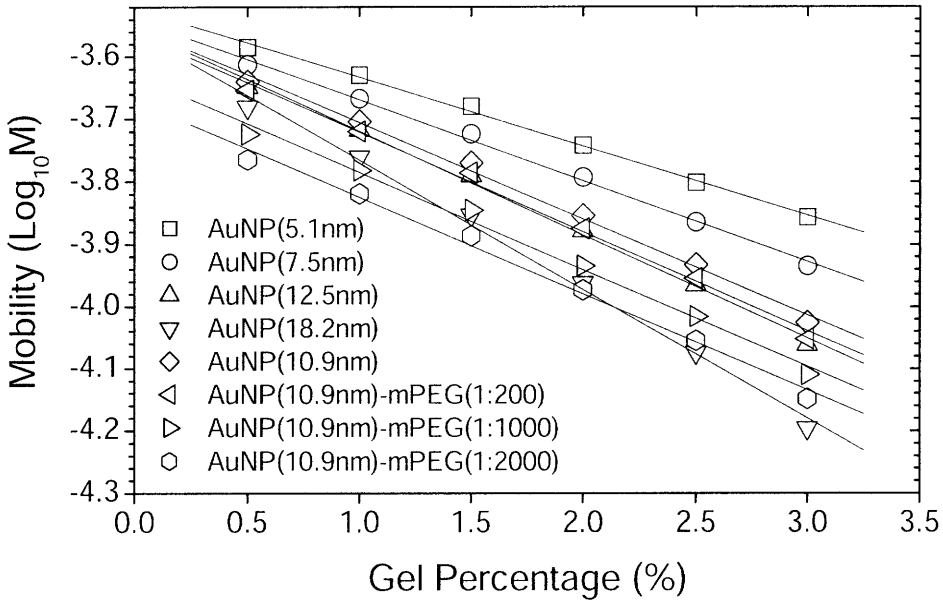

(b) 0.5×TBE

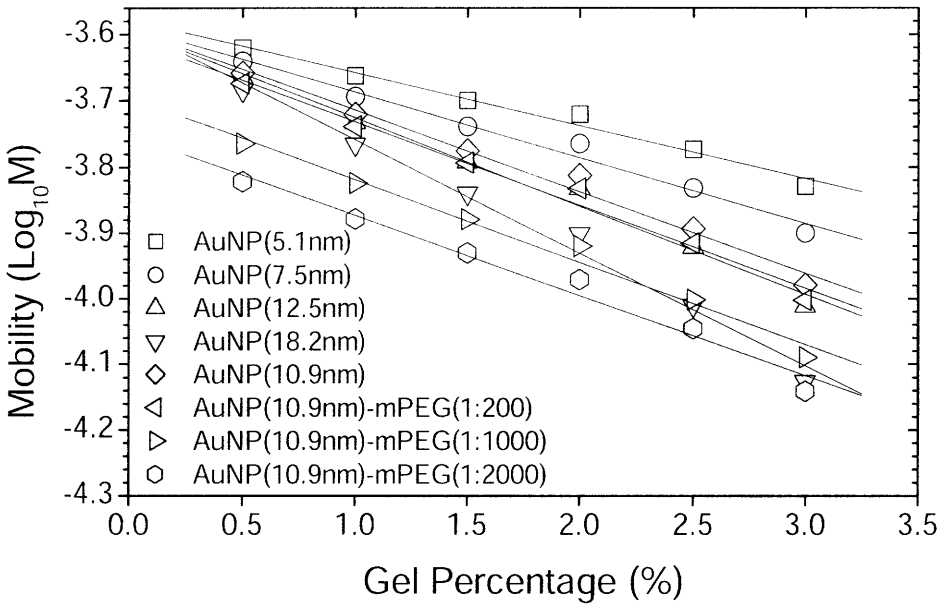

Figure 2.13 Ferguson plots of 5.1, 7.5, 10.9, 12.5 and 18.2*nm* Au NP, and Au NP with 1:200, 1:1000 and 1:2000 mPEG modifications. Gel running buffer is in (a) 0.25, (b) 0.5, (c) 1 and (d) 2×TBE. (continued on next page)

(c) 1×TBE

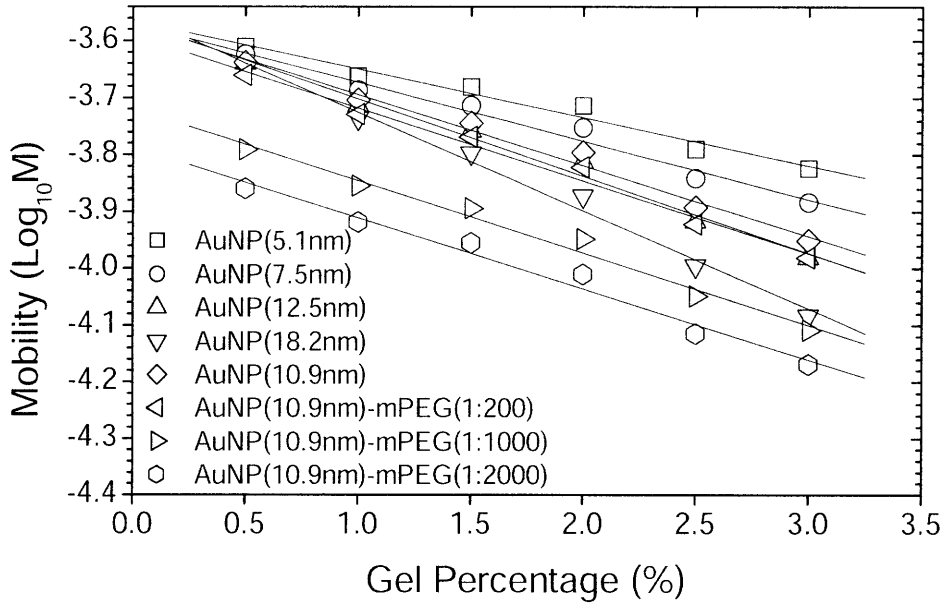

(b) 2×TBE

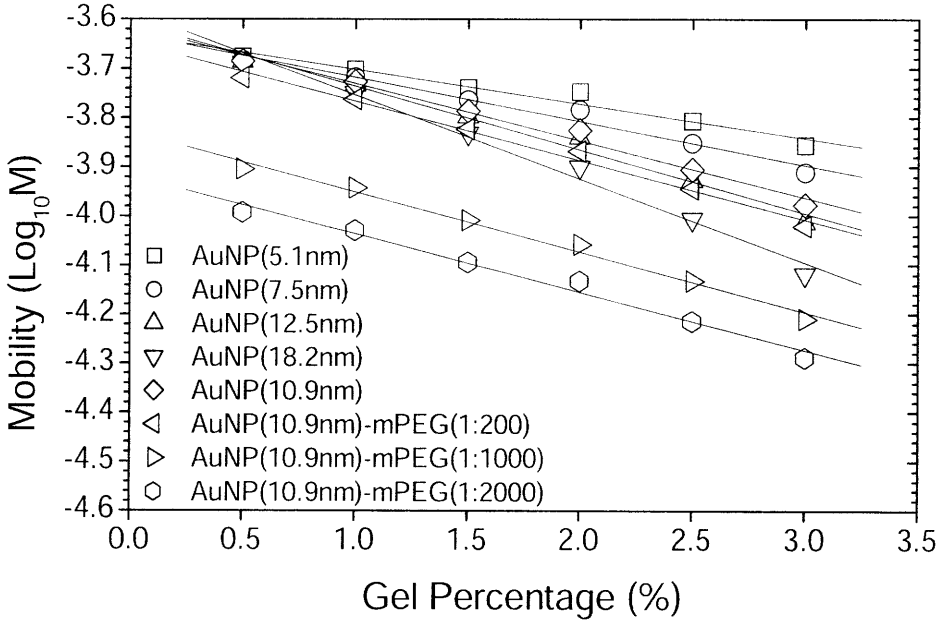

Figure 2.13 (continued) Ferguson plots of 5.1, 7.5, 10.9, 12.5 and 18.2*nm* Au NP, and Au NP with 1:200, 1:1000 and 1:2000 mPEG modifications. Gel running buffer is in (a) 0.25, (b) 0.5, (c) 1 and (d) 2×TBE.

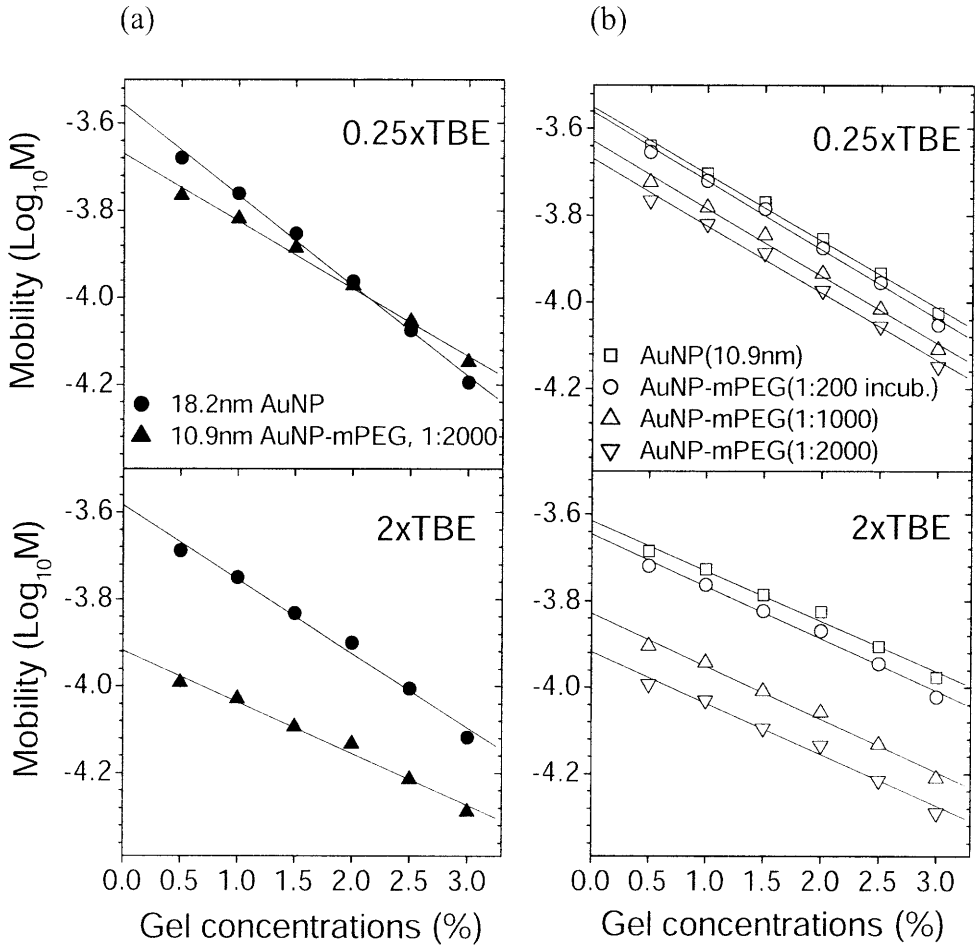

Figure 2.14 (a) Ferguson plots of 18.2*nm* Au NP (circles) and mPEG (1:2000) modified 10.9*nm* Au NP (triangles) in 0.25× and 2× TBE. Mobility M is in $[cm^2/Vs]$. (b) Ferguson plots of 10.9 *nm* Au NP with 1:0, 1:200, 1:1000 and 1:2000 ratio of mPEG-SH incubation for ~24hrs in 0.25× and 2× TBE.

The Ferguson plots also illustrate an important aspect of gel electrophoresis. Figure 2.14 (a) compares the mobility of 10.9*nm* Au NP with the greatest loading of mPEG, or the least negatively charged, to that of 18.2*nm* Au NP without mPEG modification. In 0.25×TBE 18.2*nm* Au NP has a smaller mobility in higher gel percentages due to its size, but runs faster than the 10.9*nm* Au NP in lower gel percentages ($T < 2.0\%$) due to its greater charge density. The Ferguson plots in Figure 2.14 (a) clearly show this mobility inversion upon the variation of gel concentration. However, this phenomenon was not observed in higher buffer

concentrations such as 2×TBE. This data shows that mobility is a function of both particle size and charge, and underscores the necessity of multiple gel running conditions for a proper assessment of particle characteristics.

In Figure 2.14 (b) the mobility of 10.9nm Au NPs with different mPEG loading is plotted. The M vs. T plots change in vertical offset with mPEG functionalization, but the slopes of the plots do not. This confirms that particle size does not change with surface charge variation. Since the mPEG used is small and charge-neutral, the conjugation does not change the hydrodynamic size of the particles, but results in reduced charge density that leads to a smaller M_0 (y-intercept). This vertical offset of M_0 is enhanced at higher buffer concentrations, due to the fact that zeta-potential decreases under higher ionic strength.

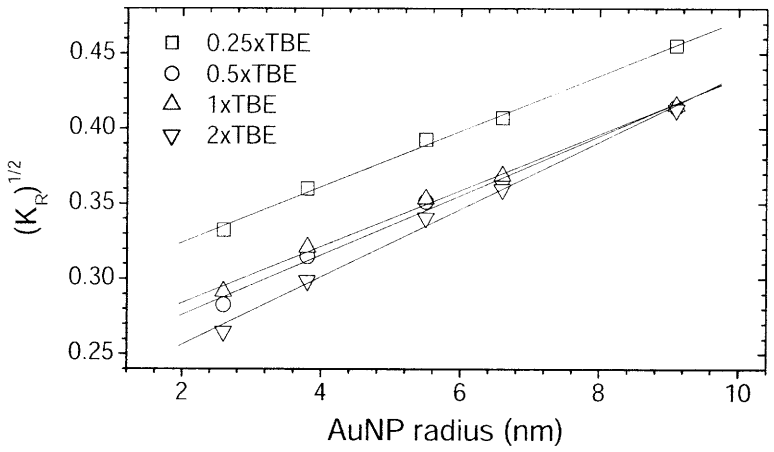

$$0.25\times\text{TBE:}\quad \sqrt{K_R} = 0.28710 + 0.01854 \cdot R$$

$$0.5\times\text{TBE:}\quad \sqrt{K_R} = 0.23648 + 0.01982 \cdot R$$

$$1\times\text{TBE:}\quad \sqrt{K_R} = 0.24649 + 0.01873 \cdot R$$

$$2\times\text{TBE:}\quad \sqrt{K_R} = 0.21134 + 0.02249 \cdot R$$

Figure 2.15 Size calibration standards for Ferguson analysis for 0.25, 0.5, 1 and 2×TBE made from mobility analysis of 5.1, 7.5, 10.9, 12.5 and 18.2*nm* Au NPs. Square roots of the slope of Ferguson plots ($(K_R)^{1/2}$) have a linear relationship with Au NP size.

Slopes of Ferguson plots are taken and square roots are drawn as a function of particle size as describe in section 2.2.1. Figure 2.15 shows graphs of $(K_R)^{1/2}$ vs. particle size in TBE of different concentrations. For Au NP and Au NP-DNA conjugate with unknown size, Figure 2.15 can be sizing standards to calculate hydrodynamic size from the slope of Ferguson plots of the samples.

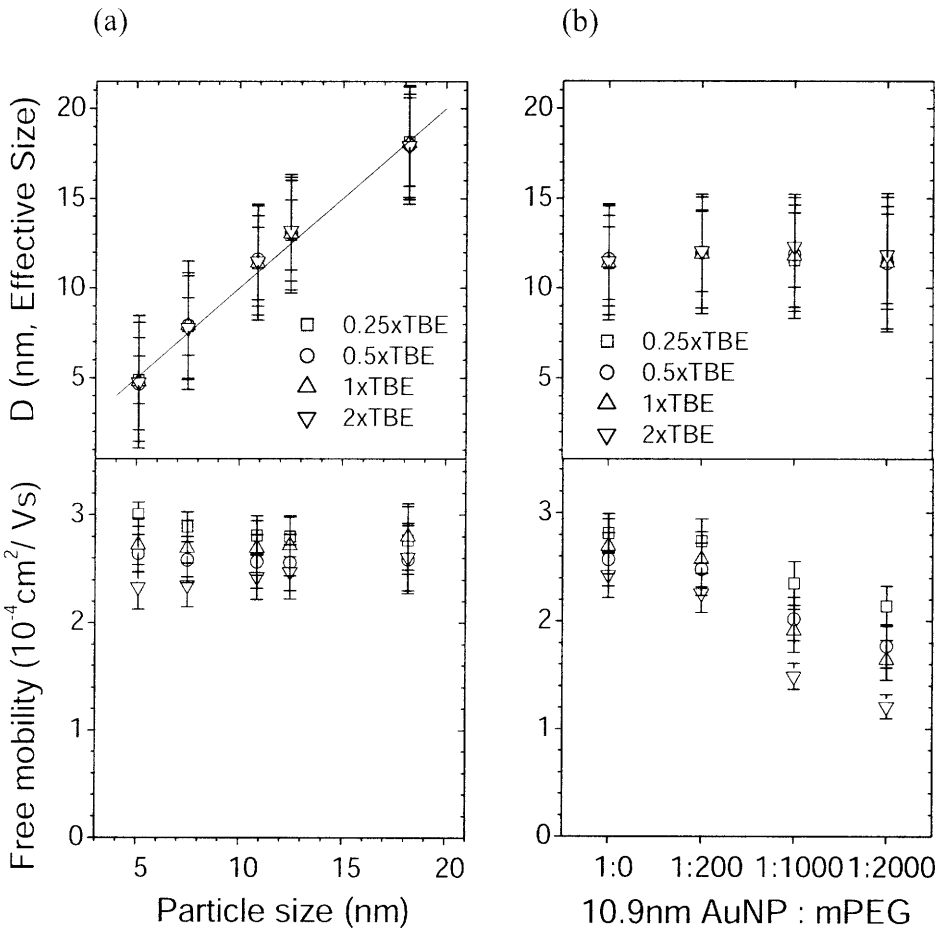

Figure 2.16 Effective size (D_{eff}, *nm*) and free mobility (M_0, cm^2/Vs) of Au NPs in 0.25, 0.5, 1 and 2×TBE calculated by Ferguson analysis with (a) different Au NP sizes (D = 5.1, 7.5, 10.9, 12.5 and 18.2*nm*) and (b) different mPEG modifications (1:0, 1:200, 1:1000 and 1:2000 Au NP:mPEG-SH incubation for ~24hrs) on 10.9*nm* Au NP. Error bars show 95% confidence intervals.

The size of the particles used as standards is reproduced with the fitted equation (Figure 2.16 (a), upper plot) and different charge modifications on 10.9*nm* Au NPs does not

change particle size (Figure 2.16 (b), upper plot). Different concentrations of buffer rarely affect evaluated size as long as the sizing standard was generated from the given buffer concentration. In contrast, M_0 (Figure 2.16, lower plots) tends to decrease in higher buffer concentration and decreases further with higher loading of mPEG. M_0 varies with surface charge and buffer concentration in addition to particle size, as expected.

In Figure 2.17 (a) and (b) ζ calculated from Henry's solutions (upper panels, equation 2.28) and Ohshima's solutions (middle panels, equation 2.30) are compared. The difference is greater than 20% for most of the samples. It should be noted that the evaluated ζ in this work are an order of magnitude higher than the particles used in a paper[18] that studied larger particles of lower mobility, for which Henry's solution can still be utilized. The correction terms in Ohshima's solutions are amplified under the condition of greater ionic drag coefficients of TBE. Therefore, Ohshima's solutions are much more suitable than Henry's solutions for this case. Regardless of the choice of formula, however, ζ decreases with increasing TBE concentration and increased loading of mPEG. Size difference of the particles does not influence on zeta-potential significantly.

Calculated total charges are also plotted (Figure 2.17 (a) and (b), bottom plots). The total charge is greater when the particle is bigger. In addition, increased mPEG functionalization leads to decreased total charge, as expected. The total charge, a physical property of the particle, is reduced when placed in higher buffer concentration. This could be due to increased binding of counter ions onto the particle surface.

By using the Ohshima's solutions, the graph in the middle panel of Figure 2.17 (a) shows size-independent zeta-potential behavior. This may be the result of the how the particle

is functionalized with the BPS ligand. During functionalization, particles and excessive BPS molecules are incubated for a long time.

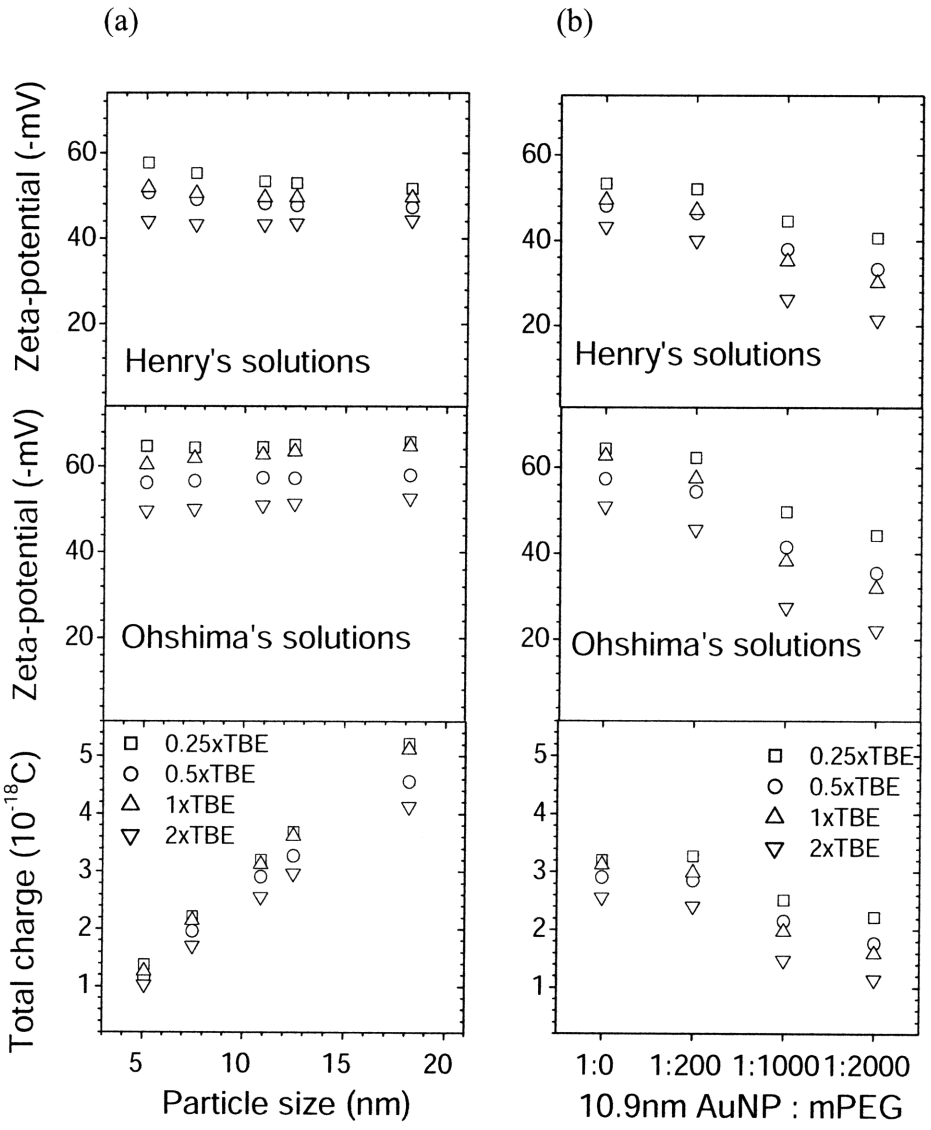

Figure 2.17 Zeta-potential is calculated by Henry's solutions (equation 2.21, upper panels) or Ohshima's solutions (equation 2.23, middle panels). Total charge (bottom panels) is based on the Ohshima's solutions and equation 2.22. Plots were generated based on (a) different Au NP size (5.1, 7.5, 10.9, 12.5 and 18.2*nm*) and (b) different mPEG modifications (1:0, 1:200, 1:1000 and 1:2000 Au NP:mPEG-SH incubation for ~24hrs) on 10.9*nm* Au NP.

Therefore the zeta-potential on the particle increases until it reaches a saturated value that balances the affinity of dipolar bonds formation between particle and BPS and repulsive energy between the zeta-potential and an incoming BPS molecule's charge. This phenomenon is most likely independent of the particle size.

2.5 Limitation of Ferguson analysis

Ferguson analysis is basically for measuring free mobility and size of particles. However, conventional dynamic light scattering (DLS) based zeta-potentiometers also can do the same work. Most of the current generation zeta-potentiometers are based on PALS (Phase Analysis Light Scattering). A laser beam is emitted from the source and split to incident beam and reference beam. Incident beam pass through the cell containing particles in solution and then put together with the reference beam. Phase of the incident beam is shifted when it is scattered by particles. The amount of shift is proportional to particle velocity, i.e. free mobility of the particle at a given electric field strength.[19, 20] The signals are detected and analyzed accordingly. While measuring, zeta-potentiometers apply sinusoidal or square form of electric field to the samples. Particles move back and forth under the electric field, and DLS measurement of he movements are processed by software.

These measurements are preferred in many cases in that results come in very quickly and only small amount of samples are necessary. In case of very small particles ($<20nm$), however, DLS is prone to unexpected fluctuations of the samples and becomes sensitive to impurities. Furthermore, when particles are modified with polymers such as DNA and mPEG the movement of the particles under the wave forms of electric field is not very ideal for PALS. Polymers have their own persistence length; therefore drag force between Au NP-polymer and fluid is not defined very well. Initiation and termination of electrophoretic movement under the electric field cycles must be different from those of hard spheres.

What zeta-potentiometers actually measure is free mobility. Displayed zeta-potentials are nothing but algebraic calculations of conventional solutions (equation 2.25, 2.27 or 2.28).

Actual zeta-potentiometer (90Plus, BIC) measurement data of Au NPs used in section 2.4 is shown in Figure 2.19. The results are highly inconsistent compared with free mobility calculations by Ferguson analysis in Figure 2.16.

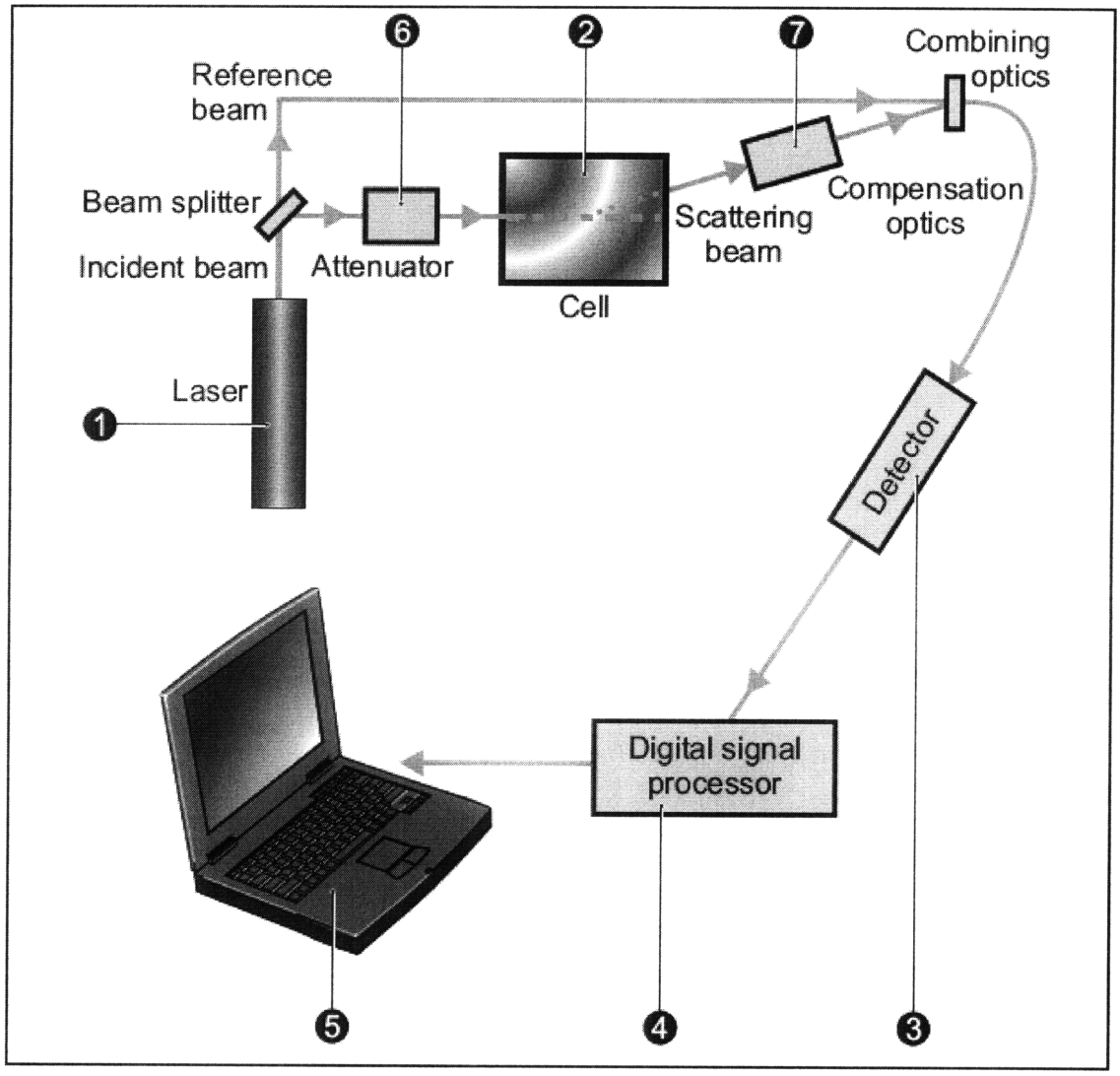

Figure 2.18 Schematic diagram of phase analysis light scattering (PALS) [19]

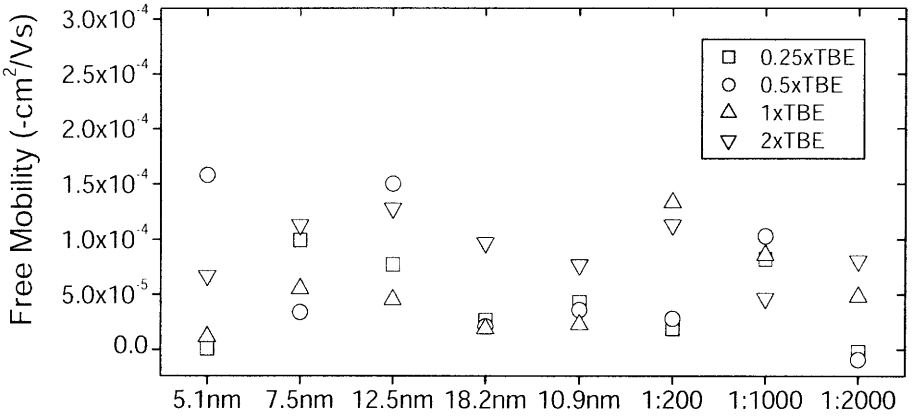

Figure 2.19 Free mobility (M_0) data measured from a zeta-potentiometer (90Plus, BIC). For each sample and TBE concentration (0.25, 0.5, 1 and 2×TBE) at least 6 measurements (> 40cycles) from the zeta-potentiometer were averaged. 5.1, 7.5, 12.5, 18.2 and 10.9nm Au NP and 10.9*nm* Au NP with 1:200, 1:1000 and 1:2000 mPEG modification (~24hrs incubation)

Capillary electrophoresis more directly measures free mobility of particles. Electrophoresis is performed in very narrow tubes (capillaries) of sub-millimeter diameter under external electric field so that the movement of the particle is well limited in 1-D. However, measured free mobility should be compensated for electroosmotic flow (EOF) generated inside the tubes. Due to surface charge of inner tube wall, fluid flow is driven by unbound counter-ion species in the buffer. Even if particles in the tubes are neutral, measured free mobility is non-zero owing to the phenomena. In other words, magnitude of EOF can be measured by reference neutral particles placed in the tube and then utilized for the compensation of measured free mobility of particles of interest. Figure 2.20 illustrates schematics of capillary electrophoresis device and electroosmosis.[21] Detectors are typically either UV-VIS spectrometer or fluorometer depending on samples' characteristic. Migration times of samples differ depending on their zeta-potential and size. Velocity profile of EOF in

tubes is flat for most of the region since flow is highly viscous and inertia effect is negligible due to very small length scale.

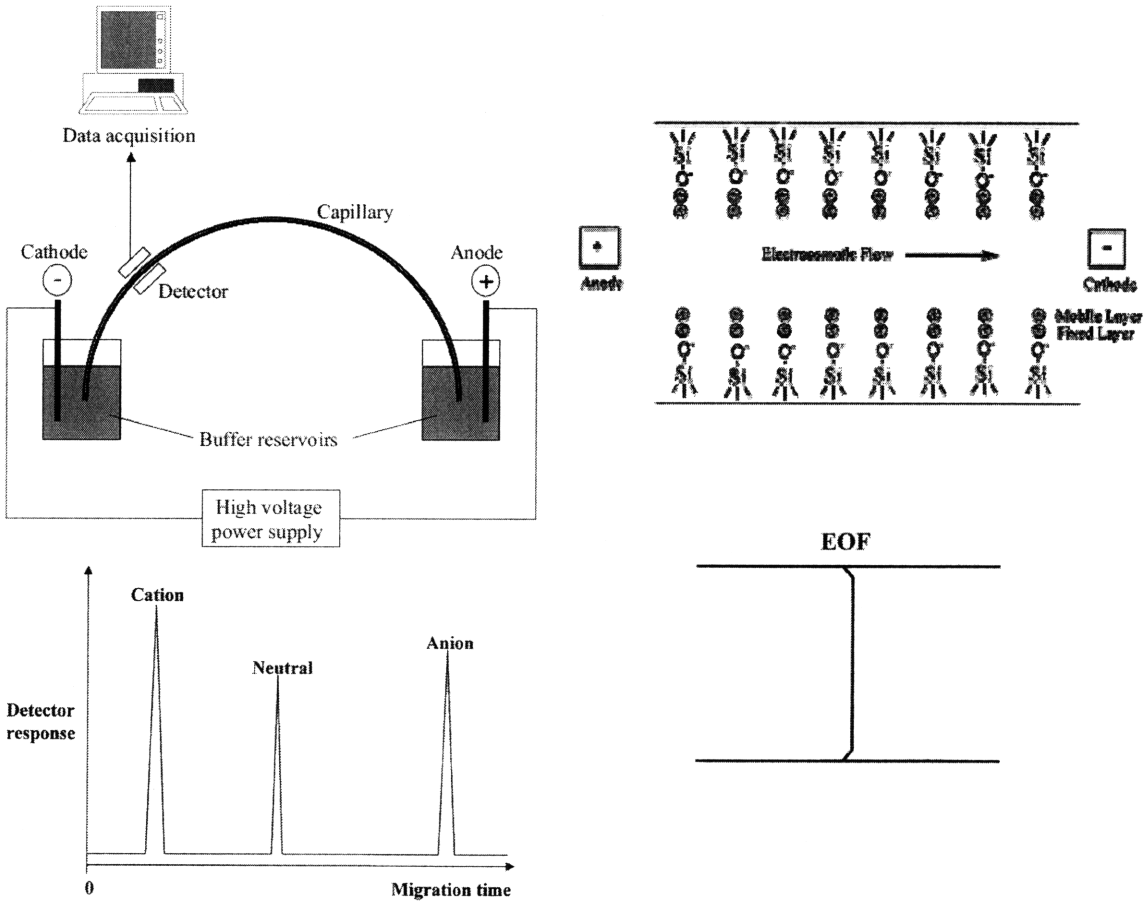

Figure 2.20 Schematic diagrams of capillary electrophoresis.[21] Inner wall of the tube is charged such that flat-profiled electroosmotic flow is generated. Depending on zeta-potential and size, particles show different time for a given migration distance.

EOF is an important issue not only for capillary electrophoresis but also for gel electrophoresis. It has been shown that polymer gel is subject to non-negligible degree of EOF depending on types of polymer and running buffer,[22, 23] and EOF is the most significant

among ordinary gels especially when TBE buffer is used for agarose gel. Borates are possibly bound to agarose fibers and make the gel structure negatively charged. It was also pointed out that free mobility extrapolated to 0% by Ferguson plot can be different from capillary electrophoresis measurement of free mobility due to EOF in agarose gel.[24] But mobility shift caused by EOF of commercial agarose gel (~ 0.3×10^{-4} cm^2/Vs) is an order of magnitude lower than observed mobility of the Au NPs used in section 2.4 so that we can safely neglect EOF. If EOF compensation is required, adjusted free mobility should be a smaller number in case of negatively charged Au NPs used in this work since EOF in negatively charged agarose gel is from cathode (-) to anode (+).

We have discussed mainly about Ogston model (equation 2.2 - 4) for Ferguson analysis, but there are some other functional forms available for the relationship between mobility of particle and polymer concentration in gel. Slater group particularly suggested that migration of particles in gel is characterized by trapping and releasing from the polymeric structure, and a polynomial relationship is a proper fitting for Ferguson analysis.[25, 26]

$$\frac{M}{M_0} = a_0 + a_1 T + a_2 T^2 + a_3 T^3 + \ldots \tag{2.38}$$

By taking logarithm and expanding the equation for small T, we can get

$$LogM = LogM_0 + a_1 T + \left(\frac{2a_2 - a_1^2}{2} \right) T^2 + \ldots \tag{2.39}$$

and the coefficients a_1, a_2, ... are determined by some important gel parameters such as particle size, electric field strength and gel pore size. An important issue that the group pointed out is that "dead-ends" formed in gel structure are a major cause for Ogston model's deviation from real experimental data. Once particles are trapped in very deep entanglement of polymers, they cannot escape from the traps especially when electric field is high such that

Brownian fluctuation doesn't allow the particles to leap from the holes. From stochastic simulation of particles in periodic or random gel structure, They have argued that scaled electric field intensity $\varepsilon' = q_e E P_E / 2k_B T_A$ is a key parameter that determines the shape of Ferguson plots. The numerator is the energy necessary for a particle of charge q_e to escape from a trap of depth P_E under electric field strength E, and the denominator is thermal fluctuation energy. The greater the scaled field intensity is the smaller the averaged mobility in the gel is expected. Figure 2.21 shows some result from numerical study. [27] Gel structure is assumed to be 2-D matrix and each element is randomly noted as either empty or occupied by polymer. Vertical axis is the ratio of mobility to free mobility and horizontal axis is gel concentration.

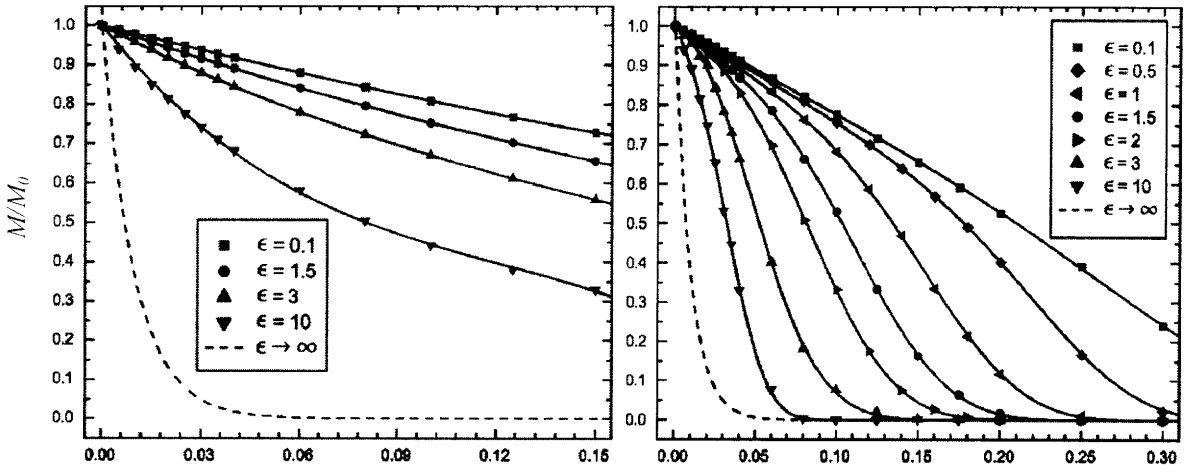

(a) No trapping (b) Trapping

Figure 2.21 Numerical simulation of particle mobility in random gel structure with or without trapping model. [27] Mobility is significantly reduced when scaled electric field intensity is high.

In our cases, however, electric field strength used is about ~$400V/m$ and particle charge is at most $5\times10^{-18}C$ from figure 2.17. Since pore size of typical agarose gel is less than $100nm$ from equation 2.13-16 associated with lab experience, the scaled electric field intensity should be around 0.02 at largest. The figure shows that this number is small enough to ignore the suggested dead-ends effect.

In conclusion, Ferguson analysis is shown to analyze size, free mobility, zeta-potential and total charge of small molecules ($<20nm$) reliably and effectively. Even though running gels takes quite a lot of time, it is possible to place several samples of interest in the same gels so that experiments are highly controlled and the overall time to test all the samples is not necessarily longer. In addition, impurities are separated out while running in gels, which is another benefit of electrophoresis. Although there are newer theories and techniques that add a little more accuracy on the analysis and measurement, suggested Ferguson analysis and Ogston model shows reasonable accuracy in the range of the particle size and zeta-potential that is mainly used.

2.6 Nomenclatures

A	Absorbance
a	A parameter in vWBR model
b	A parameter in vWBR model
α	Dissociation factor of acidic ionic species
β	Dissociation factor of basic ionic species
C	Concentration [M]
D_{eff}	Effective hydrodynamic size of molecule
δ	Numerical parameter in Henry's solutions
E	Electric field strength [V/m or V/cm]
ε	Permittivity ($=\varepsilon_0\varepsilon_r$)
ε'	Scaled electric field intensity ($=q_e EP_E/2k_BT_A$)
ε_0	Vacuum permittivity ($=8.854\times10^{-12}\,F/m$)
ε_r	Relativity permittivity
ε_{abs}	Extinction coefficient [cm^{-1}/M^{-1}]
f	Fractional volume
η	Viscosity of fluid [$kg/m\cdot s$]
I	Intensity of light [W/m^2]
K_R	Retardation coefficient
K_R'	Modified retardation coefficient
k_B	Boltzmann constant ($=1.38\times10^{-23}\,J/K$)
κ^{-1}	Debye length
L	Fiber length per unit mass [cm/g]
$\overline{L}$	Mean length of molecule
l	Fiber length per unit volume [cm/ml]
M	Mobility, U/E [$cm^2/V\cdot s$]
M_0	Free mobility
M_s	Asymptotic mobility of very small DNA fragment
M_∞	Asymptotic mobility of very long DNA
μ	Mobility of ionic species
N_A	Avogadro number ($=6.022\times10^{-23}\,mol^{-1}$)
N_0	The number of monomers in polymer chain

N_c	Critical number of monomers, a parameter in vWBR model
n	Number of atoms per each particle
n_0	The number of point-like gel fibers per unit volume [ml^{-1}]
P_E	Effective gel pore size
q_e	Charge of particle [C]
R	Radius of molecule
R_0	Reflection point of sigmoidal model of Ferguson plot
r	Radius of cylindrical gel fiber
S	Coupled surface area of molecule and 1-D gel ($=4\pi(R+r)^2$)
s	Surface area of 2-D gel plane per unit volume [cm^2/ml] or [cm^{-1}]
σ_s	Surface charge density
T	Gel percentage [$g/100ml$]
T_A	Absolute temperature [K]
U	Migration velocity
V	Coupled volume of molecule and 0-D gel ($=4/3\cdot\pi(R+r)^3$)
V_e	Available volume of gel to molecules
V_0	Void volume of gel
V_T	Total volume of gel
V_{fiber}	Volume of fiber per unit mass ($=\pi r^2 L$)
Z	Valence of ionic species
ζ	Zeta-potential (V)

2.7 References

(1) Park, S.; Brown, K. A.; Hamad-Schifferli, K. *Nano Lett.* **2004,** 4, 1925-1929.
(2) Zanchet, D.; Micheel, C. M.; Parak, W. J.; Gerion, D.; Alivisatos, A. P. *Nano Lett.* **2001,** 1, 32-35.
(3) Zanchet, D.; Micheel, C. M.; Parak, W. J.; Gerion, D.; Williams, S. C.; Alivisatos, A. P. *J. Phys. Chem. B* **2002,** 106, 11758-11763.
(4) Viovy, J.-L. *Rev. Mod. Phys.* **2000,** 72, 813-872.
(5) Griess, G. A.; Moreno, E. T.; Easom, R. A.; Serwer, P. *Biopolymers* **1989,** 28, 1475-1484.
(6) Rodbard, D.; Chrambach, A. *Proc. Natl. Acad. Sci.* **1970,** 65, 970-977.
(7) Tietz, D.; Chrambach, A. *Electrophoresis* **1986,** 7, 241-250.
(8) Ogston, A. G.; Preston, B. N.; Wells, J. D. *Proc. R. Soc. Lond. A.* **1973,** 333, 297-316.
(9) Rill, R. L.; Beheshti, A.; Winkle, D. H. V. *Electrophoresis* **2002,** 23, 2710-2719.
(10) Serwer, P. *Electrophoresis* **1989,** 10, 327-331.
(11) Slater, G. W. *Electrophoresis* **2002,** 23, 1410-1416.
(12) Deen, W. M. *AIChE J.* **1987,** 33, 1409-1425.
(13) Ohshima, H., *Theory of Colloid and Interfacial Electric Phenomena*. 1 ed.; Academic Press: London, 2006; Vol. 12.
(14) O'Brien, R. W.; White, L. R. *J. Chem. Soc., Faraday trans 2* **1978,** 74, 1607-1626.
(15) Michov, B. M. *Electrophoresis* **1984,** 5, 171.
(16) Beesley, J. E., *Colloidal Gold: A New Perspective for Cytochemical Marking*. 1 ed.; Oxford University Press: Oxford, 1989.
(17) Kittel, C., *Introduction to Solid State Physics*. 7 ed.; John Wiley & Sons, Inc.: New York, 1996.
(18) Hanauer, M.; Pierrat, S.; Zins, I.; Lotz, A.; Sonnichsen, C. *Nano Lett.* **2007,** 7, 2881-2885.
(19) Zeta-potential Theory. http://www.nbtc.cornell.edu/facilities/downloads/Zetasizer%20chapter%2016.pdf
(20) McNeil-Watson, F.; Tscharnuter, W.; Miller, J. *Colloids Surf. A* **1998,** 140, 53-57.
(21) Background Theory and Principles of Capillary Electrophoresis. http://www.rsc.org/pdf/books/capelectrosc.pdf
(22) Guo, Y.; Li, X.; Fang, Y. *Electrophoresis* **1998,** 19, 1311-1313.
(23) Stellwagen, N. C.; Gelfi, C.; Righetti, P. G. *Biopolymers* **2000,** 54, 137-142.
(24) Strutz, K.; Stellwagen, N. C. *Electrophoresis* **1998,** 19, 635-642.
(25) Slater, G. W.; Guo, H. L. *Electrophoresis* **1996,** 17, 977-988.
(26) Slater, G. W.; Guo, H. L. *Electrophoresis* **1996,** 17, 1407-1415.
(27) Gauthier, M. G.; Slater, G. W. *J. Chem. Phys.* **2002,** 117, 6745-6756.

Chapter 3. Au NP-DNA characterization and surface modification

3.1 Introduction

Gold nanoparticle (Au NP) and their conjugates with DNA have many applications in self-assembly, gene delivery, bio-molecular target sensing, and control.[1-9] One of the key issues is to preserve DNA's ability to hybridize to its complementary strands.[10-15] However, DNA strands are known to adsorb non-specifically on the surface of Au NPs depending on oligonucleotide content, oligo length, and coverage.[14, 15] These phenomena should be controlled since non-specific adsorption can significantly limit the capacity of DNA to hybridize to its target and ruin the functionality of designed Au NP-DNA for real applications.

The conformation of DNA adsorbed onto Au NPs differs from those of adsorption-free DNA and thus leads to different effective sizes (D_{eff}) of the conjugates. Evaluating NP-DNA conjugate size thus can assess the ability of the functionality of the DNA in the conjugate.[16, 17] Therefore, theories of DNA and Au NP-DNA conformations are reviewed and summarized. Ferguson analysis is re-introduced to see the feasibility of the methods for evaluating effective size and zeta-potential of Au NP-DNA. In addition, surface of Au NP-DNA is modified with 6-mercapto-1-hexanol (MCH) and examined how much of non-specific adsorptions are removed. Ferguson analysis discussed in Chapter 2 is further utilized with varying combinations of Au NP-DNA and surface modifications, and the chemistry of surface modification and the actual improvement of hybridization capacity are confirmed by fluorescence measurement techniques.

Finally, sequence dependent adsorption behavior of DNA is investigated. Bases of high affinity are placed in different region of DNA such that Au NP-DNA conjugates' conformation varies and is evaluated by Ferguson Analysis. It will be shown that Au NP-DNA conformation become similar and hybridization capacity is improved after MCH treatment on each combinations of Au NP-DNA.

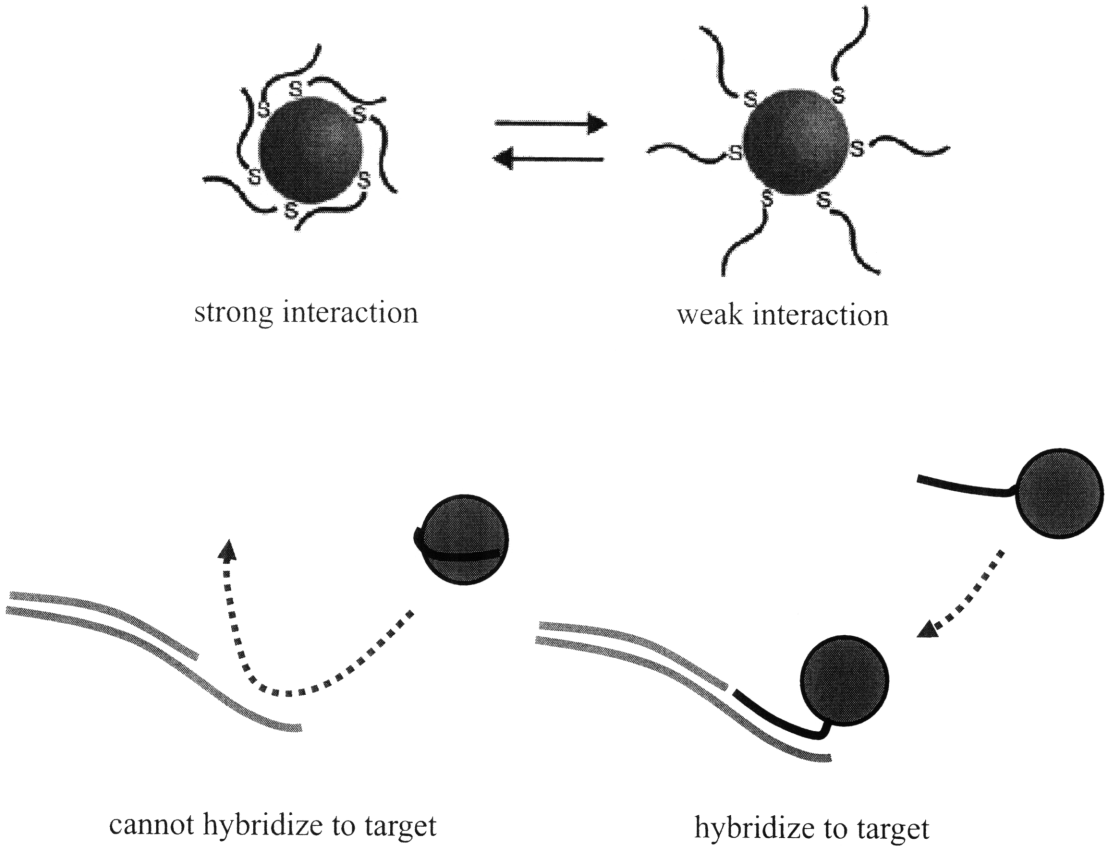

Figure 3.1 The strength of interaction between Au NP and DNA determines DNA conformation on the particle (top image[15]). Au NP-DNA can not be hybridized to target sequence if non-specific adsorptions are not properly removed.

3.2 Fluorescence measurement of Au NP-DNA

Fluorescence is one of the most commonly used methods in modern biological science. Fluorescence is the phenomenon in which absorption of light of a given wavelength by a fluorescent molecule is followed by the emission of light at longer wavelengths. There are many kinds of fluorophores having their own excitation and emission spectra. The most remarkable advantage of fluorescence over other optical techniques is its sensitivity. Absorbance measurements are generally performed with micromolar oligo concentration, whereas conventional fluorometers reliably work with nanomolar or even picomolar concentration. Another advantage is design possibility of fluorescence emission-quenching. Quencher is a molecule that has strong absorption peak at similar wavelength of a certain fluorophore's emission peak. If emission and absorption peaks of both of the molecules are close enough to each other then fluorescence signal is quenched and not detected by external measurement device. Table 3.1 shows some commercial fluorophores and quenchers.[18] It is also known that metal particles are very strong quenchers.[19, 20] For example, 10*nm* Au NPs have an absorbance peak at 520 *nm*. Thus emission of fluorescein, with an emission peak at 520 *nm*, is mostly quenched by nearby gold particles.

However, fluorescence intensity of fluorophores varies with many other parameters such as *pH* and temperature of medium. In addition, emission intensity generally decreases as the fluorophores are repeatedly exposed to excitation light due to deterioration of the molecular structure. Therefore control experiment should be done very carefully when measurement of fluorescence is for the purpose of quantification of the number or concentration of certain molecules like DNA oligos to which the fluorophores are attached.

Fluorophore	Max. Abs.	Max. Emi.
6-FAM	495nm	517nm
CY3	550	570
CY5	650	667
CY5.5	675	694
Fluorescein	495	520
HEX	537	553
JOE	520	548
LightCycler Red 640	625	640
LightCycler Red 705	680	705
Oregon Green 488	495	521
Oregon Green 500	499	519
Oregon Green 514	506	526
Rhodamine	564	603
Rhodamine6G	524	557
Rhodamine Green	504	532
Rhodamine Red	570	590
ROX	581	607
TAMRA	550	576
TET	521	538
Texas Red	589	610

Quencher	Max. Abs.	Max. Emi.
BHQ-1 Dark	535nm	None
BHQ-2 Dark	579	None
BHQ-3 Dark	672	None
DABCYL Dark	453	None
DABCYL-dT Dark	453	None
QSY-7	560	None
TAMRA	550	576nm

Table 3.1 Maximum absorbance and emission wave length of fluorophores and quenchers in common use.[18]

DNA is commercially ordered to be modified with fluorophores if quantitative analysis is necessary. The concentration of DNA in solution is easily achieved by measuring fluorescence signals. Peak emission intensity is proportional to concentration of DNA-fluorophore most of the cases (Figure 3.2). The measured intensity should not be affected by other emitters or quenchers for better accuracy. To address the degree of fluorescence quenching by Au NP in solutions, Förster (or fluorescence) resonance energy transfer (FRET) should be fully understood. Light energy that excited donor molecule is emitted at longer wavelength, thermally dissipated, or transferred to nearby acceptors. Dipole-dipole coupling between donor and acceptor is the cause of resonant energy transfer and this phenomenon

happens only within very short length scale (<10*nm*). Energy transfer rate (or efficiency) E is calculated by equation 3.1.[21]

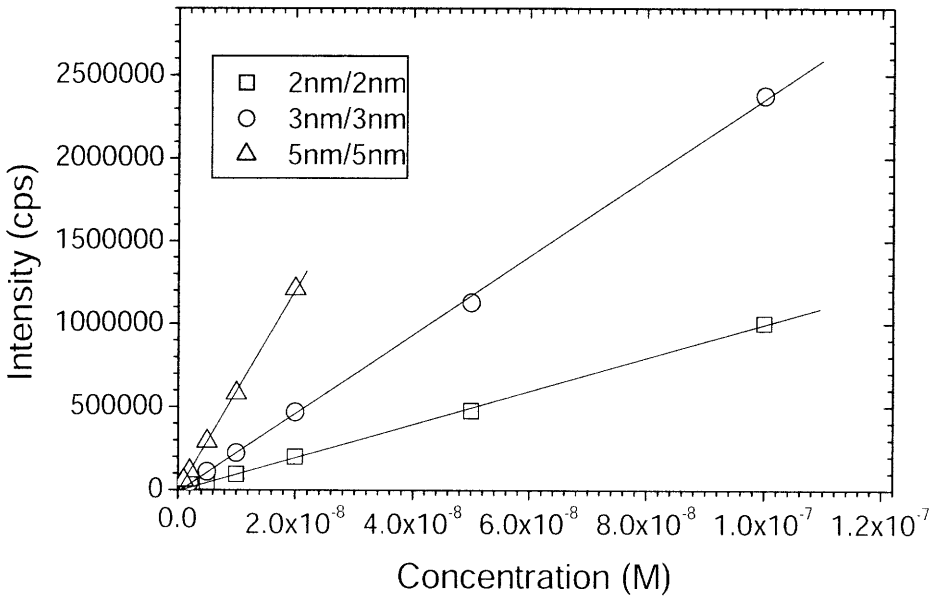

Figure 3.2 Fluorescence intensity vs. concentration of 40mer DNA-TAMRA (5'-HS-26(T)CGGCCCGTATAATT-TAMRA-3'). Samples in 1×PBS. The intensity is proportional to the concentration. The wider the slit size, the stronger the intensity is. Using machine is Fluoromax 3.

$$E = \frac{1}{\left(1 + \frac{R^6}{R_0^{\ 6}}\right)} \tag{3.1}$$

R_0 is called Förster distance where 50% of energy is resonantly transferred to acceptor. R_0 is calculated by equation 3.2[22]

$$R_0 = \left[\left(8.79\times10^{17}\right)\cdot\kappa^2\cdot n^{-4}\cdot\Phi_d\cdot J_{da}\right]^{\frac{1}{6}} \quad [nm] \tag{3.2}$$

where κ^2 orientation factor, n refractive index of solvent, Φ_d quantum efficiency of donor, and J_{da} overlap integral. κ^2 is 2/3 for freely moving and rotating dyes and Φ_d is 0-1. Overlap

integral is determined by emission spectra of donor ($F_D(\lambda)$) and absorbance spectra of acceptor ($\varepsilon_A(\lambda)$). The more the overlap of both specta is the higher the efficiency of energy transfer is.

$$J_{da} = \frac{\int F_D(\lambda) \cdot \varepsilon_A(\lambda) \cdot \lambda^4 d\lambda}{\int F_D(\lambda) d\lambda} \quad \left[M^{-1} \cdot cm^3\right] \tag{3.3}$$

$F_D(\lambda)$ should be normalized such that the maximum emission intensity is scaled to 1. The absorbance spectra $\varepsilon_A(\lambda)$ is also scaled to the intensity of $1M$ solution of donor.

To demonstrate energy transfer from fluorophores to Au NPs, fluorescein and TAMRA modified DNAs are commercially obtained (Table 3.2). Au NPs of $11nm$ diameter were also synthesized and BPS modified as in section 2.3. For calculation of overlap integral, emission and absorbance spectra were measured and scaled accordingly (Figure 3.3).

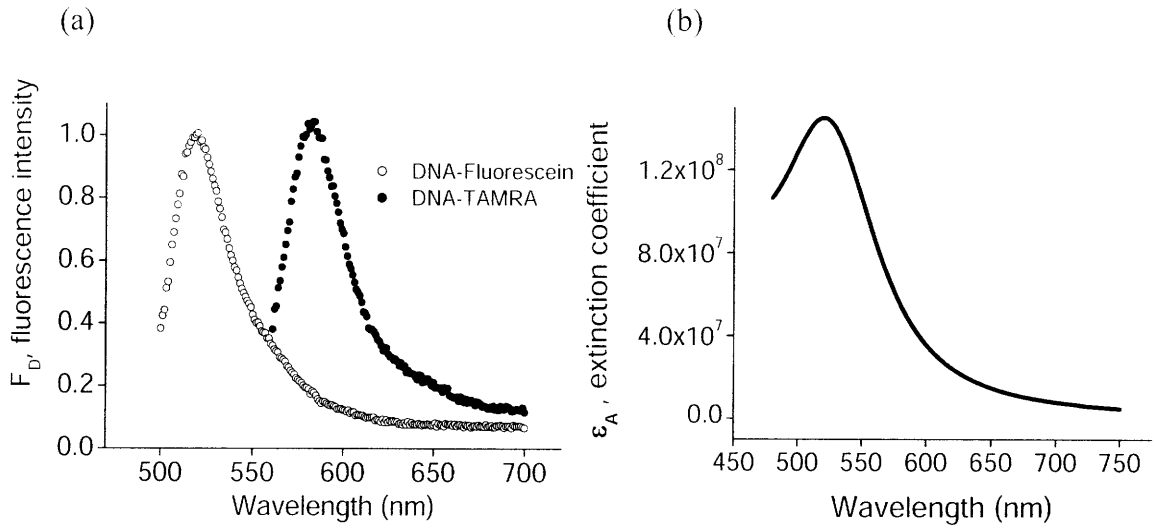

Figure 3.3 (a) Emission spectra of DNA-Fluorescein and DNA-TAMRA normalized to 1 at the peak. (b) Absorbance spectra of $11nm$ Au NP normalized to the intensity of $1M$ solution. All the samples are placed in 1×PBS buffer.

	Sequence
DNA-Fluorescein	5'-(Fluorescein)CGGGCCGAATTATA-3'
DNA-TAMRA	5'-(TAMRA)CTAATCCACAATGGG-3'

Table 3.2 Sequence of using DNAs

All the necessary numbers were plugged into equation 3.2 and Φ_d is assumed to be 1. Then R_0 calculated is $342nm$ for DNA-Fluorescein and $311nm$ for DNA-TAMRA. Their numbers are much grater than the order of magnitude of typical resonance energy transfer ($<10nm$).

To determine experimentally the quenching effect of Au NPs, different amount of $11nm$ Au NPs were put into DNA-Fluorescein and DNA-TAMRA solution at $2\times10^{-8}M$ concentration and $1M$ PBS buffer, and then fluorescence intensity at peak was measured and normalized to pure DNA-flourophore emission intensity (Figure 3.4). At low concentration of Au NP ($<\sim1\times10^{-9}M$) fluorescence intensity is not much quenched, but the intensity vanishes when concentration of Au NP is high ($(>\sim5\times10^{-8}M$). It is shown from the measurement that fluorescence from DNA-fluorophore is half-way quenched when the concentration of $11nm$ Au NP is around $1\times10^{-8}M$.

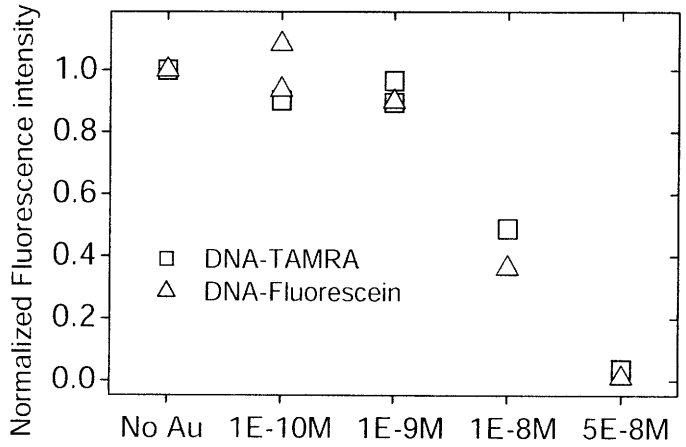

Figure 3.4 Fluorescence intensity of $2\times10^{-8}M$ DNA-TAMRA and DNA-Fluorescein in 1×PBS. As Au NPs are put into the solution fluorescence intensity vanishes to zero.

It can be shown that this result matches with the result from the calculation of Förster distance (either 311*nm* or 342*nm*). To roughly estimate energy transfer efficiency, it is assumed that fluorophores within the Förster distance from an Au NPs are all quenched and the ones outside the distance are not affected (solid line, Figure 3.5). If overlaps of the quenching volumes of different Au NPs are neglected, then the energy transfer efficiency is roughly

$$E \approx \frac{1L}{\frac{4}{3}\pi R_0^{\,3} \cdot C_{Au} \cdot N_A} \tag{3.4}$$

where C_{Au} is concentration of Au NP and N_A is Avogadro number. Estimation of the necessary 11*nm* Au NP concentration that quenches 50% of fluorescence intensity (E=0.5) is listed in Table 3.3. The results show that calculated values are quite similar to the actual experimental result in Figure 3.4. Although fluorescence quenching by Au NP is not attributed to resonance energy transfer in terms of much different length scales, the calculation based on overlap of emission and absorbance spectra is still valid.

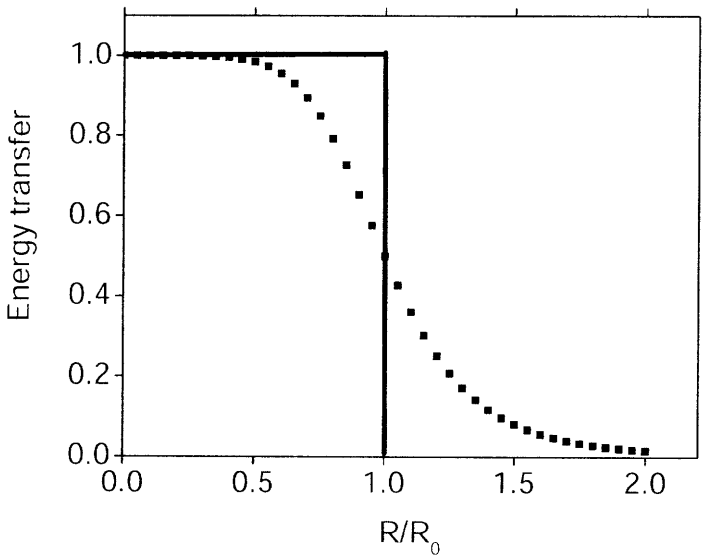

Figure 3.5 Energy transfer rate (or efficiency) vs. normalized distance between donor and acceptor. Dotted line shows equation 3.1. For easier calculation of equation 3.4 solid line is used instead.

	R_0	C_{Au} of 50% quenching
DNA-Fluorescein	342nm	1.0×10^{-8}M
DNA-TAMRA	311nm	1.3×10^{-8}M

Table 3.3 11nm Au NP concentration that quenches 50% intensity of DNA-Fluorescein or DNA-TAMRA. Solutions are in 1×PBS.

Better accuracy is achieved by using equation 3.1 and allowing the overlapped effect of the energy transfer profiles. Au NPs are ordered in 3-D lattices with the same intervals that are determined by the concentration of Au NP and a fluorophore is randomly placed in the space (Figure 3.6). Energy transfer from the fluorophore to nearby Au NPs is added up until the sum converges. By repeating the calculations for different positions of fluorophore and by averaging them the relation between the degree of quenching and Au NP concentration is achieved. In Figure 3.7, it is recognized that fluorescence emission is mostly quenched when acceptor (or quencher) concentration is above $5\times10^{-8}M$ in case Förster distance is around 200-300nm.

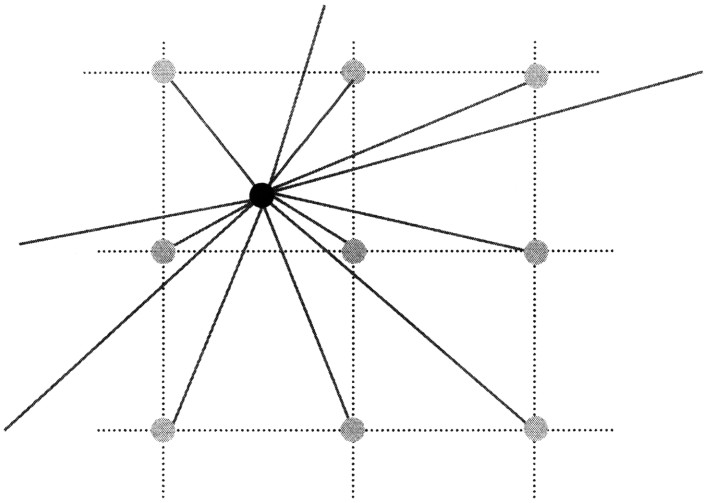

Figure 3.6 A fluorophore is quenched by nearby Au NPs. The quenching effect is added up until the summation of the energy transfer converges. Calculations are repeated for different positions of the fluorophore and then the results are averaged.

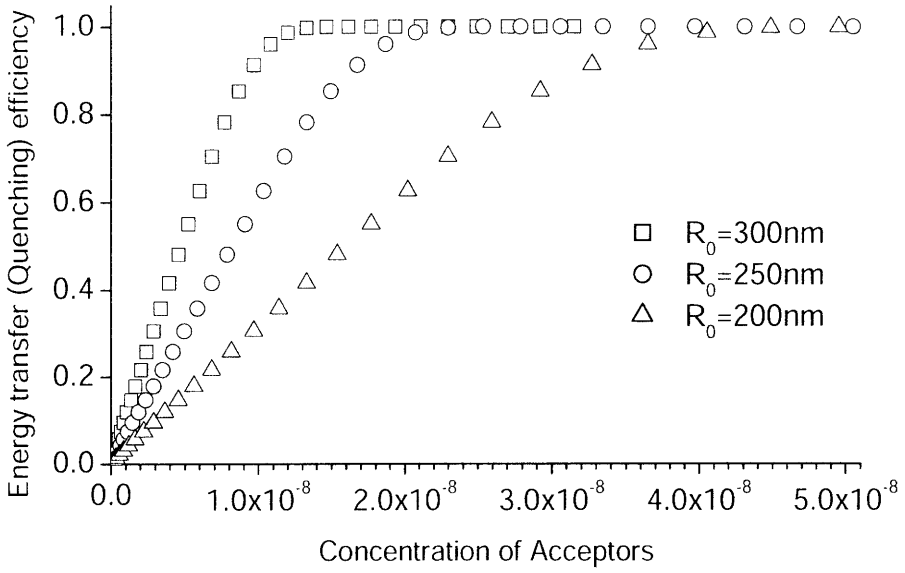

Figure 3.7 Energy transfer efficiency is calculated by equation 3.1 and Au NP arrangement shown in Figure 3.5. Fluorescence emission is mostly quenched when acceptor (or quencher) concentration is above $5\times10^{-8}M$.

In conclusion, concentration of Au NP ($\sim10nm$) should be low enough ($<1\times10^{-9}M$) to avoid disrupting measurement of fluorophore's emission intensity when the measurement is done for the purpose of quantification of DNA.

3.3 Theories of DNA and Au NP-DNA conformation

3.3.1 Basic theories on persistence length

Measurement and/or calculation of the persistence length of polymer have been an extensive topic for the last a few decades because the rigidity of polymer is a main parameter for its conformation. Persistence length is conceptually defined as the length over which the average deflection of the polymer axis caused by thermal agitation is one radian.[23] More rigorously, it is the sum of the average projections of all chain segments on the direction of a given segment or simply the first segment.[24, 25] Due to recent emphasis on biology and biotechnology, the persistence length of biomolecules including DNA has become an important issue. Conformational changes of biomolecules are directly related with their activity, and inversely we can influence them by changing external force and stress.[26] For example, a single-stranded DNA (ssDNA) has different ability to hybridize with its complementary strand according to their conformation. In addition, when transcriptions occur, double stranded DNA (dsDNA) partially open their double helix structures. It might be possible to control these phenomena by understanding the exact picture of the behavior.

Generally two kinds of persistence length are mentioned in DNA related research. One is from enthalpic contribution and the other is from entropic contribution.[27, 28] The latter is due to the statistical distribution of DNA conformation, while the former is mainly because of the rigidity of DNA itself. In general, short DNA strands have fewer number of possible conformations, the enthalpic persistence length thus dominates. Some other researchers using DNA electrophoresis employ different classifications such as intrinsic and electrostatic contributions.[29-32] Since DNA strands have charges on their backbones, ionic strength of the

medium becomes very important to describe charge-screening behavior, which induces reduction of charge repulsion between DNA bases. In any case, the overall persistence length p is considered as the sum of the two persistence lengths, because the entropic or electrostatic term gives additional stiffness.

$$p = p_0 + p_e \tag{3.5}$$

p_0 denotes the enthalpic (or intrinsic) persistence length, and p_e means the entropic (or electrostatic) persistence length for different situation. When electrostatic contribution to the persistence length is considered, Debye length κ^{-1} becomes important parameter. It is associated with Bjerrum length,[29, 33]

$$l_B = \frac{e^2}{\varepsilon k_B T_A} \tag{3.6}$$

the distance where the electrostatic energy between two counter ions with unit charge e is the same as thermal fluctuation $k_B T_A$, where k_B is Boltzmann constant and T_A is absolute temperature. Then κ^{-1} (equation 2.23) can be expressed as

$$\frac{1}{\kappa} = \frac{1}{\sqrt{N_A l_B I}} \tag{3.7}$$

, and p_e is approximated for intrinsically stiff polymer like short DNA strand as[29, 33]

$$p_e = \frac{l_B q^2}{4z^2}\left(\kappa^{-1}\right)^2 \tag{3.8}$$

where z is the valence of the ions, q is line charge density, and I is the ionic strength of the buffer solutions (equation 2.20).[29, 34] Although the equation is not applicable to all cases, it shows that smaller Debye length, which can be caused by high salt concentration or high valence, induces less electrostatic stiffness.

One more description on the classification is found in other literature,[23, 35] where static(p_s) and dynamic(p_d) contribution of persistence length are mentioned. Dynamic contribution is the persistence based on thermal fluctuation. Hence the static persistence length may contain all the other effect such as intrinsic and electrostatic contributions. The authors defined the overall persistence length in a different way.[23, 35]

$$\frac{1}{p} = \frac{1}{p_s} + \frac{1}{p_d} \tag{3.9}$$

It is understood from the formula that both contributions making the DNA "pliable" give rise to the decrease of the overall persistence length.

From the understanding of persistence length, some theories for the conformation of polymer chains were suggested. Among them, Freely Jointed Chain (FJC) model and Worm-Like Chain (WLC) model are most commonly used. FJC model assumes that polymer is a series of orientationally independent statistical segments (Kuhn segments).[36] On the contrary, WLC model consider polymers continuous, thin and flexible chains, which give[23, 36]

$$\left\langle \overrightarrow{t(s)} \cdot \overrightarrow{t(s+\Delta s)} \right\rangle = \exp\left(-\frac{\Delta s}{p} \right) \tag{3.10}$$

where $\overrightarrow{t(s)}$ is the unit tangential vector of the contour. Persistence length p is involved in WLC model. From well established theories, the root-mean-square end-to-end length R under the absence of force is given as

$$R = \left\langle \left| \vec{R} \right|^2 \right\rangle^{1/2} = \sqrt{Nb^2} = \sqrt{Lb} \qquad \text{: FJC} \tag{3.11}$$

$$R = \sqrt{2}p\left[\frac{L}{p} + \exp\left(-\frac{L}{p} \right) - 1 \right]^{1/2} \qquad \text{: WLC} \tag{3.12}$$

For FJC, the chain length L can be expressed as the product of the Kuhn length b and the number of Kuhn segments N. It also can be written as simply monomer length times the number of monomers, but practically not for FJC. Sometimes b of FJC is treated as $2p$ due to the fact that R of WLC becomes close to $\sqrt{2Lp}$ as L becomes much larger than p. More specifically, the probability distribution of R for WLC model is known by[64]

$$P(r,t) = \frac{4\pi A r^2}{(1-r^2)^{9/2}} \exp\left(\frac{-3t}{4(1-r^2)}\right) \tag{3.13}$$

where

$$A = \frac{4(3t/4)^{3/2}\exp(3t/4)}{\pi^{3/2}\left(4 + \frac{12}{(3t/4)} + \frac{15}{(3t/4)^2}\right)} \tag{3.14}$$

with $t=L/p$ and $r=R/L$.

All these equations can be argued by excluded-volume interaction, which means that a position in space cannot be occupied by two monomers simultaneously.[32, 37] When the volume scale of polymer Ld^2 (d: polymer diameter) is much larger than the cube of Kuhn length, the excluded-volume may affect the end-to-end size of the polymer.

$$R = N^{\nu} b = L^{\nu} b^{1-\nu} \tag{3.15}$$

where ν is known as Flory exponent, approximately equal to 0.6[32, 37, 38] Also if κ^{-1} is comparable to or bigger than the polymer diameter, the excluded volume becomes the order of $(\kappa^{-1})^3$, and the end-to-end length may follow a different rule.[32]

Some useful approximations are found also from force-extension relation.[28, 33, 39]

$$R = L\left[\coth\left(\frac{2Fp}{k_B T_A}\right) - \frac{k_B T_A}{2Fp}\right]\left(1 + \frac{F}{K}\right) \qquad \text{: FJC} \tag{3.16}$$

$$F = \left(\frac{k_B T_A}{p}\right)\left[\frac{1}{4(1-R/L+F/K)} - \frac{1}{4} + \frac{R}{L} - \frac{F}{K}\right] \qquad : \text{WLC} \qquad (3.17)$$

where K is elastic bending stiffness of the chain. Above equations contain enthalpic contribution term F / K that is due to elastic stretching of polymer structure itself. But practically this term is negligible in case of random coil.[39] An approach for more exact solution is given in literature.[33, 39] Based on WLC model, energy stored in chain can be expressed as

$$E_{WLC} = \int_0^L \left(\frac{K}{2}\left|\frac{d\vec{t}(s)}{ds}\right|^2 - F\cos\theta(s)\right)\cdot ds \qquad (3.18)$$

The first term of the integrand is the stored energy due to bending, and the relation $p=K / k_B T_A$ holds. The Boltzman factor $e^{-E_{WLC}/k_B T_A}$ is used to get partition function Z, and finally the relation

$$\frac{R}{L} = \frac{k_B T_A}{L}\frac{\partial \ln Z}{\partial F} \qquad (3.19)$$

is used for numerical calculation of force-extension relation. By comparing with equation 3.13, the author[39] simply added correction terms up to 7th order,

$$F = \left(\frac{k_B T_A}{p}\right)\left[\frac{1}{4(1-l)} - \frac{1}{4} + l + \sum_{i=2}^{7} a_i \cdot l^i\right] \qquad (3.20)$$

where $l=R / L - F / K$.

An important thing to note is that force-free end-to-end length or force-extension relation contain persistence length term, though its definition in the formula changes somewhat (e.g., a half of Kuhn length or bending stiffness over thermal fluctuation). Therefore we can get persistence length of DNA by comparing the theoretical models with

some experimental result showing the above relations. Also it can be more exactly compared with direct simulation of FJC or WLC model.

3.3.2 Double-stranded DNA's persistence length

There has been intensive research on dsDNA's persistence length, and it has been a typical way of the research to figure out the relationships between force and DNA's configuration. One way of DNA stretching is to use electrophoresis. External electric field gives rise to motion of DNA, and the force is balanced by drag force from relative fluid motion.[30] Therefore DNA moves with constant velocity during electrophoresis (or at rest). DNA is stained by fluorescence materials, which gives the information about its conformations. From FJC model, a relationship is given as[30]

$$R = \frac{1}{\alpha} \ln\left[\frac{\sinh \alpha L}{\alpha L}\right] \tag{3.21}$$

where $\alpha = E_0 qb/k_B T_A$, E_0 is electric field strength and q is line charge density. Therefore $E_0 qb$ is a local force acting on one Kuhn segment. The author compared experimental data of λ-phage DNA with equation 3.21 with varying q, finally got q=15e^- per p(=b/2). To get the persistence length through FJC simulation, electric field was removed to compose a random coil. By measuring the average end-to-end length, p ~80nm was achieved. The approaches in the article may be argued because excluded volume effect was not considered. Since κ^{-1} is in the order of 1~3nm for highly charged polymer such as DNA in general salt condition[29, 32] and the case of TBE in Figure 2.5, effective diameter of DNA is similar to $d+2\kappa^{-1}$ rather than just d. Electro-osmotic flow may affect the force balance in the case.[40]

Actually there have been some arguments on the situation involving both hydrodynamic force and electrostatic force, because the electro-osmosis flow is sometimes underestimated (see section 2.5). In addition, fluid motion induced by one monomer (or a part equivalent to Kuhn length) also may affect other monomers. It is not appropriate to say that the local force balanced by fluid drag is simply E_0qb.[32, 40] At the same time, the total force is not E_0qb. A more realistic overall force balance equation is given below.[32, 40]

$$F - \xi(v_{fluid} - \mu_0 E_0) = 0 \tag{3.22}$$

μ_0 is the mobility under the absence of external fluid flow. When external fluid velocity is zero (i.e. most of the gel electrophoresis cases),

$$F = \xi\mu_0 E_0 = 6\pi\eta R_h \mu_0 E_0 \sim \eta R_g \mu_0 E_0 \tag{3.23}$$

where ξ is excluded volume parameter, R_h is hydrodynamic radius and R_g is the radius of gyration originated from intrinsic viscosity of polymers.[41] Considering equation 3.11 or 3.15, and 3.23, we can reach the below relation.

$$F \sim R_g \sim R \sim L^{0.5} \text{ (or } L^{0.6}) \tag{3.24}$$

Note that the mobility μ_0 is almost constant regardless of its length when reptation occurs. [42] This force-chain length behavior was confirmed experimentally by use of fluid flow,[43] by fixing one end of DNA with optical trapping. The experiment shows that the free end of DNA is not very stable.[33, 42] The fluctuation is caused by a variation in the hydrodynamic drag force as the DNA conformation changes.

Since there is uncertainty for the conformation when we let one or both ends of the DNA free, direct stretching of both ends may be preferred to get clearer picture. Due to recent technology like optical trap, it is possible to control both force ($\sim pN$) and position in a very precise manner. Very popular experiment was done on B-form λ-Phage DNA to get enthalpic contribution to the persistence length.[38] As described earlier, stretching random coiled DNA mainly depends on entropic feature, whereas nearly linear polymer is subjected to enthalpic behavior. Equation 3.16 or 3.17 can be recalled. The author reported that force-extension experiment gives linear relationship up to $F \sim 60pN$. Around 65 pN, the DNA suddenly stretched to ~1.7 times its B-form contour length, which means the rupture of one of its strands. Twisted coil becomes straight at this stage. But it recovers its shape when released, though there is a certain time scale for the recovery. It is stated that the required force for the sudden behavior becomes small when ionic strength becomes low. Low degree of charge screening causes electrostatic repulsion between DNA backbones. Another experiment with optical tweezer[28] shows that multi-valent ions in solution gives low persistence length compared to mono-valent ions. It is in agreement with the explanation given on equation 3.7 and 3.8. In $10mM$ Na^+ salt condition, the persistence length achieved is $47nm$, but reduces to $39nm$ in $100\mu M$ Mg^{2+} solution, which is much lower concentration compared to Na^+. But no further drop of the persistence length is observed for higher salt condition, thus we can infer that the intrinsic persistence length is about $39nm$.

Regarding with equation 3.9, cryo-electron microscopy can be used to instantaneously immobilize and image the DNA[23]. dsDNA trapped between 40~50nm slabs is rapidly cooled with the rate of $10^6 K$/s. It is fast enough to capture a single state out of many different dynamic fluctuations. By comparing the actual DNA conformation with numerical simulation

of equation 3.10, dynamic persistence p_d is evaluated as $80nm$. If we assume the overall persistence length is $50nm$ (or $45nm$ from this article), then the static persistence length is about $130nm$ from equation 3.9. This static persistence length is much longer than the values called "intrinsic" persistence length from the above. The author explains that the overall persistence length is basically containing the pliability originated from thermal fluctuation, therefore DNA becomes stiffer if thermal effect is got rid of.

Besides the methods mentioned above, some other imaging and stretching methods such as scanning force microscopy[36, 44] and moving meniscus[45] have been utilized. Through wide range of research, the persistence length of dsDNA is believed to be in the order of $50nm$ with some variation.

3.3.3 Persistence length of single-stranded DNA

In general, single-stranded DNA (ssDNA) has much smaller persistence length compared to dsDNAs which compose sturdy double helix structures. From the force-extension relation given in equation 3.16 and 3.17, we can see that a small persistence length requires greater force to stretch, but results in small end-to-end length according to equation 3.11 and 3.12.

Stretching experiment with optical tweezers was done on single-stranded DNA (ssDNA).[38] The procedure is identical with that of dsDNA experiment given in the previous sections. In the early stage of stretching, ssDNA is much more contractile than dsDNA, but overstretch behavior is similar to dsDNA because only one of the two strands is dominant during the dsDNA overstretching. From the experiment and FJC model, calculated p ($=b/2$) was only $0.75nm$ which is comparable to the length of two bases only.

The ssDNA's persistence lengths were calculated for different salt conditions and chain length.[31] It was done by measuring the diffusivity of each random coil ssDNA, by use of fluorescence recovery after photobleaching(FRAP). Stokes-Einstein relation is given in equation 3.25.

$$D_s = \frac{k_B T_A}{6\pi\eta R_h} = \frac{k_B T_A}{6\pi\eta\left(\xi R_g\right)} \tag{3.25}$$

Radius of gyration R_g is given as[41]

$$R_g = \frac{R}{\sqrt{6}} = \frac{\sqrt{2Lp}}{\sqrt{6}} = \sqrt{\frac{Lp}{3}} \tag{3.26}$$

for long WLC. Intrinsic viscosity is considered in equation 3.25, and excluded volume effect comes in ξ, rather than in the end-to-end length. The author[31] took $0.5<\xi<0.664$ from various sources. In addition, L is the product of the number of bases L_0 and monomer length b_0 ($\sim 0.43nm$ for ssDNA in this article, but may be argued). From equation 3.25 and 3.26, we can see $D_s \sim N_0^{-0.5}$ for fixed p. If excluded volume effect is considered in end-to-end length, $D_s \sim N_0^{-\nu}$ should hold. Since the diffusivity data exactly fit in these relation,[31, 38] ssDNA length dependent behavior of p was not observed. It is understood from the fact that the smallest ssDNA used for the experiment is N_0=280, long enough to be WLC.[31]

An important point made by the experiment is that the persistence length of ssDNA highly depends on ionic strength (Figure 3.8). Data from another article[38] agree with the graph in rich salt condition, which gives intrinsic persistence length.

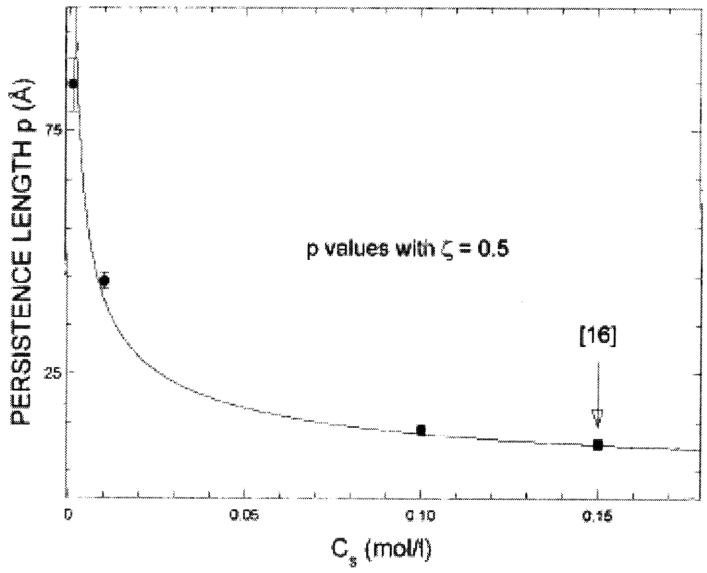

Figure 3.8 Persistence length change with the ion concentration $C_s(mol/L)$ with ξ=0.5. The arrow denotes the data from[38]. Image is from[31].

Rather than using randomly sequenced long chain, we may be interested in short ssDNA. However, it is difficult to image the actual contour due to its very small size. Recently fluorescence resonance energy transfer (FRET, see section 3.2) experiment was carried out with short ssDNA (N_0=10~70) wholly composed of thymines.[46] Figure 3.9 shows a schematic of the DNA used for the experiment. One advantage of the experiment is that we do not concern about each strand, but measure the overall intensity from the bulk solution. R, donor-acceptor distance in the energy transfer efficiency E (equation 3.1) is equal to the average end-to-end length of dT_{N0} from the Figure 3.9, and R_0 depends on salt condition and the characteristics of donor and acceptor,[47] but it is about 6nm for various NaCl concentrations (25mM~2M) and Cy3-Cy5 pair used in the experiment.

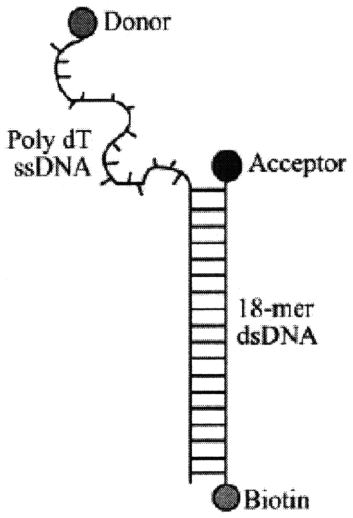

Figure 3.9 A Schematic of dT_N tailed, fluorescence labeled DNA. N_0 varies from 10 to 70.[46]

If the probability distribution of the end-to-end length is considered given in equation 3.13, we can modify the transfer efficiency as

$$E = \int_0^1 P(r) \frac{1}{\left[1+\left(rL/R_0\right)^6\right]} dr \tag{3.28}$$

where $r=R/L$. To get chain length L, the monomer length is assumed to be $0.63nm$, calculated from computerized molecular construction software. This value is a little different from that of another article[31] due to sequence dependent persistence behavior that will be explained later.

Figure 3.6 shows the change of E with the number of bases and salt concentration. Each line for different salt concentration comes from the numerical simulation with the optimal persistence length that gives the best fit with the experiment data of E. This also shows that high salt concentration induces intrinsic persistence length due to charge screening of DNA backbones. The range of the persistence length is $1.5nm$~$3nm$, similar to the result of diffusivity experiment on long chains.[31]

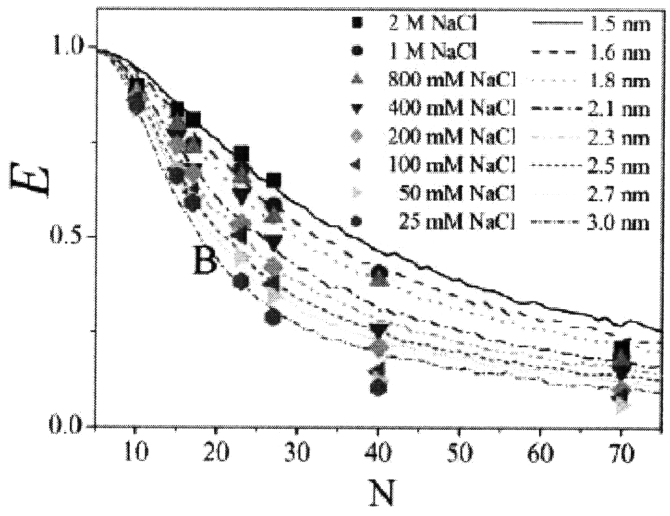

Figure 3.10 FRET efficiencies for different sizes of DNA and salt concentration. Image from[46].

Short and homogeneous series of thymines were also used in other experiments.[36, 48] To get detectable conformation change, dT_{N0} is introduced only in the middle of dsDNA (Figure 3.11). Double stranded parts are nearly straight since their lengths are within the range of the persistence length of dsDNA.

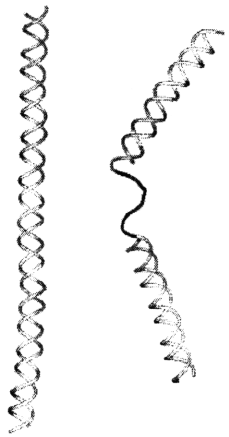

Figure 3.7 A schematic of ssDNA having dsDNA wings. Image from [48].

The DNA chain given in Figure 3.11 is comprised with sections of different persistence length. The overall end-to-end length is related with all of the p's, section lengths, and angles of each joint. The formula is given in the literature.[36]

$$R_{(\beta_1,\ldots,\beta_N;p_1,\ldots,p_N)} = \sqrt{2}\left\{\sum_{n=1}^{N+1} p_n^{\,2}\left[\frac{L_n}{p_n} - \left(1-e^{-L_n/p_n}\right)\right]\right.$$
$$+\sum_{n=1}^{N} p_n \cdot p_{n+1}\cos\beta_n\left(1-e^{-L_n/p_n}\right)\left(1-e^{-L_{n+1}/p_{n+1}}\right) \qquad (3.29)$$
$$\left.+\sum_{n=1}^{N-1}\sum_{m=n+2}^{N+1} p_n \cdot p_m \cos\left(\sum_{i=n}^{m-1}\beta_i\right)\left(\prod_{j=n+1}^{m-1} e^{-L_j/p_j}\right)\left(1-e^{-L_n/p_n}\right)\left(1-e^{-L_m/p_m}\right)\right\}^{\frac{1}{2}}$$

N+1 is the total number of sections and N is the number of joints. p_n and L_n are the persistence length and section length of n^{th} segment. β_n is the angle between the tangent vectors of n^{th} and $(n+1)^{\text{th}}$ segment at the joint. Smooth chain gives β_n =0. The only unknown is ssDNA's persistence length, and all other parameters are supposed to be known including end-to-end length available from SFM image. Experiments were done on several kinds of chains with various number and length of sections. Under the presence of divalent ions, p is about $1.3nm$ for short dT_{N0}.[36]

There is some consideration for the difference caused by DNA sequence.[48, 49] Since the strand being comprised entirely of thymines has minimal stacking interactions,[36] a series of whole adenine may give higher persistence length. It was confirmed by WLC simulation and the experiment done the similar DNA's given in Figure 3.9.[48] p and monomer length b_0 of dT_{N0} are $2\sim3nm$ and $0.5\sim0.7nm$, respectively. In case of dA_{N0}, however, they are $7.8nm$ and $0.32nm$ at $4^{o}C$. It seems that poly-adenines are more closely stacked (low b_0) due to strong interaction between bases, thus high persistence length is induced. More generally, the information on stacking free energy for different combinations of bases can be found in

literature.[50] It can be inferred that the additional rigidity of dA_{N0} is mostly enthalpic, rather than entropic. Another thing to note is that if only one different kind of base is introduced in the homogenous short chain, the stiffness is significantly reduced[49] by making a kink on the position. Some authors argue that the traditional model of DNA structure must be revised to include these sequence dependent rigidity of single-stranded DNA.[49]

3.3.4 Application to Au NP-DNA conjugates

Each of the using Au NP-DNA molecules in the thesis consist of an Au NP, a possible single-stranded offset, and a double-stranded part which can have a fluorophore-quencher pair. Figure 3.12 shows how we can model this system to use equation 3.29. L_1 is the same as particle's radius and the persistence length of the section is infinite. The joint angle between section 1 and 2 (=β_1) is more or less vague. We may use chemical bond angle between gold and sulfur at the joint, but also we can think that the ssDNA is perpendicular to the gold surface (β_1= 0) due to ligand and surface modification layer on the surface. β_2 is zero if smooth chain is assumed. R_1 denotes the average length from particle center to the end of ssDNA and R_2 is measured from the particle center to the end of dsDNA.

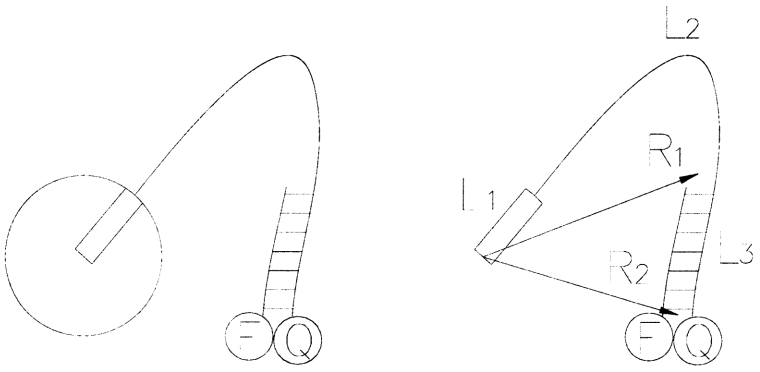

Figure 3.12 Equivalent polymer chain of Au-ssDNA-dsDNA series.

Since short dsDNA is nearly straight due to its long persistence length, we can think that the dsDNA section exists between R_1 and R_2 in average. The weakness of this modeling is that the gold particle really excludes a lot of volume. It will change the actual conformation of the DNA. If the size of the gold is not very big compared to the chain length of DNA, however, the model may give a close answer.

Table 3.4 gives an example. The offset strand is a homogeneous 25mer poly-T with the assumption of p_1=2*nm*, dsDNA is 15mer, and β_1, β_2 are zero. To deal with the infinite persistence length, we need to use the relation below.

$$1-e^{-\frac{L_n}{p_n}} = 1-\left\{1-\frac{L_n}{p_n}+\frac{1}{2}\left(\frac{L_n}{p_n}\right)^2-\cdots\right\} \approx \frac{L_n}{p_n}-\frac{1}{2}\left(\frac{L_n}{p_n}\right)^2 \quad \text{as } p_n \to \infty \tag{3.30}$$

This leads to the following two equations.

$$p_n^{\,2}\left[\frac{L_n}{p_n}-\left(1-e^{-\frac{L_n}{p_n}}\right)\right] \approx \frac{1}{2}L_n^{\,2} \quad \text{as } p_n \to \infty \tag{3.31}$$

$$p_n\left(1-e^{-\frac{L_n}{p_n}}\right) \approx L_n \quad \text{as } p_n \to \infty \tag{3.32}$$

Finally we can simplify equation 3.29 for R_1 and R_2.

$$R_1 = \sqrt{2}\left\{\frac{1}{2}L_1^{\,2}+p_2^{\,2}\left[\frac{L_2}{p_2}-\left(1-e^{-\frac{L_2}{p_2}}\right)\right]+L_1p_2\left(1-e^{-\frac{L_2}{p_2}}\right)\right\}^{\frac{1}{2}} \tag{3.33}$$

$$\begin{aligned} R_2 = \sqrt{2}\Bigg\{&\frac{1}{2}L_1^{\,2}+p_2^{\,2}\left[\frac{L_2}{p_2}-\left(1-e^{-\frac{L_2}{p_2}}\right)\right]+p_3^{\,2}\left[\frac{L_3}{p_3}-\left(1-e^{-\frac{L_3}{p_3}}\right)\right] \\ &+L_1p_2\left(1-e^{-\frac{L_2}{p_2}}\right)+p_2p_3\left(1-e^{-\frac{L_2}{p_2}}\right)\left(1-e^{-\frac{L_3}{p_3}}\right)+L_1p_3\left(e^{-\frac{L_2}{p_2}}\right)\left(1-e^{-\frac{L_3}{p_3}}\right)\Bigg\}^{\frac{1}{2}} \end{aligned} \tag{3.34}$$

	Section 1 (gold)	Section 2 (ssDNA)	Section 3 (dsDNA)
b_0	5*nm*	0.63 *nm*	0.34 *nm*
N_0	1	25	15
$L = N_0 b_0$	5 *nm*	15.75 *nm*	5.1 *nm*
p	∞	2 *nm*	50 *nm*
R_1	10.0 *nm*		
R_2	12.0 *nm*		

Table 3.4 End-to-end length of Au-ssDNA-dsDNA chain. 10*nm* Au particle, 25mer poly-T, and 15mer dsDNA are considered.

From the table 3.2, dsDNA of the Au NP-DNA conjugate is supposed to be away from the particle center by 10*nm*~12*nm*. Although overall chain length is greater than 20*nm*, the actual size of Au NP-DNA is much less. This fact will be confirmed again by doing Ferguson analysis on Au NP-DNA in following chapters.

3.4 Au NP-DNA conjugation and coverage evaluation

Linking of bio-molecules to inorganic nanoparticles has been widely studied.[1, 51] A pair of linker and functional group can be selected from either nature like streptavidin and biotin or chemical means like introducing C-6 thiol group at the end of DNA oligos. Thiol chemistry is especially convenient and effective when Au NPs are used to conjugate with DNA strands. 5' or 3' end of short DNA oligs are commercially ordered to be modified with thiol groups and easily attached to Au NPs surface by forming very strong covalent bonds between gold and sulfur atoms.

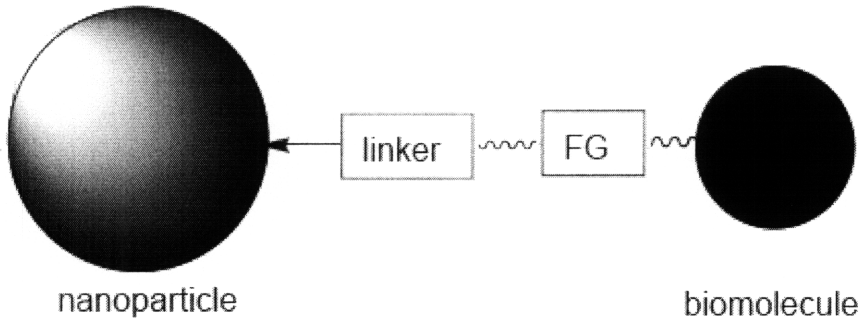

Figure 3.13 General methods of coupling nanoparticles and biomolecules. FG stands for functional group. [1]

Stock thiol-modified DNA oligos, however, form disulfide bonds originated from the thiol groups and are rarely conjugated to Au atoms as they are. Disulfide bonds should be reduced to thiol groups again. This is done by incubating DNA oligos in Dithiolthreitol (DTT) solutions. From lab experience, $0.1 \mu g/\mu l$ DNA is mixed with $0.05M$ DTT for ~24hrs for the best result. Then DTT should be removed from the solution before being put together with Au

NPs since it also reduce Au-S bonds such that Au NP and DNA conjugations are not achieved. DTT is removed by adding 3 or 4 times as much as ethyl acetate to the solution and then vortexing and centrifuging. After centrifuged, the solution is separated into two layers. The bottom layer is water and DNA mixture, and the top is ethyl acetate layer that contains DTT that is discarded. By repeating the washing process at least 4 times, the content of DTT is minimized in the DNA solution.

Once DTT is removed, DNA solution is immediately put into Au NP (see section 2.3) solution of desired concentration. The solutions are put together and then brought into a lyophilizing chamber. Although thiol bond is highly favorable to form, formations of the bonds can be accelerated by concentrating, i.e. drying the solution. It should be noted that the solution must be in ionic buffer such that electrostatic repulsion between negatively charge Au NPs and DNAs can be shielded when they are get closer while being dried.

After the sample is completely dried, it is re-dispersed in ~2×TBE or ~1×PBS and kept in refrigerator for 1 or 2 days to allow further conjugation. Free DNAs are separated either by agarose gel electrophoresis or by repeating centrifuging and re-dispersing as described in section 2.3. Final concentration of Au NP-DNA is measured by evaluating absorbance of the Au NPs by assuming that conjugating DNAs does not affect the absorbance of Au NPs much.

Coverage (average # DNA strands / particle) is measured by completely displacing the DNA from the NP in concentrated MCH solutions (1mM MCH) for extended time (~24 hrs), doing centrifugation, and measuring intensity of fluorescence marker in the supernatant.[19] Intensity vs. DNA concentration relation like Figure 3.2 should be prepared with using DNA-fluorophores to interpret measured intensity into concentration of DNA. If the DNA used

doesn't have fluorescence marker, the DNA strands in the supernatant can be fluorescence-stained by use of commercial dyes like Cyber gold. Figure 3.14 shows schematic of the process.

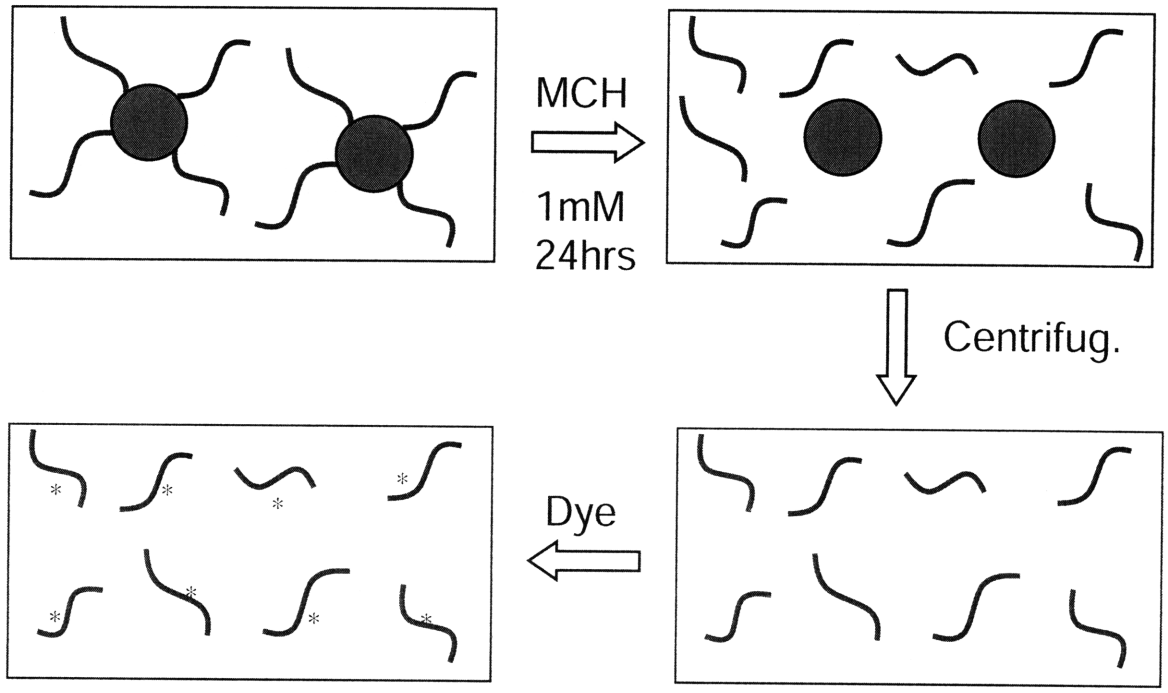

Figure 3.14 Steps of quantification of coverage. Au NP-DNAs are incubated in excessive MCH environment (1*mM* MCH) for a day. Aggregated Au NPs are discarded by centrifugation. Fluorescence of supernatent is either from fluorophores attached to DNAs or commercial staining dye like Cyber-gold.

3.5 Ferguson analysis on Au NP-DNA conjugates

It is shown in Chapter 2 that nanoparticles can be characterized via Ferguson analysis. In this section, the method is extended to Au NP-DNA for evaluating effective size and zeta-potential of the conjugates. Effect of ionic strength on Au NP-DNA is also discussed.

10.9*nm* Au NPs (sample 1) were prepared as in section 2.3. The Au NPs were incubated with mPEG-SH (1:200, [Au NP] = 5×10^{-7} *M*) for ~24hrs (sample 2). A portion of sample 2 was lyophilized in the presence of TAMRA functionalized thiol-DNA (5'-HS-TTTTTTCGGCCCGTATAATT-TAMRA-3') and re-dispersed (sample 3). Au NPs without mPEGs (sample 1) were directly lyophilized with DNA (sample 4), then put in 0.1*mM* 6-mercapto-1-hexanol (MCH) solutions for 1 min. and washed with ethyl acetate three times at 3× volume (sample 5). The same treatment was done also with mPEG-SH (sample 6) instead of MCH. All the DNA lyophilization processes were done with the ratio of Au NP:DNA=1:13, followed by incubation in ~2× TBE for 2 days to maximize DNA loading on the NPs. The Au NP concentration was 5×10^{-7} *M* for mPEG-SH and MCH modification. Free mPEG-SH and DNA were separated from the NPs and NP-DNA conjugates by centrifuging the solutions and removing the supernatant. All the samples were finally re-dispersed in 0.5× TBE. Note that the method of MCH modification (Sample 5) reduces non-specific adsorption of DNA onto Au NP and induces conformational change of Au NP-DNA. This will be discussed in the next section in detail.

Agarose gel electrophoresis was done for the prepared samples. Gel percentage varies from 0.5% to 3% and running buffer used are 0.25, 0.5, 1 and 2×TBE. Electric field strength

is 3.7-3.8*V/cm* and gel running time is 1.5-2 hrs. One of the gel pictures is shown in Figure 3.15 (0.5×TBE, 0.5% agarose gel).

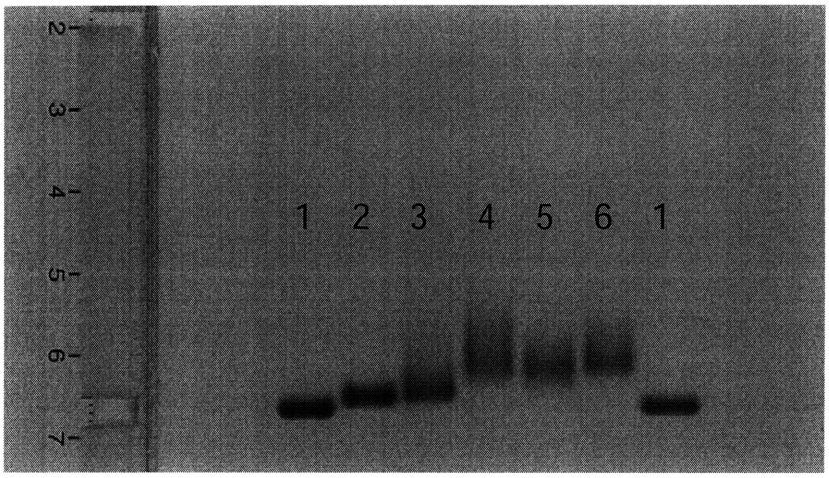

Figure 3.15 Example gel. 0.5% Agarose gel run for 2hrs in 0.5× TBE under electric field strength 3.8*V/cm*. Sample 1: Au NP, 2: Au NP-mPEG (1:200 incubation), 3: Au NP-mPEG followed by DNA conjugations, 4: Au NP-DNA, 5: Au NP-DNA followed by MCH modification (0.1*mM* MCH, 1min, ethyl acetate washing), 6: Au NP-DNA followed by mPEG modification.

Size evaluation by Ferguson analysis on the samples is shown in Figure 3.16 (a) (upper plot). Coverage is plotted in the lower plot of Figure 3.16 (a). Sample 3 has a relatively low coverage and smaller D_{eff} compared to those of samples 4-6, indicating that the pre-coating with mPEG before DNA conjugation limits the amount of thiolated DNA that can react with the Au NP. MCH or mPEG modified Au NP-DNA (samples 5 and 6) have a slightly lower DNA coverage than unmodified Au NP-DNA (sample 4) due to loss of DNA during the surface modification process. However, the D_{eff} of samples 5 and 6 are larger, suggesting that the conformation of the DNA on the particle surface is extended more radially from the NP upon the surface modification, and that non-specific adsorption is reduced. This is discussed further in detail in the next section. Another observation is that the change in D_{eff} of samples

4-6 decreases at higher TBE concentrations. This can be attributed to stronger charge screening effect that makes DNA strands more floppy (section 3.3) diminishing the hydrodynamic size of the Au NP-DNA conjugates. Finally, the magnitude of size increase upon DNA conjugation and further increase with MCH/mPEG reaction is smaller than the contour length of DNA strands used, which confirms again the Au NP-DNA conformation modeling presented in section 3.3.

Figure 3.16 (b) shows calculated ζ and the effective total charge of the species by use of Ohshima's solutions (equation 2.29 and 2.30). As DNA is added to NP surface, the total charge of the conjugate increases, as expected. However, the difference of the charge between Au NP (sample 1) and Au NP-DNA (sample 4) is only on the order of $1\times10^{-18}C$, which is less than the actual charge added by conjugating 10 stands of 20bp DNA on each particle ($32\times10^{-18}C$). Therefore, this suggests that charge screening of the DNA in the conjugate exists at these TBE concentrations. Screening is probably more complicated for Au NP-DNA than for a simple spherical particle as counterions can screen the DNA and NP from each other (Figure 3.16 (c)). This model highlights the fact that the charge distributions and screening effects in Au NP-DNA conjugates are not spherically homogeneous.

In Figure 3.17 DLS zeta-potentiometer (Plus 90, BIC) measurement of Au NP-DNA's free mobility is shown. It is again confirmed that Ferguson analysis is superior to DLS measurement of Au NP-DNA's free mobility. Not only the averaged free mobility fluctuates but also standard error of measurements is much greater for the zeta-potentiometer.

In conclusion, Ferguson analysis can reliably analyze the size and zeta-potential of not only Au NPs but also Au NP-DNAs and surface modified Au NP-DNAs. With the assurance, surface modification on Au NP-DNA is studied in more detail in the next section.

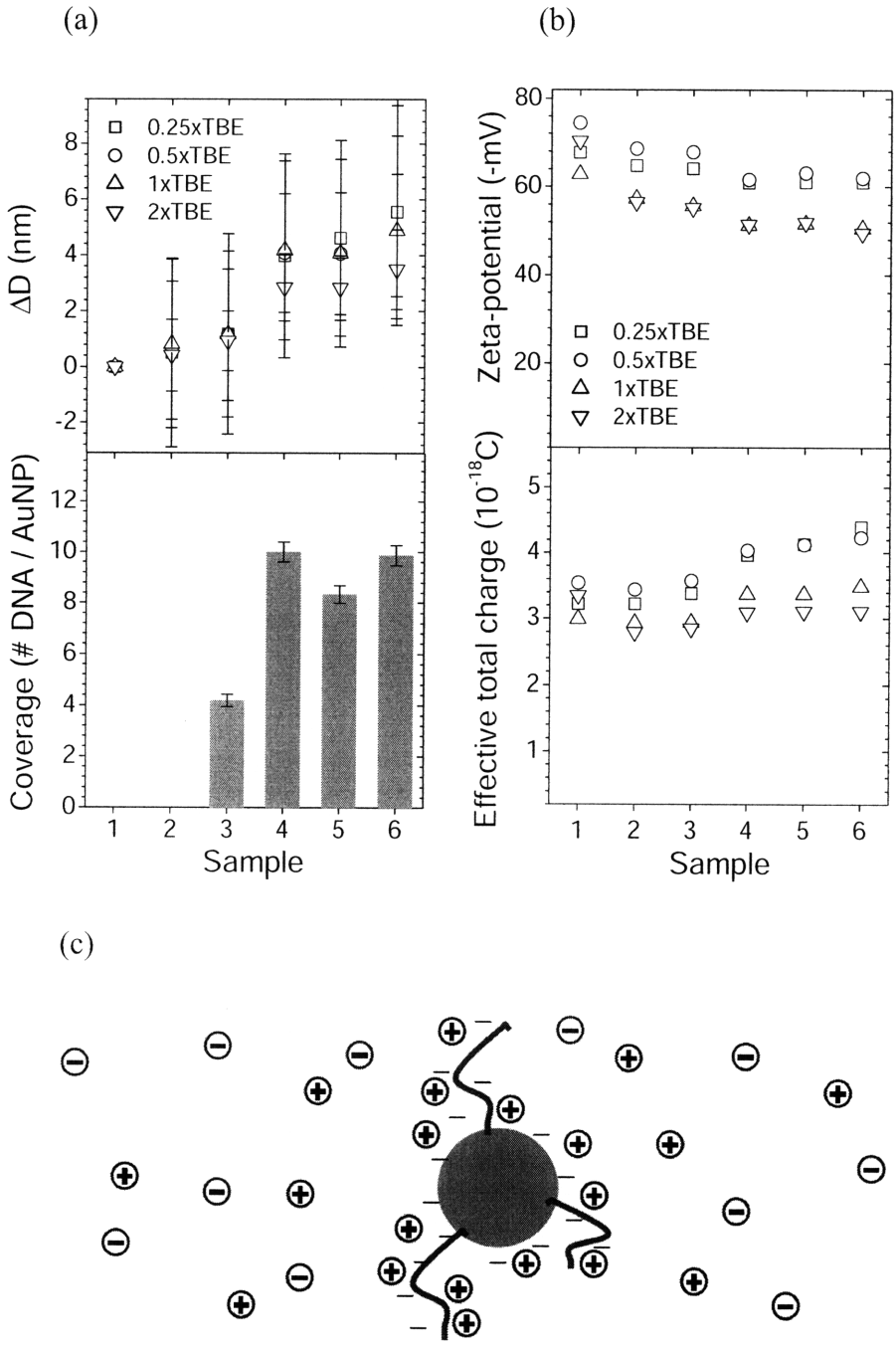

Figure 3.16 (a) Effective size (D_{eff}) of Au NP and Au NP-DNA with different chemical modifications and in different TBE concentrations for 10.9*nm* Au NPs. Sample 1: Au NP, 2: Au NP-mPEG (1:200 incubation), 3: Au NP-mPEG followed by DNA conjugation, 4: Au NP-DNA, 5: Au NP-DNA followed by MCH modification (0.1*mM* MCH, 1min, ethyl acetate washing), 6: Au NP-DNA followed by mPEG modification. [Au NP] was held at $5\times10^{-7}M$ for both mPEG-SH and MCH reactions. Coverage is measured by complete displacement of conjugated DNA by incubating the particles in 1*mM* MCH bath for ~24hrs and measurement of fluorescence intensity of TAMRA. Error bars show 95% confidence intervals. (b) Calculated zeta-potential (ζ) and effective charge of the same samples via equation 2.22 and 2.23. (c) An illustration that shows complicated conformation and charge distribution of Au NP-DNA. Salt ions bind to Au NP-DNA and alter charge status of the conjugates.

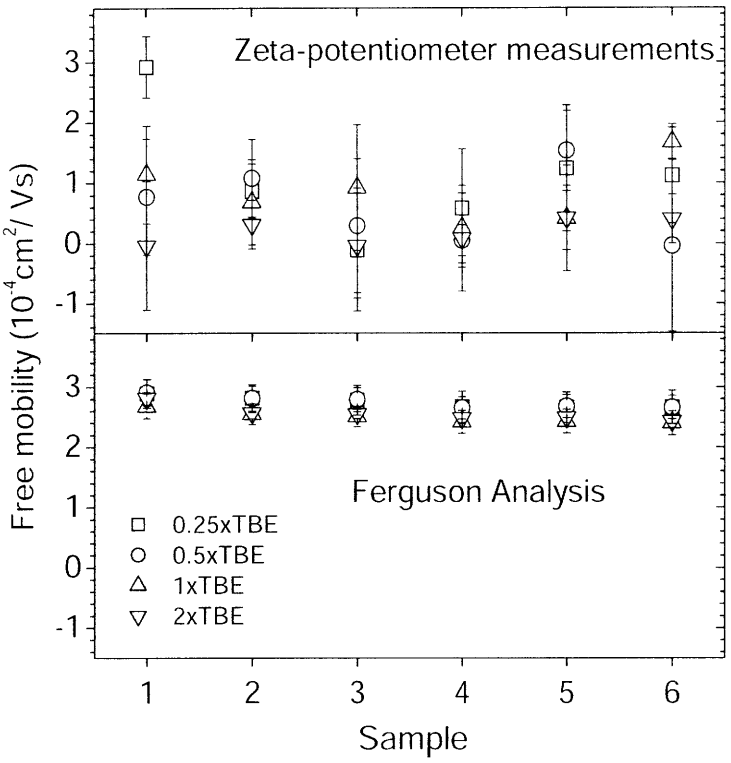

Figure 3.17 Comparison of M_0 data measured from a zeta-potentiometer (90Plus, BIC) and those estimated from Ferguson analysis. For each sample and TBE concentration (0.25, 0.5, 1 and 2× TBE) at least 6 measurements (> 40cycles) from the zeta-potentiometer were averaged. Sample 1: Au NP (10.9*nm*), 2: Au NP-mPEG (1:200 incubation), 3: Au NP-mPEG followed by DNA conjugations, 4: Au NP-DNA, 5: Au NP-DNA followed by MCH modification (0.1*mM* MCH, 1min, ethyl acetate washing), 6: Au NP-DNA followed by mPEG modification. Error bars show 95% confidence intervals.

3.6 Surface modification with 6-mercapto-1-hexanol

According to previous research, 6-mercapto-1-hexanol (MCH) composes self-assembled monolayer (SAM) on flat gold surface.[52] The monolayer prevents DNA adsorption, thus enhancing the ability to hybridize with their complementary strands. This gives us an idea on how to modify our Au-DNA system to be suitable for biological applications. However, gold particles are much more difficult to deal with compared to flat surface since they easily aggregate in liquid if they do not have enough charge to repel each other. From the experience of MCH treatment, MCH replaces not only bases' adsorption sites but also displaces the charged ligand from the nanoparticle surface.

The molecular structure of MCH is given in Figure 3.18. The structure is the same as thiol modification part of DNA oligo except for *-OH* group that gives a little solubility in water. Thus MCH molecules don't screen any of bases of oligo on particle surface (Figure 3.19).

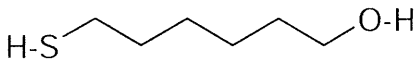

Figure 3.18 Molecular structure of 6-mercapto-1-hexanol (MCH)

Figure 3.19 shows how MCH reaction changes the conformation of Au NP-DNA conjugates. Oligos on gold particles are mostly adsorbed to the particle's surface before MCH being introduced. After MCH (short rod in the Figure 3.19) is added to the solution, MCH molecules start replacing the adsorption sites with themselves (step 2 in Figure 3.19).

Consequently, the DNA oligo strands point outward, although they are still attached to the particle by thiol linkage. Further MCH reaction, however, displaces charged ligand and oligos as well as the adsorption sites (step 3) from the NP surface. For extended time the particles lose all the ligands and oligos on the surface, and then aggregate in the solution. To get Au-DNA samples at step 2 that can be used for the applications like antisense, MCH reaction should stop during some time at step 2. This can be done by selective extraction of MCH with ethyl acetate.

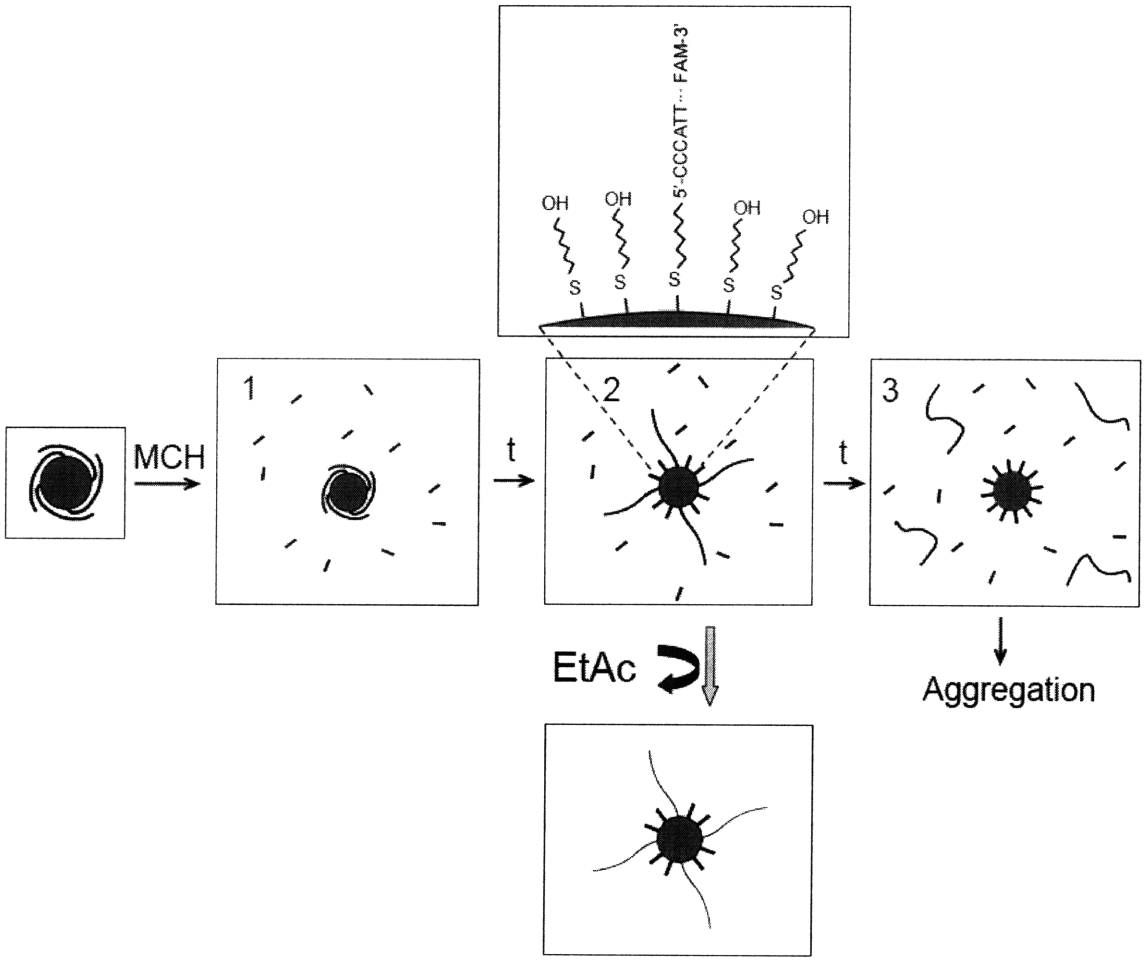

Figure 3.19 Conformation change of Au NP-DNA conjugate upon MCH reaction.

Gold nanoparticles with mean diameters 9.4*nm* were commercially obtained and functionalized with BPS as in section 2.3. DNA oligonucleotides are purchased with C-6 thiol group on the 5' end and a FAM on the 3' end. The oligos were 15mers with a sequence 5'-HS-CCCATTGTGGATTAG-FAM-3' (DNA-SH) and purified by HPLC. Conjugation of the Au NPs and DNA-SHs was done by the method as in section 3.4. Au NP-DNAs were then re-suspended in buffer 0.5×TBE.

	Sequence
DNA-SH	5'-HS-CCCATTGTGGATTAG-FAM-3'
DNA-c	5'-TAMRA-CTAATCCACAATGGG-3'

Table 3.5 Sequence of using DNAs

The conjugates were then exposed to MCH in water, at concentrations ranging from $1\mu M$ to $1mM$ with reaction times 1 minute to 10 minutes. The reaction concentration of Au-DNA conjugate was $1.5\text{x}10^{-7}$ *M*. Reactions were halted by adding 3× volume of ethyl acetate (EtAc) three times, which extracts the excess MCH into EtAc away from the DNA in H_2O. The extraction of MCH is crucial as it permits control of reaction time. The samples after removal of MCH were stable as aqueous solutions at least for a month, though it is subject to the initial DNA coverage in that negative charges on DNA act as surface charge of Au NP that repells other particles. If the samples are exposed to MCH for extended periods of time, they aggregate, as the particles become neutrally charged and are no longer fully soluble in aqueous solutions due to the loss of BPS and DNA from their surface.

Ferguson analysis is used in order to test the change in effective size D_{eff} upon reaction with MCH. Figure 3.20 shows a 3% agarose gel containing Au NP-DNA (~1:3.7 Au NP-DNA coverage) samples that have been exposed to various MCH reaction conditions. Electric field

strength was at 3.87*V/cm*. Lane 1: Au NP alone, 2: Au NP-DNA, 3: Au NP-DNA with 1μM MCH for 1min, 4: Au NP-DNA with 1μM MCH for 10min, etc. 0.5×TBE was used as running buffer. The bands shift slightly upon treatment with low concentration MCH. However, samples that have been exposed to MCH at high concentration do not shift as much, which suggests that reaction with concentrated MCH displaces the oligo from the nanoparticle surface and results in size decrease.

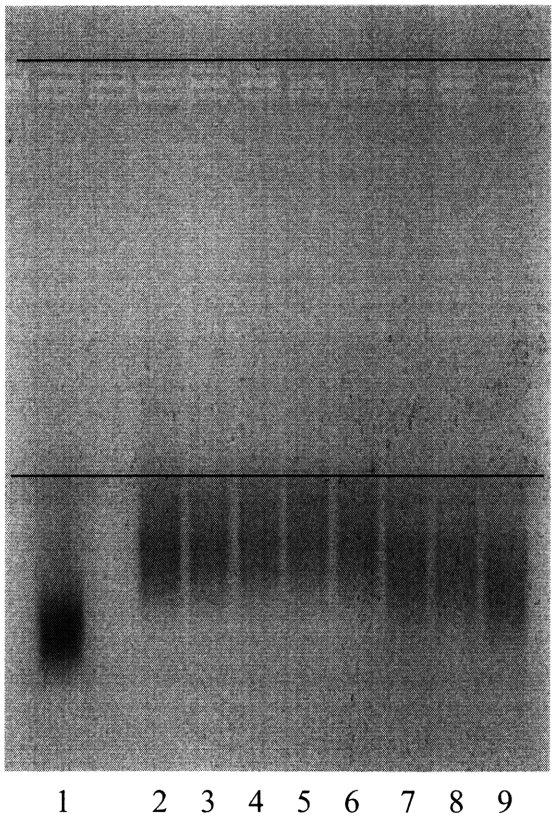

Figure 3.20 Agarose gel (3%) electrophoresis of 9.4*nm* Au – DNA-SH conjugate (~1:3.7) with various MCH treatment. Electric field strength at 3.87*V/cm*. Lane 1: Au only, 2: Au-DNA, 3: Au-DNA with 1μM MCH, 1min reaction, 4: 1μM, 10min, 5: 10μM, 1min, 6: 10μM, 10min, 7: 0.1mM, 1min, 8: 0.1mM, 10min, 9: 1mM, 1min

Gel electrophoresis was repeated for 1.5, 2, 2.5, 3 and 3.5% agarose gel in 0.5×TBE. Figure 3.21 shows a Ferguson plot generated by collection the mobility for Au NP-DNA under different MCH treatments as a function of gel percentage. As control experiments, MCH was treated on plain Au NPs (dotted line). It is confirmed that treating 10mM rarely

change mobility of Au NP (triangles) in all gel percentage range. However, treating the same concentration MCH on Au NP-DNA (inverted triangles) actually change the slope of the Ferguson plot, which means that conformation of DNA is different from that of untreated Au NP-DNA (diamonds). The inset shows that extrapolation to 0% gel mobility reflects the charge status of the samples. Au NP-DNA with 1*mM* MCH/1min treatment has smaller free mobility such that a great portion of surface charge which is from both BPS and DNA has been replaced with charge-neutral MCH.

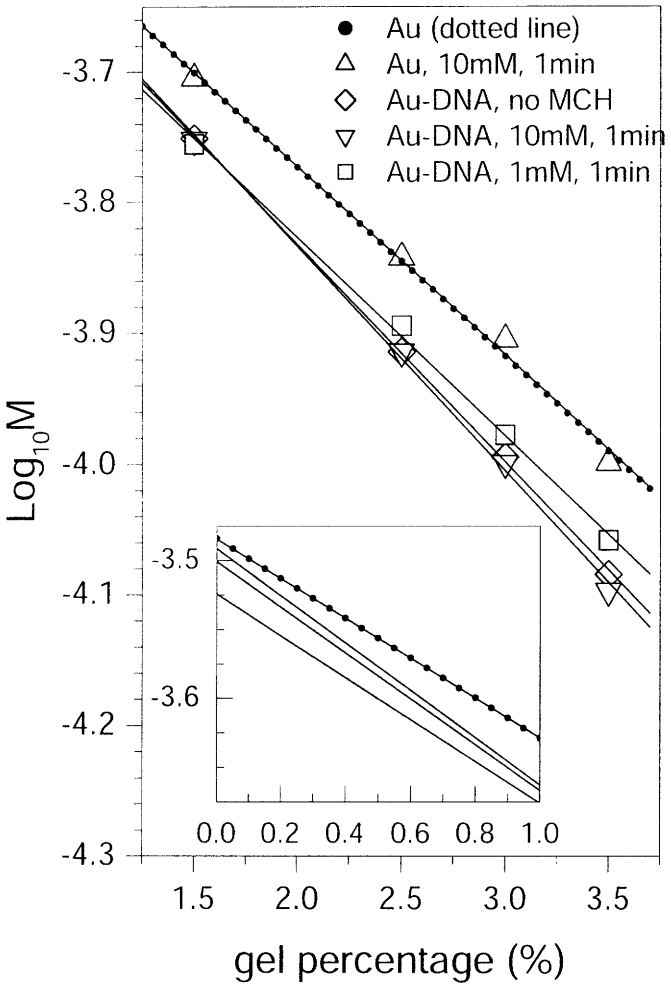

Figure 3.21 $Log_{10}M$ vs gel percentage for Au NP and Au NP-DNA (9.4*nm*/1:3.7) with different MCH treatments. Inset: enlargement of low gel percentage region (<1%)

By using equation 2.9 and sizing standard in Figure 2.4 effective size of the samples is calculated. Figure 3.22 (a) shows the ΔD_{eff}, the difference between the diameter of Au NP-DNA and the diameter of the plain Au NP, obtained as a function of the MCH concentration ($1\mu M$-$1mM$) for a reaction time of 1 min or 10 min. Only samples stable for at least a month after reaction with MCH are shown. ΔD_{eff} of Au:DNA of 1:3.7, 1 min curve (open circles), shows an initial increase upon functionalization with the DNA strands. With $10\mu M$ MCH, D_{eff} increases additionally by $0.6nm$, indicating that the oligo adopts a slightly more radial configuration, increasing the effective size of the conjugate. This level of increase is smaller than the length of DNA, as dealt in section 3.3. At MCH concentrations $\geq 0.1mM$, the D_{eff} decreases to below the value of the Au-DNA conjugates. The reaction at high MCH concentration was sometimes accompanied by particle aggregation, suggesting that the MCH completely displaced the DNA-SH and BPS. This shows that controlling the MCH concentration is key to obtaining the proper conformation of the DNA. For longer reaction times (10 min, filled circles) the behavior is similar to the 1 min reactions except at high concentrations ($\geq 0.1mM$) D_{eff} approaches a smaller value. Au-DNA ratios after these MCH treatments are shown in Figure 3.22 (b) as a function of MCH concentration. The coverage is constant for MCH concentrations up to $10\mu M$, but decreases $\geq 0.1mM$, illustrating that the DNA is not removed until this threshold value.

No significant size changes were observed from MCH reaction of plain Au particles (stars). MCH treatment was also repeated for Au NP:DNA ratios of 1:0.4 (squares), 0.7 (inverted triangles), 1.5 (diamonds), and 2.1 (triangles). $10\mu M$ MCH still resulted in an increased D_{eff} for 2.1 and 1.5. For coverages <1:1, no increase in D_{eff} was observed, probably due to the fact that there were not enough DNAs on the particles to change hydrodynamic

behavior in the gel regardless of conformation. Increased aggregation was also observed for concentrations $\geq 1mM$, making it unfeasible to obtain mobility information.

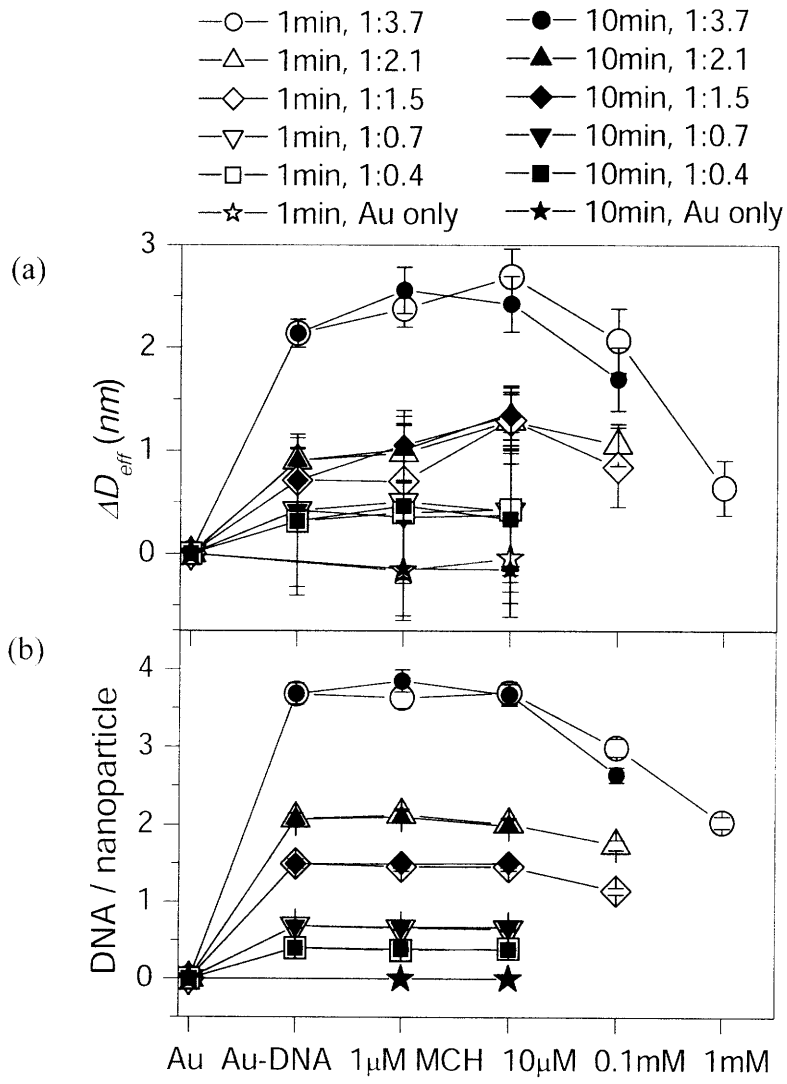

Figure 3.22 (a) ΔD_{eff} obtained for MCH of different reaction conditions as a function of MCH concentration for Au NP(9.4*nm*)-DNA. Open symbols: 1 min reaction time, filled symbols: 10 min reaction time. Coverage ratio of Au NP-DNA before MCH treat is from 1:0.4 (squares), 1:0.7 (inverted triangles), 1:1.5 (diamonds), 1:2.1 (triangles), 1:3.7 (circles). ΔD_{eff} of plain Au NPs (stars). (b) DNA per Au NP as a function of MCH treatment for different starting Au NP:DNA coverage ratios.

It has been shown that $10\mu M$ MCH reaction does not affect the coverage of Au NP but change the conformation of DNA. DNA displacement by MCH is quantified by fluorescence measurements of detached DNA of which FAM is emitting at $520nm$. The concentration of the Au NP-DNA solutions should be low enough to avoid quenching by Au NP. Even if Au NP concentration is high, however, the trend of graph should not be changed as long as the intensity data are somehow normalized. Figure 3.23 clearly shows that $0.1mM$ MCH reaction reduces the coverage but $10\mu M$ MCH does not.

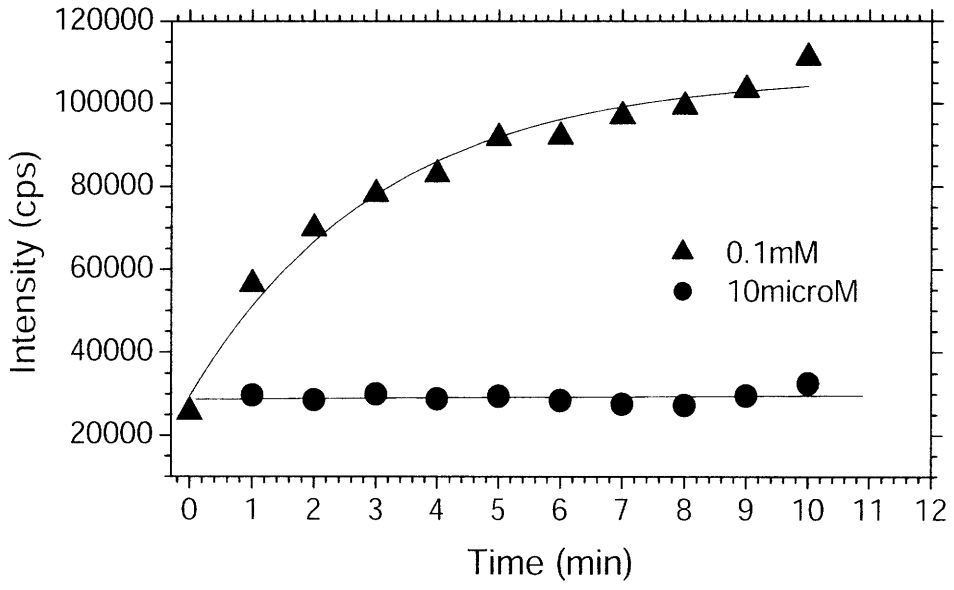

Figure 3.23 Fluorescence measurement of kinetics of MCH reaction on $1.5\times10^{-7}M$ Au NP($9.4nm$)-DNA. DNA strands replaced with MCH are set free to the medium and fluorescence signal of FAM is not quenched by Au NPs. $10mM$ MCH rarely change the coverage ratio of Au NP-DNA, but $0.1mM$ MCH do change.

It is proven that MCH reaction can change conformation of DNA by use of Ferguson analysis. Now we need to test if MCH reaction really changes the DNA conformation in such a way that the actual capacity for forming a hybrid pair is improved. Au NP-DNA conjugates

were hybridized to a complementary strand modified with TAMRA (DNA-c, 5'-TAMRA-CTAATCCACAATGGG-3'). Dehybridized DNA-c is no longer quenched due to proximity of Au NPs[19, 20] and thus quantification of TAMRA fluorescence provides a measure of the hybridization capacity of the DNA on the Au NP surface (Figure 3.24).

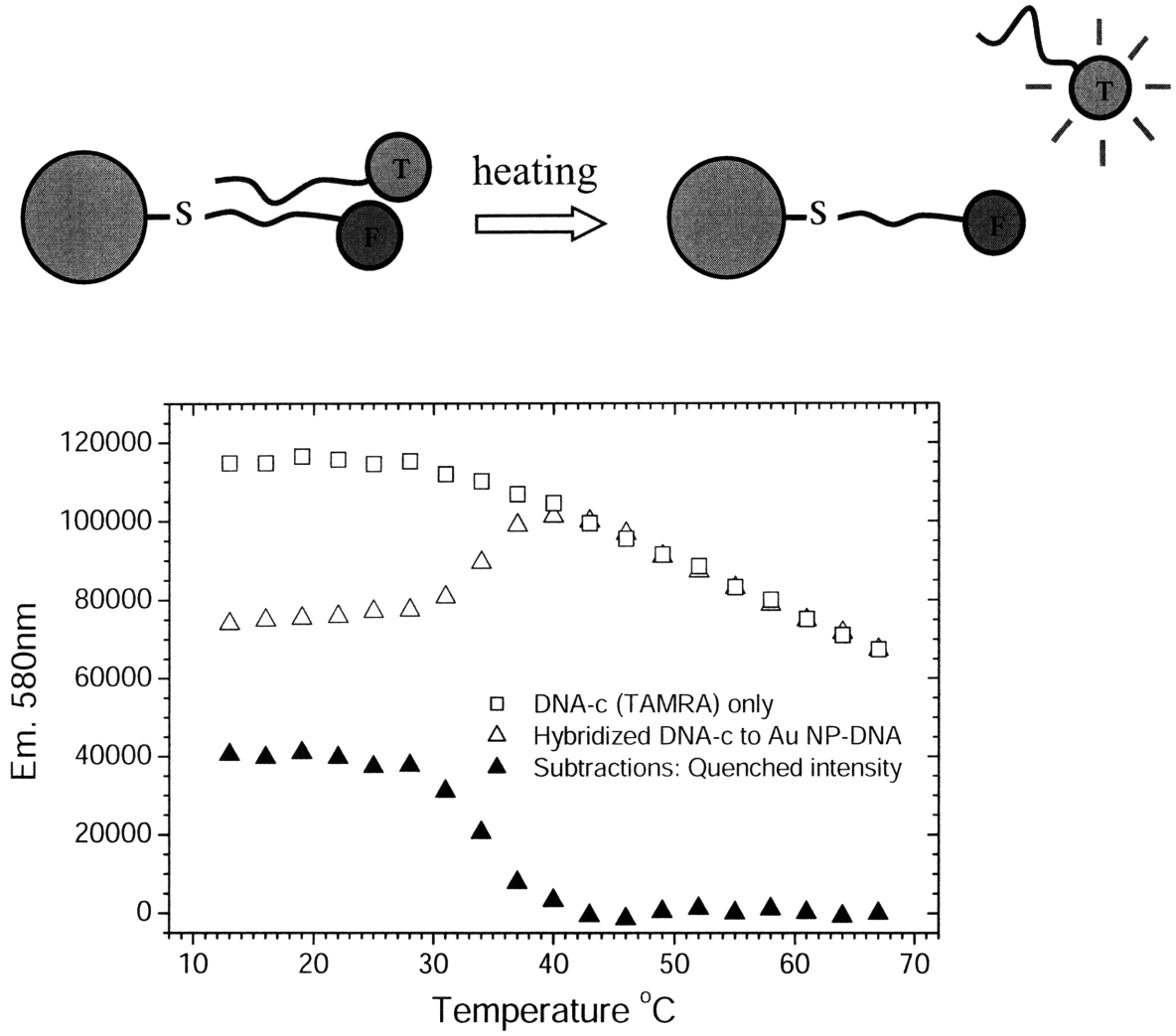

Figure 3.24 Fluorescence measurements. Excitation at 555*nm* and emission at 580*nm*. Samples are in 0.5×TBE. Measurement of free DNA-c solution shows temperature dependence of TAMRA fluorescence (open squares). Hybridized Au NP-DNA and DNA-c give non-zero intensity at the lowest temperature, which is considered as the effect from free DNA-c. At high temperature DNA-c is dehybridized and not quenched by Au NP such that the total fluorescence intensity is from both originally free DNA-c and dehybridized DNA-c (open triangles). By matching the values at the highest temperature and subtracting the two curves (solid triangles) only the quenched intensity by DNA-c hybridization is calculated and converted to the number of hybridized DNA-c.

Au NP-DNA conjugates with a coverage ratio 1:2.9 were used and the ratio remained the same after the $10\mu M$/10min MCH reaction, but decreased to 1:2.3 after the $0.1mM$/1min MCH reaction. After MCH treatment, Au NP-DNA samples were adjusted to be at concentration of $5\times10^{-8}M$ and DNA-c was in excess to enhance the hybridization ($1\times10^{-6}M$), and the samples were annealed from $70^{o}C$ to $4^{o}C$ for about 30min. Excess DNA-c was partially removed by agarose gel electrophoresis. Control measurement of DNA-c shows that fluorescence intensity of TAMRA on DNA-c decreases at high temperature, which is mainly due to *pH* change of the buffer (0.5×TBE) at high temperature (open squares in Figure 3.24). When DNA-c is hybridized to Au NP-DNA, emission from TAMRA on DNA-c is quenched by Au NP at low temperature, but DNA-c is dehybridized and not quenched by Au NP any more at elevated temperature (open triangles in Figure 3.24). Therefore non-zero fluorescence intensity at the lowest temperature is exclusively from free DNA-c still existing in the solution. At the highest temperature, both hybridized DNA-c and free DNA-c contribute to the fluorescence intensity. By matching the fluorescence intensity curves of free DNA-c and Au NP-DNA:DNA-c at the highest temperature and calculating the difference, it is possible to discard the intensity from free DNA-c and get the quenched fluorescence from only the hybridized DNA-c (solid triangles in Figure 3.24).

Figure 3.25 shows the number of dehybridized DNA-c per DNA-SH on the Au NP as a function of temperature. All samples show a sigmoidal step centered about 35°C, the T_m of the oligo confirmed by a melting curve of the plain DNA-SH–DNA-c hybrid under identical salt conditions. Both MCH treated samples show a higher capacity for DNA-c hybridized to the surface DNA than the non-MCH treated samples [52, 53], in which only <20% of the oligos are available for hybridization. The $0.1mM$ MCH/1min sample shows that ~70% of DNA-

SH's on the nanoparticle were hybridized with DNA-c, while the $10\mu M$/10min sample shows only a nominal enhancement (25%) of hybridization over no MCH. Thus, it is believed that not all the adsorption sites were passivated by MCH in the $10\mu M$/10min reaction.

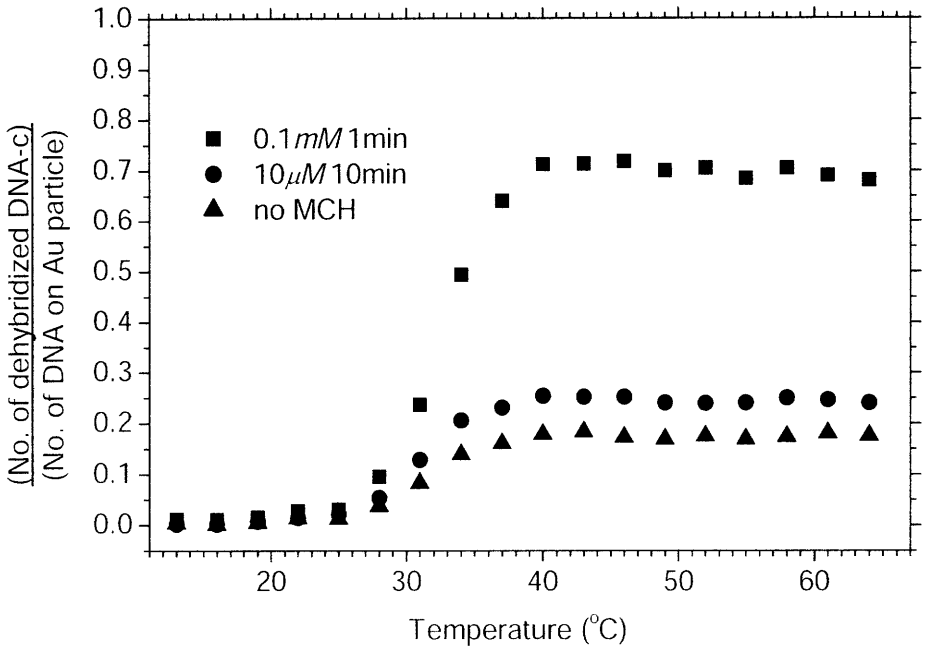

Figure 3.25 the number of hybridized DNA-c per DNA-SH on the surface of the nanoparticle, as a function of temperature, obtained by fluorescence spectroscopy. Au NP-DNA without MCH reaction (triangles), with $10\mu M$/10min MCH reaction (circles), and $0.1mM$/1min (squares). The initial coverage of Au NP-DNA is 1:2.9.

Figure 3.26 illustrates possible hydrodynamic behavior induced by the change in DNA conformation. The contour length of a single stranded 15mer DNA is ~$6.5nm$ [31], suggesting that the DNA is not completely straight on the NP surface even if the C-6 linker were perfectly packed. This is expected based on estimates for the persistence length of single stranded DNA, which is $0.75–3nm$ depending on salt conditions (section 3.3). Therefore, the oligo would have at least a few bends. The $10\mu M$/10min MCH reaction (b) has some oligo adsorption, resulting in an increased D_{eff} from the no MCH sample (a). Due to this adsorption,

its capacity for hybridization is minimally enhanced. In the case of the $0.1mM/1$min reaction (c), the MCH covers enough of the particle surface such that the DNA does not adsorb. Although some of the DNA is displaced, it has an enhanced capacity for hybridization to a complement. The DNA-SH, which has an inherently different mobility than Au NPs, are not adsorbed to the surface, and may have a tendency to align with the direction of motion during electrophoresis ("free draining") [32]. Consequently, this phenomenon results in a smaller measured D_{eff}. However, it should be noted that the behavior described in Figure 3.26 is only a hypothesis. It is difficult to predict the real conformation of Au NP-DNA with the type of (c) during the gel electrophoresis because hard spheres and polymer chains have very different electrophoretic properties (section 2.2).

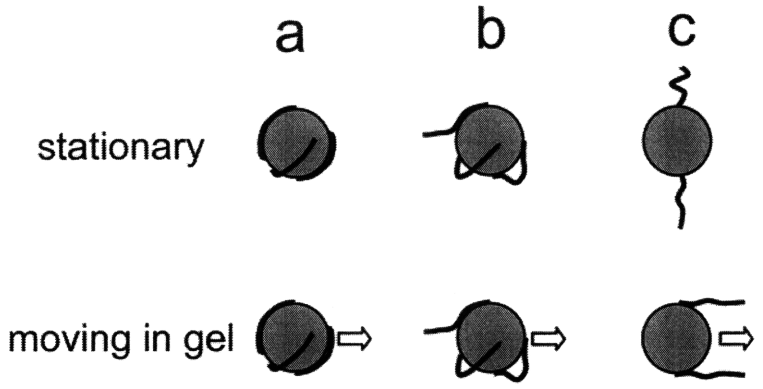

Figure 3.26 An illustration of Au NP-DNA conformation in gel when the samples are stationary or moving. Au NP-DNA without MCH reaction (a), with $10\mu M/10$min MCH reaction (b), and $0.1mM/1$min MCH reaction (c). Arrows indicate relative motion of the sample through a gel.

In summary, MCH can be utilized on nanoparticle surfaces to control the conformation of covalently linked DNA oligos. Upon the reaction with MCH, oligo adsorption to Au via bases is destabilized, changing the conformation of the oligo to one which is more amenable for hybridization. Control of both MCH concentration and reaction

times are crucial for achieving the desired effect of oligo conformation change but not significant displacement from the nanoparticle surface. Further study is necessary to clearly reveal the electrophoretic behavior of Au NP-DNA conjugate.

3.7 Sequence effects on non-specific adsorptions

DNA adsorption onto Au NP is a strong function of sequence and content of each base. Experiments studying the adsorption of free nucleotides onto Au NPs by rates of particle aggregation [11, 15] have shown an affinity order of G > C > A > T, while temperature programmed calorimetry (TPC) and desorption (TPD) have determined affinity orders of C > G > A> T [12] and G ≥ A > C > T.[10] In contrast, homo-oligonucleotide competition assays have shown relative affinities of A > G ≥ C > T.[13] Typically, addition of poly-T spacers has been successful in reducing non-specific adsorption.[19] However, biological applications using NP-DNA conjugates put constraints on sequence choice. Target oligonucleotidess and binding sites may be rich in high affinity nucleotides. The effect of oligonucleotide length on non-specific adsorption has been studied,[14] but variation with position relative to the NP has not.

Therefore the effect of oligonucleotide sequence on non-specific surface adsorption is investigated. 7.5*nm* Au NPs were conjugated to DNAs differing in nucleotide composition and placement within the sequence. Reactivity of the DNAs toward the NP and hybridization capacity of the conjugates varied with sequence. Removal of non-specific adsorption by MCH displacement shows that DNA and conjugate behavior can be explained by non-specific adsorption.[16]

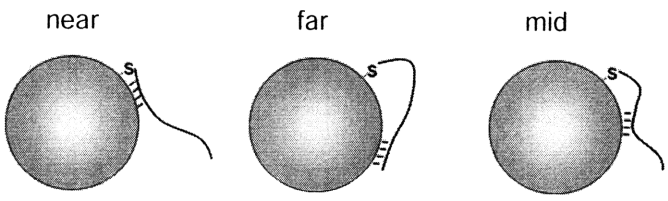

Figure 3.27 Non-specific adsorption of DNA oligonucleotides on NPs.

Table 3.6 DNA oligo sequence

	Sequence	Complement
A-near	5'-HS-AATAATTTTTTTTTT-3'	5'-FAM-AAAAAAAAAATTATT-3'
A-middle	5'-HS-TTTTTAATAATTTTT-3'	5'-FAM-AAAAATTATTAAAAA-3'
A-far	5'-HS-TTTTTTTTTTAATAA-3'	5'-FAM-TTATTAAAAAAAAAA-3'
G-near	5'-HS-GGTGGTTTTTTTTTT-3'	5'-FAM-AAAAAAAAAACCACC-3'
G-middle	5'-HS-TTTTTGGTGGTTTTT-3'	5'-FAM-AAAAACCACCAAAAA-3'
G-far	5'-HS-TTTTTTTTTTGGTGG-3'	5'-FAM-CCACCAAAAAAAAAA-3'
C-near	5'-HS-CCTCCTTTTTTTTTT-3'	5'-FAM-AAAAAAAAAAGGAGG-3'
C-middle	5'-HS-TTTTTCCTCCTTTTT-3'	5'-FAM-AAAAAGGAGGAAAAA-3'
C-far	5'-HS-TTTTTTTTTTCCTCC-3'	5'-FAM-GGAGGAAAAAAAAAA-3'
T-control	5'-HS-TTTTTTTTTTTTTTT-3'	5'-FAM-AAAAAAAAAAAAAAA-3'

To investigate sequence and sequence location effects, ten DNA oligos were compared (Table 3.6). Each of the high affinity nucleotides (A, G, C) are surrounded by poly-T stretches as a low affinity background. The oligos were conjugated with Au NPs by varying Au NP:DNA ratio and coverage was analyzed as in section 3.4. The same initial ratio of Au NP to DNA does not guarantee the same coverage after conjugation depending on the samples. Therefore Au NP-DNA of target coverage ~1.5, ~3.5 and ~7 were collected from variety of the conjugates after coverage analysis. Conjugated Au NP-DNA was annealed with 2× concentration of complementary strands in 1×PBS. Temperature was initially elevated to $30^{o}C$ and brought to $4^{o}C$, and then maintained at the temperature for 16hrs. High temperature annealing was avoided to make sure that there is no thermal disruption of non-specific adsorption. The number of hybridized strands was measured by fluorescence scan of FAM in the complement. Excessive MCH ($0.1mM$) was added to hybridize Au NP-DNA to

completely detach oligos from Au NP and then the solution is centrifuged to separate aggregated Au NPs.

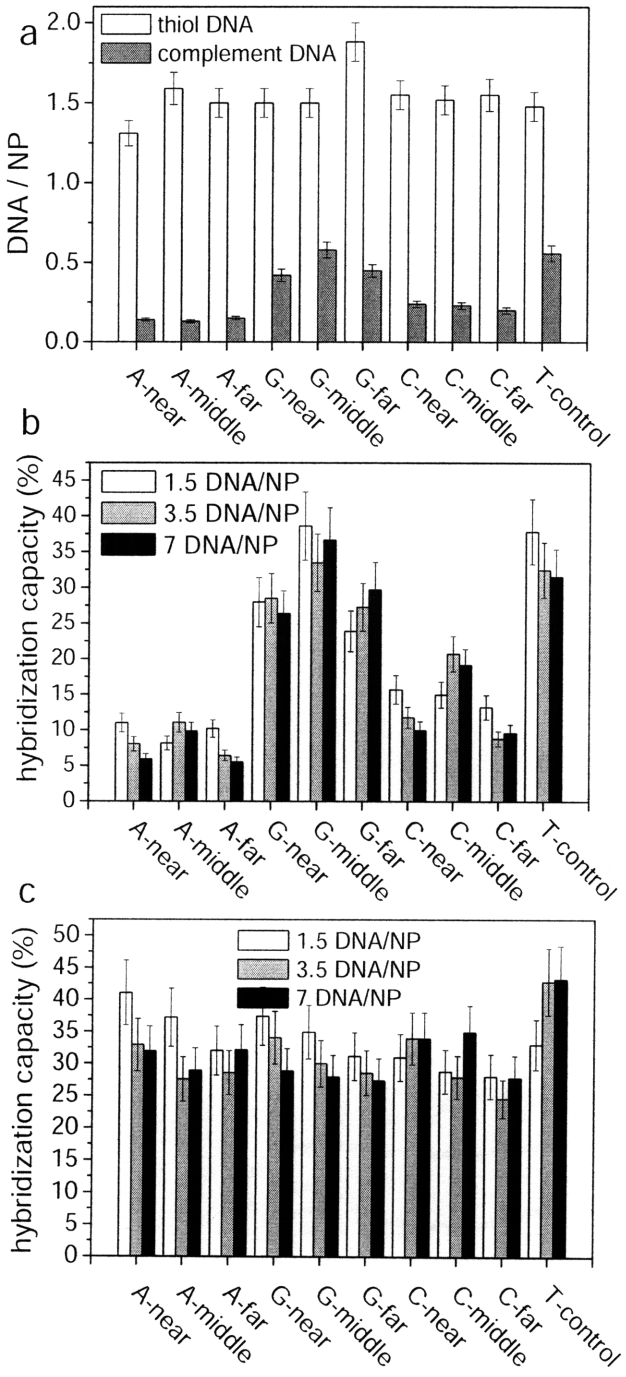

Figure 3.28 Hybridization capacity of 7.5*nm* Au NP-DNA conjugates. (a) Au NP-DNA of 1.5 Coverages. # Thiolated DNA/Au NP (white), # complements/NP (grey) (b) hybridization capacity (%) for 1.5 coverage Au NP-DNA (white), 3.5 (grey), and 7 (black) (c) hybridization capacity (%) for conjugates treated with MCH to remove non-specific adsorption. Coverage 1.5 (white), 3.5 (grey), and 7 (black).

Figure 3.28 (a) shows the real coverage of each Au NP-DNA of nominal coverage 1.5. The amount of hybridized complement strands are in grey bars. Hybridization capacity of each Au NP-DNA is shown in Figure 3.28 (b). Au NP-(T-control) has the maximum hybridization capacity as expected. By placing a sticky sequence in the oligos, hybridization capacity decreases in the order of A > C > G, which may demonstrate the order of adsorption affinity to Au NP surface. However, hybridization capacity becomes similar and does not show any sequence dependence after MCH treatment (Figure 3.28 (c)). This clearly shows that non-specific adsorption of DNA onto Au NP limit hybridization capacity of the DNA and this phenomenon depends on oligo base type and sequence, which can be cured by surface modification by using MCH.

3.8 Nomenclatures

b	Kuhn length
C	Concentration [M]
D_{eff}	Effective size
d	Polymer diameter
E	Energy transfer efficiency
ε	Permittivity (= $\varepsilon_0 \varepsilon_r$)
ε_0	Vacuum permittivity (=$8.854\times10^{-12}\ F/m$)
ε_r	Relativity permittivity
F	Force
Φ_d	Quantum efficiency
J_{da}	Overlap integral
κ^{-1}	Debye length
κ^2	Orientation factor
k_B	Boltzmann constant (=$1.38\times10^{-23}\ J/K$)
L	Contour (chain) length of polymer
l_B	Bjerrum length
λ	Wavelength
M	Mobility [$cm^2/V\cdot s$]
M_0	Free mobility
N	The number of Kuhn segments
N_A	Avogadro number (=$6.022\times10^{-23}\ mol^{-1}$)
n	Refractive index
ν	Flory exponent
p	Persistence length
p_d	Dynamic contribution in persistence length
p_e	Entropic (or electrostatic) persistence length
p_s	Static contribution in persistence length
p_0	Enthalpic (or intrinsic) persistence length
q	Line charge density [C/m]
R	End-to-end length of polymer or distance between two molecules
R_0	Förster distance

T	Gel percentage [$g/100ml$]
T_A	Absolute temperature [K]
U	Migration velocity
ξ	Excluded volume parameter
Z	Partition function
z	Valence of ionic species
ζ	Zeta-potential (V)

3.9 References

(1) Niemeyer, C. M. *Angew. Chem., Int. Ed. Engl.* **2001,** 40, 4128-4158.
(2) Fischer, N. O.; Tarasow, T. M.; Tok, J. B.-H. *Curr. Opin. Chem. Biol.* **2007,** 11, 316-328.
(3) Taton, T. A.; Mirkin, C. A.; Letsinger, R. L. *Science* **2000,** 289, 1757-1760.
(4) Hamad-Schifferli, K.; Schwartz, J. J.; Santos, A. T.; Zhang, S.; Jacobson, J. M. *Nature* **2002,** 415, 152-155.
(5) Thomas, M.; Klibanov, A. M. *Proc. Natl. Acad. Sci. USA* **2003,** 100, 9138-9143.
(6) Loweth, C. J.; Caldwell, W. B.; Peng, X.; Alivisatos, A. P.; Schultz, P. G. *Angew. Chem., Int. Ed. Engl.* **1999,** 38, 1808-1812.
(7) Qin, W. J.; Yung, L. Y. L. *Nucleic Acids Res.* **2007,** 35, e111.
(8) Shiddiky, M. J. A.; Shim, Y.-B. *Anal. Chem.* **2007,** 79, 3724-3733.
(9) Hazarika, P.; Ceyhan, B.; Niemeyer, C. M. *Small* **2005,** 1, 844-848.
(10) Demers, L. M.; Ostblom, M. M.; Zhang, H.; Jang, N.-H.; Liedberg, B.; Mirkin, C. A. *J. Am. Chem. Soc.* **2002,** 124, 11248-11249.
(11) Elghanian, R.; Storhoff, J. J.; Mucic, R. C.; Letsinger, R. L.; Mirkin, C. A. *Science* **1997,** 277, 1078-1081.
(12) Gourishankar, A.; Shukla, S.; Ganesh, K. N.; Sastry, M. *J. Am. Chem. Soc.* **2004,** 126, 13186-13187.
(13) Kimura-Suda, H.; Petrovykh, D. Y.; Tarlov, M. J.; Whitman, L. J. *J. Am. Chem. Soc.* **2003,** 125, 9014-9015.
(14) Parak, W. J.; Pellegrino, T.; Micheel, C. M.; Gerion, D.; Williams, S. C.; Alivisatos, A. P. *Nano Lett.* **2003,** 3, 33-36.
(15) Storhoff, J. J.; Elghanian, R.; Mirkin, C. A.; Letsinger, R. L. *Langmuir* **2002,** 18, 6666-6670.
(16) Park, S.; Brown, K. A.; Hamad-Schifferli, K. *Nano Lett.* **2004,** 4, 1925-1929.
(17) Xu, J.; Craig, S. L. *Langmuir* **2007,** 23, 2015 -2020.
(18) Proligo. Reporters & Quenchers Available for Bi-labeled Fluorescent Probes. http://www.proligo.com
(19) Demers, L. M.; Mirkin, C. A.; Mucic, R. C.; Robert A. Reynolds, I.; Letsinger, R. L.; Elghanian, R.; Viswanadham, G. *Anal. Chem.* **2000,** 72, 5535-5541.
(20) Dubertret, B.; Calame, M.; Libchaber, A. *Nat. Biotechnol.* **2001,** 19, 365-370.
(21) Srinivas, G.; Yethiraj, A.; Bagchi, B. *J. Chem. Phys.* **2001,** 114, 9170-9178.
(22) Fluorescence Resonance Energy Transfer. http://en.wikipedia.org/wiki/FRET
(23) Bednar, J. *J. Mol. Biol.* **1995,** 254, 579-594.
(24) Beaucage, G.; Rane, S.; Sukumaran, S. *Macromolecules* **1997,** 30, 4158-4162.
(25) Eisenberg, E.; Baram, A. *J. Phys. A: Math. Gen.* **2003,** 36, L121-L124.
(26) Maier, B.; Bensimon, D.; Croquette, V. *Proc. Natl. Acad. Sci. USA* **2000,** 97, 12002-12007.
(27) Smith, S. B.; Cui, Y.; Bustamante, C. *Science* **1996,** 271, 795-799.
(28) Wang, M. D.; Yin, H.; Landick, R.; Gelles, J.; Block, S. M. *Biophys. J.* **1996,** 72, 1335-1346.
(29) Ariel, G.; Andelman, D. *Phys. Rev. E* **2003,** 67, 011805(11).
(30) Smith, S. B.; Bendich, A. J. *Biopolymers* **1990,** 29, 1167-1173.
(31) Tinland, B.; Pluen, A.; Sturm, J.; Weill, G. *Macromolecules* **1997,** 30, 5763 - 5765.
(32) Viovy, J.-L. *Rev. Mod. Phys.* **2000,** 72, 813-872.
(33) Marko, J. F.; Siggia, E. D. *Macromolecules* **1995,** 28, 8759-8770.
(34) Skolnick, J.; Fixman, M. *Macromolecules* **1977,** 10, 944-948.
(35) Schellman, J. A.; Harvey, S. C. *Biophys. Chem.* **1995,** 55, 95-114.
(36) Rivetti, C.; Walker, C.; Bustamante, C. *J. Mol. Biol.* **1998,** 280, 41-59.
(37) Flory, P. J., *Statistical Mechanisms of Chain Molecules*. Interscience: New York, 1969.
(38) Smith, D. E.; Perkins, T. T.; Chu, S. *Macromolecules* **1996,** 29, 1372-1373.
(39) Bouchiat, C. *Biophys. J.* **1999,** 76, 409-413.

(40) Long, D.; Viovy, J.-L.; Ajdari, A. *Phys. Rev. Lett.* **1996,** 76, 3858-3861.
(41) Debye, P. *J. Chem. Phys.* **1946,** 14, 636-639.
(42) Tietz, D.; Chrambach, A. *Electrophoresis* **1986,** 7, 241-250.
(43) Perkins, T. T.; Smith, D. E.; Larson, R. G.; Chu, S. *Science* **1995,** 1995, 83-87.
(44) Wang, W.; Lin, J.; Schwartz, D. C. *Biophys. J.* **1998,** 75, 513-520.
(45) Bensimon, D.; Simon, A. J.; Croquette, V.; Bensimon, A. *Phys. Rev. Lett.* **1995,** 74, 4754-4757.
(46) Murphy, M. C.; Rasnik, I.; Cheng, W.; Lohman, T. M.; Ha, T. *Biophys. J.* **2004,** 86, 2530-2537.
(47) Deniz, A. A. *Proc. Natl. Acad. Sci. USA* **1999,** 96, 3670-3675.
(48) Mills, J. B.; Vacano, E.; Hagerman, P. J. *J. Mol. Biol.* **1999,** 285, 245-257.
(49) Goddard, N. L.; Bonnet, G.; Krichevsky, O.; Libchaber, A. *Phys. Rev. Lett.* **2000,** 85, 2400-2403.
(50) Friedman, R. A.; Honig, B. A. *Biophys. J.* **1995,** 69, 1528-1535.
(51) Katz, E.; Willner, I. *Angew. Chem., Int. Ed. Engl.* **2004,** 43, 6042-6108.
(52) Herne, T. M.; Tarlov, M. J. *J. Am. Chem. Soc.* **1997,** 119, 8916-8920.
(53) Mbindyo, J. K. N.; Reddy, L. H.; Keating, C. D.; Natan, M. J.; Mallouk, T. E. **2001,** 13, 249-254.

Chapter 4. Au NP - Antisense DNA

4.1 Introduction

It has been proposed in the previous chapters that quantitative approach to conformation and charge can improve the functionality of Au NP-DNA conjugates so that the efficiency of the conjugates for biological applications can be improved. It would be beneficial if those concepts are utilized for beginning steps such as determination of Au NP size, length and sequence of DNA and coverage as well as following steps like any necessary chemical surface modifications after the conjugates are made. One of the most significant sources of unexpected behavior of Au NP-DNA in bio-systems is non-specific adsorptions as pointed out earlier, and the proposed methods possibly optimize the Au NP-DNA systems for the best result by eliminating or utilizing the adsorptions. In this chapter, Au NP-DNA conjugates are introduced as an antisense agent which regulates gene expressions *in vitro*, and it will be examined how the efficiency can be improved by varying the design of Au NP-DNA systems.

The central dogma of biology is that messenger ribonucleic acid (mRNA) is transcribed from DNA and modified within nucleus, then transported to cytoplasm and acts as a template for protein translation which is catalyzed by ribosome that binds to certain sequences of mRNA and proceeds along the mRNA strand. Antisense approaches are all about interfering any of the biological steps that mRNA experiences.[1, 2] Especially antisense DNA, which has specific sequences that are hybridized to target mRNA, has been intensively explored recently.[2, 3] Antisense DNA strategy mainly focuses on limiting translation activity

by degrading or interfering mRNA functionality. Presence of RNA-DNA double strands, for example, induces RNase H which nonspecifically binds to the double stranded part and cleaves the mRNA strands. Another approach is using antisense DNA that is complementary to ribosome binding / protein synthesis initiating sites, which is called Kozak sequence that includes start codon (AUG) and induces ribosome binding in case of eukaryotic mRNA.[2] Antisense DNA designed to hybridize to Kozak sequence sterically hinders ribosomal activity without irreversible degradation of mRNA.

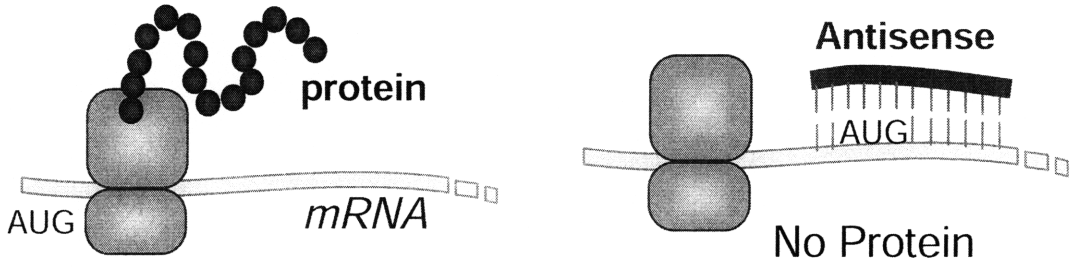

Figure 4.1 Protein translations from mRNA under ribosomal activity. Antisense DNA blocks the start codon (AUG) of mRNA and sterically hinder ribosome binding or proceeding so that gene expression is limited.

However, placing only antisense DNA onto mRNA does not provide enough resistance to ribosome binding / proceeding owing to significant enzymatic strength of the ribosome. Excessive amount of antisense DNA is typically used to regulate gene expression and the efficiency is generally low. Therefore we propose that the efficiency of mechanical blocking of ribosome activity is significantly enhanced by attaching gold nanoparticles (Au NPs) to antisense DNA. The size of Au NP used is about 10nm such that it is large enough to block the ribosome (~20nm) but also small enough not to interact non-specifically too much with the ribosome and other biomolecules.

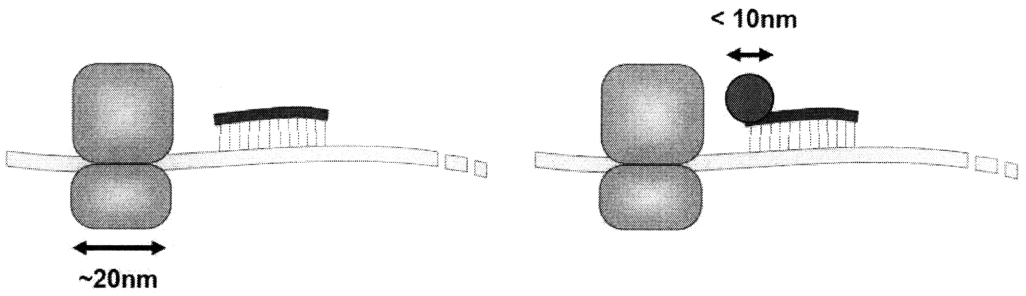

Figure 4.2 Au NP – Antisense DNA conjugates offer better mechanical blocking efficiency compared with the case using only antisense DNA strands.

Another advantage of using Au NP is that Au NPs are excellent vectors that deliver DNA-based therapeutics into cytoplasm or even into nucleus.[4, 5] There are many DNA delivery systems developed so far such as viruses, cationic polymers, dendrimers, liposomes and nanoparticles with their own advantages and disadvantages.[1-3] It has been particularly reported that conjugation of Au NPs to DNA or DNA with conventional vectors enhances the efficiency of delivery into cytoplasm or nucleus.[5] It was also shown in recent research that not only cellular uptake of antisense but also gene regulation within cells is enhanced by using Au NPs.[3]

Previous research has demonstrated possibilities of bio-applications of Au NP-DNA systems, however, mostly ignored optimizing some important parameters such as coverage and charge of Au NP-DNA systems while functionality of DNA on Au NP must be different from its free state. Non-specific adsorptions, a key limiting factor of the applicability of the conjugates, have never been considered either. In this chapter, *in vitro* regulation of enhanced green fluorescent protein (eGFP) expression using Au NP-antisense DNA is mainly discussed to show how conjugation of Au NP affects antisense DNA's functionality. Fluorescence intensity of translated eGFP directly tells the degree of gene regulation in the samples. eGFP

gene transcription and translation steps are described and the effects of antisense DNA or Au NP-antisense DNA on translation are compared by varying antisense molecules concentration, coverage and Au NP concentrations. It would be surprising that Au NP-antisense DNA conjugates turn out not to regulate but to enhance the translations under a certain reaction conditions, which suggests that Au NP-DNA conjugates can be used as an enhancer in translation systems *in vitro*. Non-specific adsorptions between translation molecules and Au NP-DNA conjugates may play a significant role in the enhancement phenomena.

4.2 Transcription and translation of eGFP

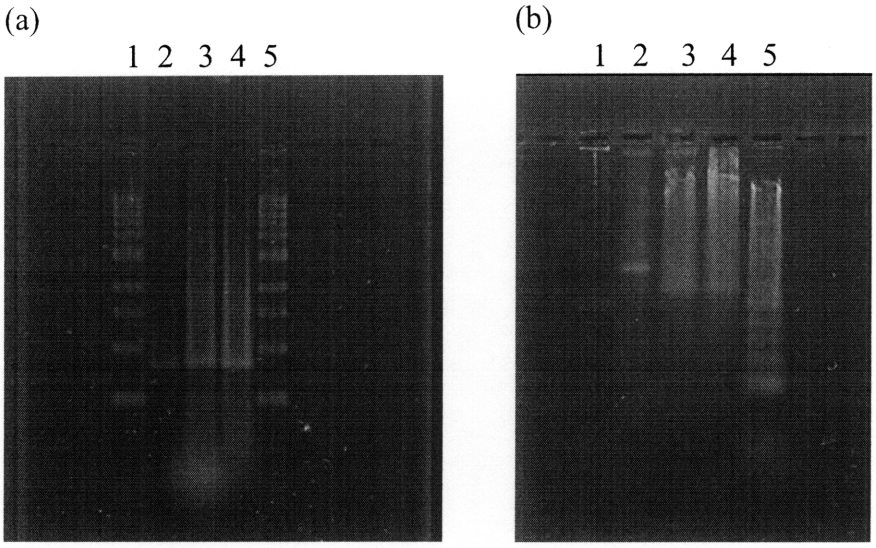

Figure 4.3 Agarose gel in 0.5×TBE under E~2V/cm and running time ~2.5hrs. Gel was stained with CyberGold (Invitrogen) for 15min and pictures were taken under ultra-violet light illumination. (a) 1% agarose gel. Lane 1 and 5: 1kbp DNA ladder, Lane 2: Template DNA for PCR reaction, Lane 3: PCR-amplified DNA without purification, Lane 4: PCR-amplified DNA with purification. (b) 2% agarose gel. Lane 1: 1kbp DNA ladder, Lane 2: Template DNA for transcription reaction, Lane 3 and 4: transcribed mRNA with purification and DNase reaction (different batches), Lane 5: 100bp DNA ladder.

Green fluorescent protein (GFP) is naturally found from *Aequorea* jellyfish and has two excitation peaks at 395nm and 470nm. eGFP is a modified form of GFP and only one excitation peak exists at 488nm. eGFP is chemically more stable, and emission intensity is about 6 times as high as that of wild type GFP.[6, 7] eGFP used in the thesis is encoded in pEGFP-C1 plasmid (Clontech). Standard T7 promoter is inserted during eGFP DNA replications using Taq DNA polymerase (New England BioLab). Replicated eGFP DNA is amplified using PCR and the products are purified with QIAquick PCR Purification Kit (Qiagen). Concentration of eGFP DNA is determined by measuring optical absorbance at 260nm. Then mRNA is transcribed from the DNA using PROTEINscript II T7 Kit (Ambion) and purified with RNeasy Mini Kit (Qiagen). Template DNA remaining in the solution is degraded by RNase-free DNase Kit (Qiagen). Achieved mRNA is quantified by optical

absorbance at 260nm and stored at -80°C. All the processes are performed by manufactures' protocols suggested. Figure 4.3 (a) shows that PCR reaction amplifies the amount of eGFP DNA in the solution (compare Lane 2 and 3 or Lane 2 and 4) and the purification process effectively removes most of the unnecessary molecules like primers from the DNA solutions (compare Lane 3 and 4). Translated and purified mRNA shows electrophoresis band at different position from that of template DNA (see Figure 4.3 (b)). All the agarose gel was made with 0.5×TBE and electric field strength is ~2V/cm and gel running time is ~ 2.5hrs.

Purified mRNA is used as template for translation reaction with Retic Lysate IVT™ Kit (Ambin). Fluorescence measurement of the solutions (Figure 4.4) after translation reaction confirms that eGFP has been actually synthesized. Excitation wavelength of eGFP is 488nm and emission peak is at ~510nm. Putting 0.2μg of mRNA into 1 batch reaction of translation results in much more amount of translated eGFP compared with 0.1μg mRNA condition, but doubling from 0.2μg to 0.4μg mRNA does not give that much of increase in eGFP expression. (see Figure 4.4 (b)) Therefore the mRNA amount of 0.25μg has been chosen as a standard amount used per each translation reaction performed in this thesis.

One very important issue about conducting RNA related experiment is the random effect of RNase existing everywhere. All the tools and disposable tubes/sharps must be clean, and water used for the experiments should be RNase-free. RNase-free water is either commercially purchased (Promega) or made by following conventional process using Diethyl Pyrocarbonate (DEPC). 0.1% of DEPC-water solution is incubated at 37°C for 12hrs and then autoclaved. TBE buffer used for gel electrophoresis of mRNA related samples is made from DEPC-treated water and powdered TBE substances commercially available.

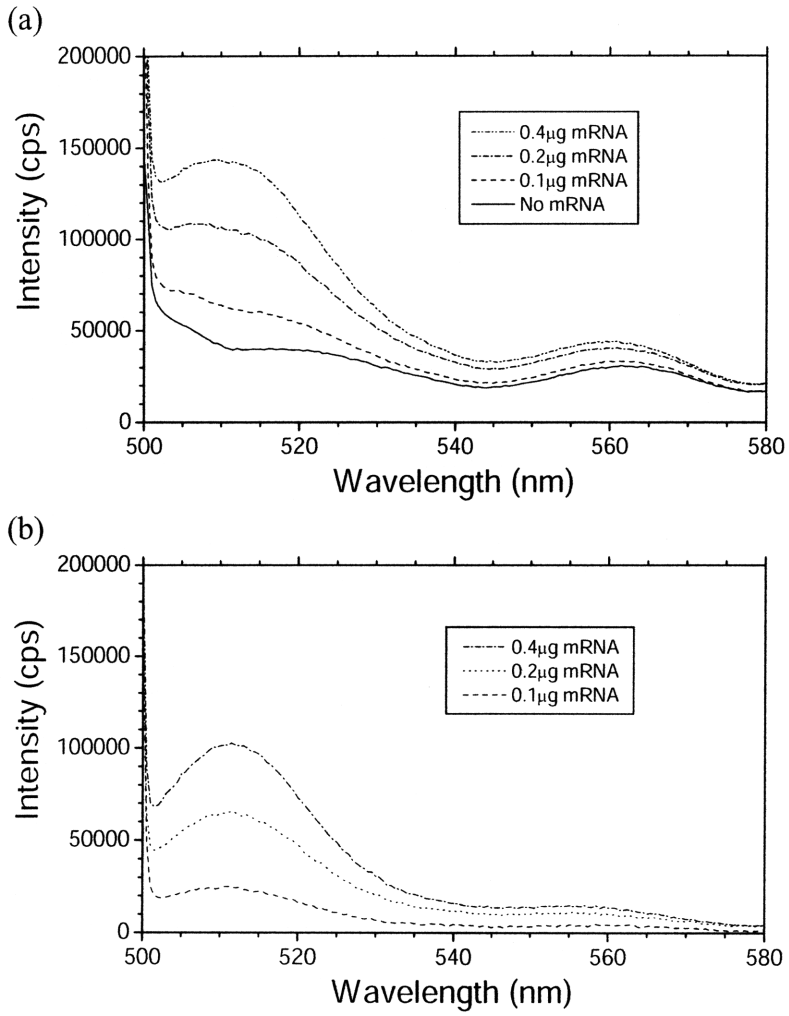

Figure 4.4 Translation reaction was performed with synthesized mRNA and Retic Lysate IVT™ Kit (Ambion). Fluorescence measurement of translated solutions was done at 488nm excitation wavelength. (a) Emission spectra of fluorescence measurement. The amount of template mRNA is 0, 0.1, 0.2 and 0.4μg per each batch of translation reaction. (b) Emission spectrum of No mRNA condition was subtracted from the other emission scans. Peaks at 510nm are more clear and secondary peak at 560nm almost vanished.

4.3 Antisense DNA and Au NP-Antisense DNA

eGFP mRNA used in this experiment has Kozak sequence which includes start codon of the mRNA. Antisense DNA was designed to target Kozak sequence as shown in Figure 4.5. Nonsense DNA which has similar structure but does not bind to Kozak sequence was also designed for control experiments. Additional 10 T's and thiol group (-SH) are placed at 5' end of the DNA for conjugation to Au NPs. Poly(T) sequence acts as a spacer between Au NP and antisense (or nonsense) DNA as T is known to be the least sticky to Au NP's surface.[8] In addition, DNA strands of 25 of only T's are designed as a control that has the least binding affinity to mRNA.

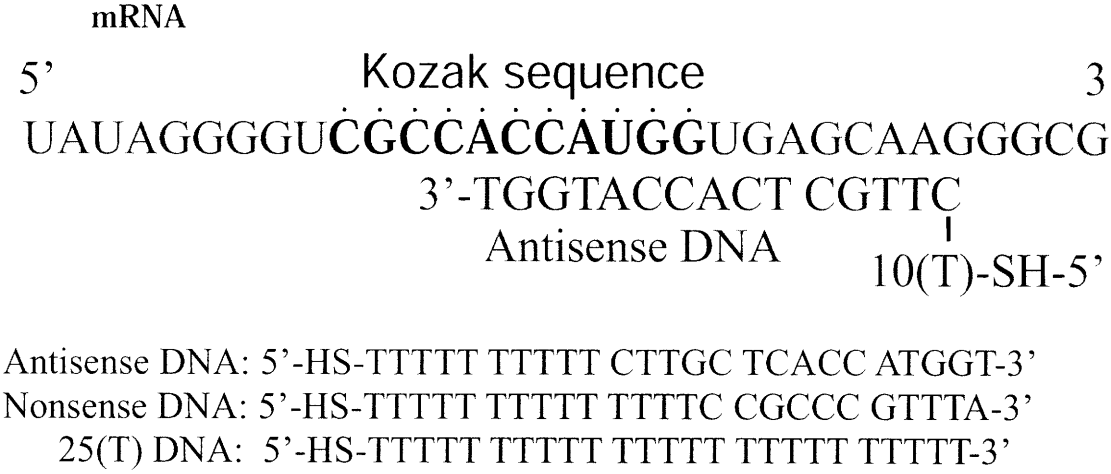

Figure 4.5 Design of antisense DNA, nonsense DNA and 25(T) DNA. Consecutive T's are inserted at 5' as a spacer between Au NP and actual sequence. 25(T) DNA has the least binding energy to mRNA.

To examine the effect of using antisense DNA on translation reaction, different amount of antisense DNA, nonsense DNA or 25(T) DNA was put into mRNA solutions and cured at room temperature for ~1 hr. Then translation reaction was performed as described in the previous section. Fluorescence emission at 510nm was measured and plotted in Figure 4.6.

Using antisense DNA apparently reduces eGFP expression. We expected nonsense DNA's inhibition is minimal in that it does not interfere with mRNA in Kozak Sequence region, however, nonsense DNA also limits translation as like DNA does although there is a little difference in the degree of gene regulation. It is practically impossible to design a DNA strand with a random sequence that avoids any consecutive nucleotides' hybridization to mRNA, which is about 900 bases long. Furthermore, non-Watson-Crick base pairing between U(or T) and G of RNA leads to more binding energy available for the mRNA and DNA strands. A simulation result[9] indicates that the designed nonsense DNA has non-negligible amount of bindings near the start codon of mRNA (Figure 4.7) so that it should have some gene regulation effect, too. In reality, 25(T) DNA strands shows the least amount of bindings to mRNA and gene regulation is minimal. Therefore, antisense or nonsense sequence found in literature[3, 10] is not much optimized in this point of view.

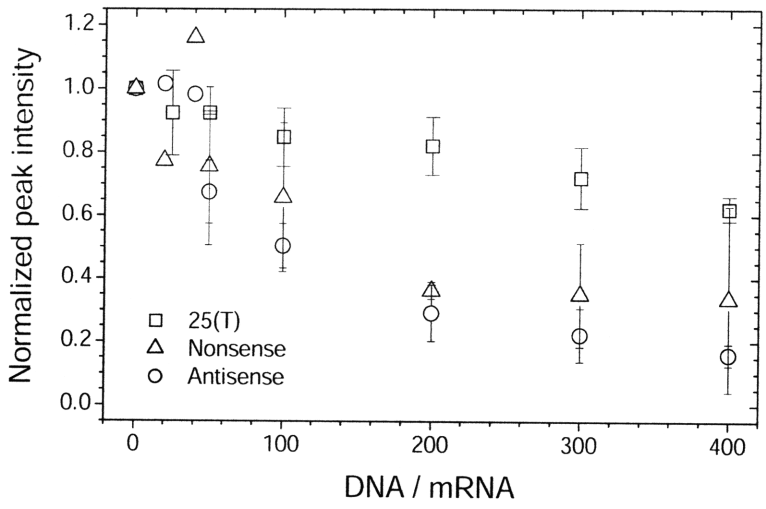

Figure 4.6 Fluorescence measurement of eGFP at 510nm. Translation was done with varying ratio of DNA:mRNA strands from 25 to 400. 0 ratio indicates control translation experiments conducted without antisense, nonsense or 25(T) DNA. Squares: Translation with 25(T) DNA. Circles: Translation with antisense DNA. Triangles: Translations with Nonsense DNA. Intensities were normalized to the intensity of control experiment in each case.

Effect of Au NP on translation also has been tested. Au NPs were synthesized and average size (~9.5nm) was evaluated from TEM images. Then the particles were put into translation reactions and fluorescence intensities were measured. As shown in Figure 4.8 (a), Au NP alone also regulates *in vitro* eGFP expression. The effect of Au NP on gene regulation is even greater than antisense DNA in that only the number of Au NP's comparable with that of mRNA can effectively inhibit the gene expression. The decreased fluorescence intensity at higher Au NP concentration is not by fluorescence quenching of Au NP itself. Figure 4.8 (b) shows that only small decrease in fluorescence intensity has been observed when Au NP's were put into the solutions which contain expressed eGFP already.

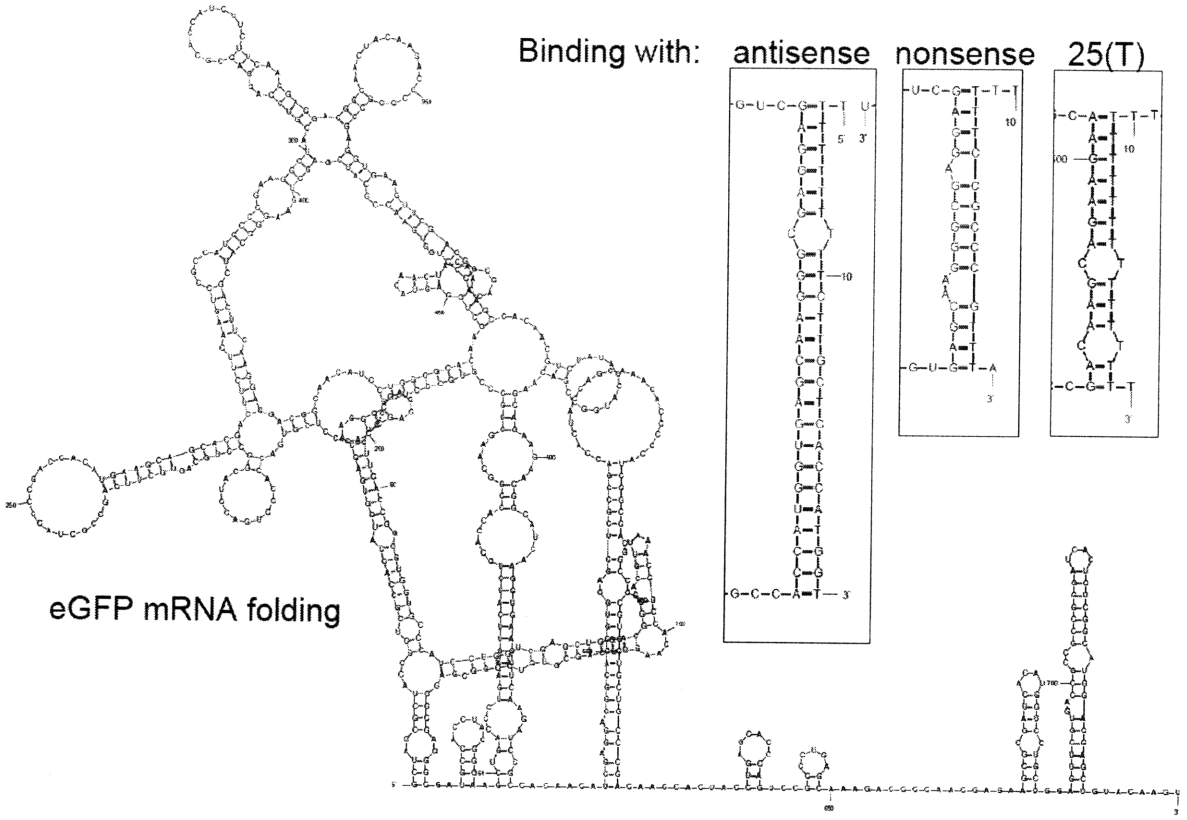

Figure 4.7 Simulation result of eGFP mRNA folding and bindings between mRNA and antisense DNA, nonsense DNA or 25(T) DNA. Binding energy (ΔG) is: -29.6, -11.8 and -3.4 kcal/mol, respectively. 37°C and $[Na^+]$ = 1M are assumed. Simulation tool used is available on the website.[9]

It may be argued that Au NP alone can be used as a gene regulator without DNA conjugation; however, the effect of Au NP in biological systems *in vivo* must be very non-specific so that unexpected interaction with other bio-activities also can happen. Therefore Au NP should be conjugated with DNA for better targeting to a specific mRNA, and surface modification technique must be followed if charge interaction with other bio-molecules is significant.

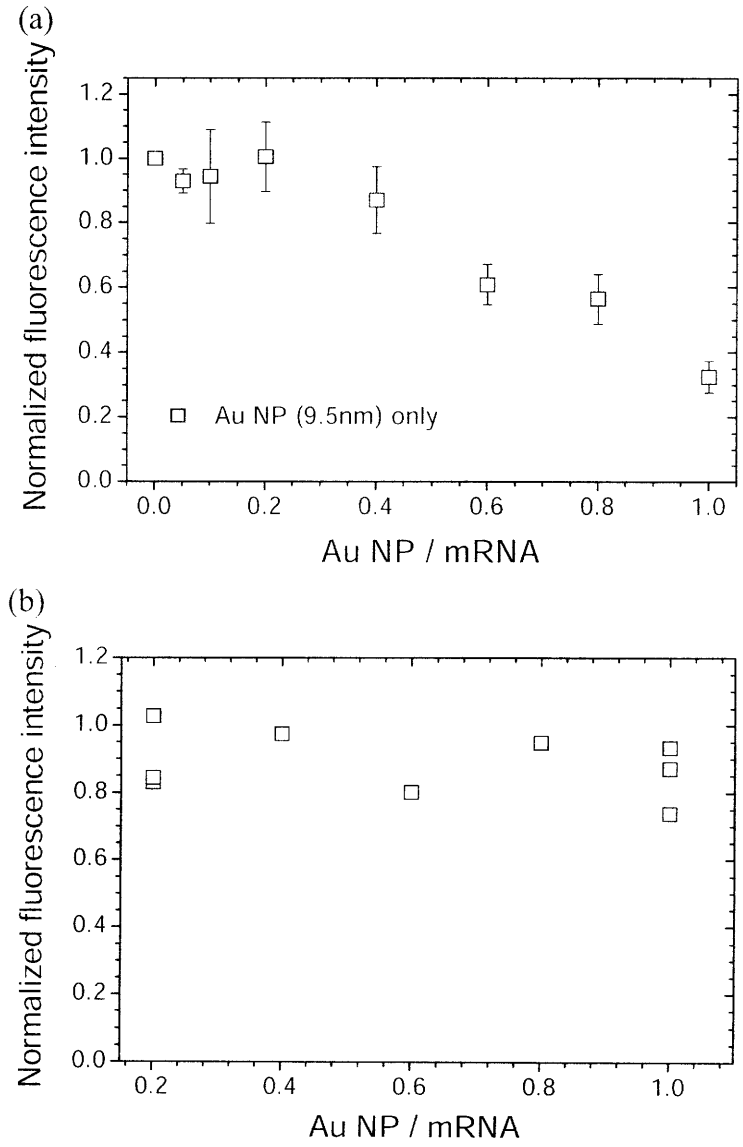

Figure 4.8 (a) Fluorescence measurement of eGFP at 510nm. Translation was done with varying ratio of Au NP(9.5nm):mRNA strands from 0.5 to 1. 0 ratio indicates control translation experiments conducted without Au NP. Intensities were normalized to the intensity of control experiment. (b) Au NP's were put in after control translation reactions were done.

To test the Au NP-DNA systems proposed, particles were conjugated with antisense, nonsense, and 25(T) DNA at the varying Au NP:DNA strands ratio(1:40 to 1:120). Then the actual coverage of each Au NP-DNA was evaluated by staining free DNA strands after 100mM MCH treatment and measuring fluorescence by following the methods in Chapter 3. Then some of the samples that have similar coverage are chosen and listed (Table 4.1). One thing to note is that the concentration of MCH is 100 times higher compared to the cases in previous chapters since the coverage of Au NP-DNA here is much higher so that more MCH molecules are necessary to remove DNA strands from the particle surfaces. Another fact of Au NP-DNA with higher coverage is that the conformation of DNA strands on the Au NP is almost radial.[11] since the hydrodynamic size of lower-coverage samples (26 or 34) revealed from Ferguson analysis is almost twice of that of bare Au NPs (Figure 4.9). This means that DNA is in better conformation to hybridize with target mRNA sequence. Au NP-DNA with higher coverage is supposed to be even more radial according to literature.[12] This Ferguson analysis result also matches well with the theoretical calculations done in Table 3.4. Section 2 of Au NP-DNA given in Figure 3.12 is 25mer ssDNA like antisense or nonsense DNA used here, and the calculated radius of Au NP-ssDNA, R_1, is 10nm (D=20nm) when the NP radius, L, is 5nm (D=10nm), which is very similar to the case being investigated in this chapter. Therefore we can conclude that there is not much non-specific adsorption between Au NP surface and 25mer DNA strands for the coverage utilized in this experiment.

Table 4.1 Actual coverage of Au NP-DNA samples

Coverage	Au NP-antisense DNA	Au NP-nonsense DNA	Au NP-25(T) DNA
High	65	59	54
Low	26	34	31

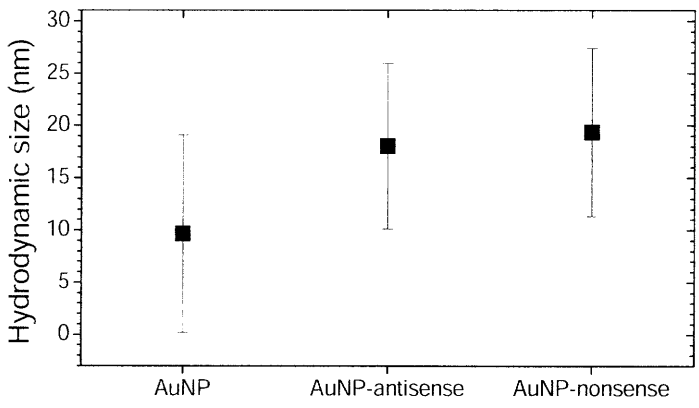

Figure 4.9 Hydrodynamic size of Au NP (9.5nm), Au NP-antisense DNA (coverage 26) and Au NP-nonsense DNA (coverage 34). Error bars are from the standard errors of linear Ferguson plots.

With keeping in mind those properties, Au NP-antisense DNA (1:65) was put into translation reaction. However, it can be seen in Figure 4.10 (a) that eGFP expression is not regulated, but enhanced by putting into Au NP-DNA. This is a clear negative result to the original hypothesis. Free Au NP and free DNA that are not bound to each other do not enhance the translation and the inhibition effects from both species are added up as shown in Figure 4.10 (b), but the conjugated molecules of Au NP and DNA act as an enhancer of *in vitro* translations while unbound Au NP or DNA works as an inhibitor. It may be claimed that the enhancement effect is related with the enlarged size by conjugation of Au NP and DNA, however, the result of a control experiment with 18.2nm Au NP, which is comparable with Au NP (9.5nm)-DNA conjugates in the size, shows that larger particle alone perturbs translation reactions even more. (triangles in Figure 4.10 (b)) Note that fluorescence quenching is not negligible at high concentration of 18.2nm Au NP due to the large volume of the particles.

The same experiments were repeated with Au NP-antisense DNA with lower coverage (1:26) and varying coverage for Au NP-nonsense DNA and Au NP-25(T) DNA. The result shows that the enhancement effect becomes weak when coverage gets smaller in case of Au

NP-antisense DNA (Figure 4.11(a)), and the effect quickly fades away at higher Au NP concentration when Au NP-nonsense DNA's are used (Figure 4.11(b)). Au NP-25(T) DNA does not show significant enhancement effect over the varying Au NP:mRNA ratio. Therefore the translation enhancement must be a function of DNA sequence and coverage of the Au NP-DNA conjugates.

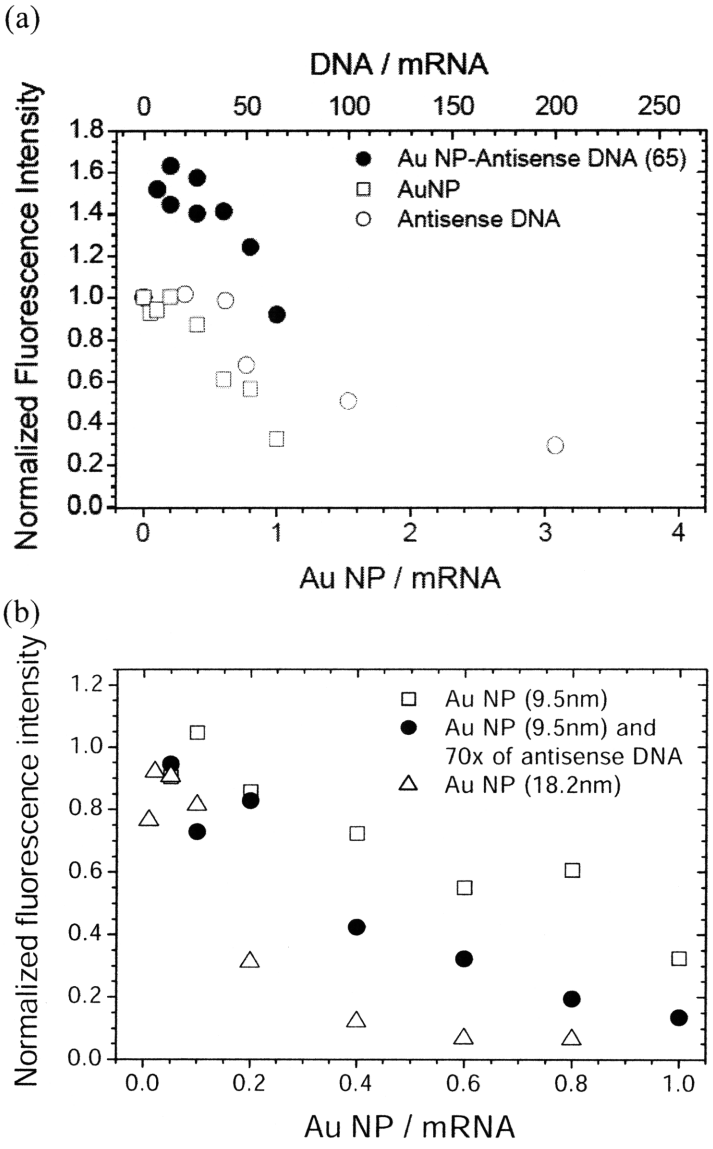

Figure 4.10 (a) Fluorescence measurement of eGFP at 510nm. Translation was done with varying amount of Au NP-antisense DNA (coverage 65, solid circles), Au NP (open squares) or antisense DNA (open circles). Upper horizontal axis shows the ratio of DNA to mRNA, and lower horizontal axis is for the ratio of Au NP to mRNA. Fluorescence intensity was normalized to the intensity of the translated sample without Au NP or DNA. (b) Effect of Au NP (9.5nm, open squares) is compared with that of the mixture of unbound Au NP and 70 fold as many as antisense DNA strands (solid circles), or with larger Au NP (18.2nm, open triangles).

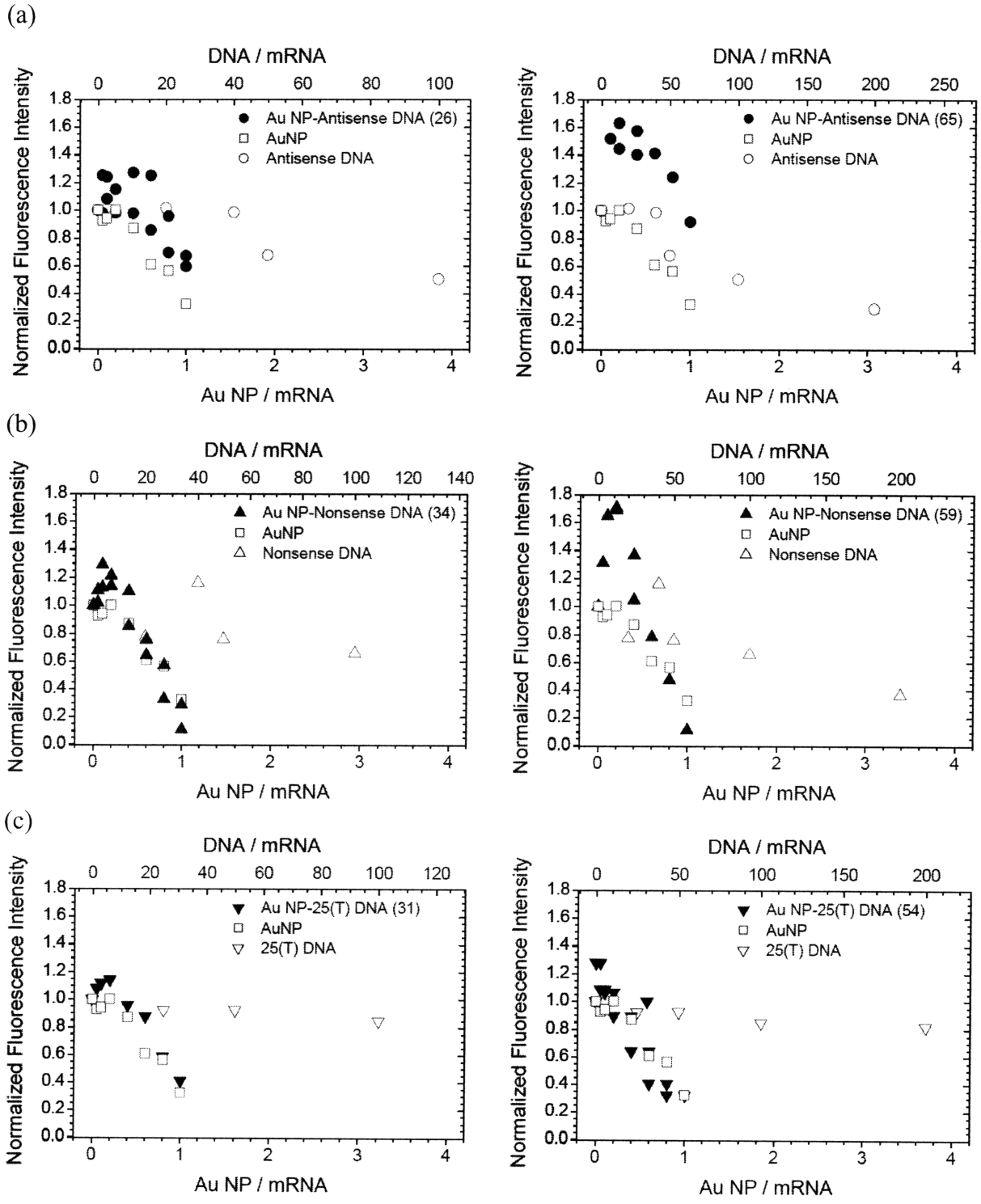

Figure 4.11 (a) Left: Au NP-antisense DNA of coverage 26 was used. Right: the same graph given in Figure 4.10 (a). Solid circles: Au NP-antisense DNA, open squares: Au NP, open circles: antisense DNA. Upper horizontal axis shows the ratio of DNA to mRNA, and lower horizontal axis is for the ratio of Au NP to mRNA. Fluorescence measurement of eGFP at 510nm. Fluorescence intensity was normalized to the intensity of the translated sample without Au NP or DNA. (b) Repeated for Au NP-nonsense DNA. Left: coverage 34, right: coverage 59. Solid triangles: Au NP-nonsense DNA, open squares: Au NP, open triangles: nonsense DNA. (c) Au NP-25(T) DNA. Left: coverage 31, right: coverage 54. Solid triangles (inverted): Au NP-25(T) DNA, open squares: Au NP, open triangles (inverted): 25(T) DNA.

4.4 Au NP-DNA as a translation enhancer

Antisense DNA has been commonly utilized as a translation inhibitor, and Au NP also can interfere with translation process due to non-specific adsorptions including charge interactions with biomolecules. The original hypothesis of the thesis is based on the idea that gene regulation efficiency may be much improved by putting those two inhibitors together. Surprisingly the result shows an unexpected trend in that Au NP-DNA conjugate actually enhances translation reaction, and this is an opposite result compared with the *in vivo* application from another research group.[3] The experiment here is done *in vitro* and the result may be different from that of *in vivo* applications, however, some of their results may be questioned. Charge distribution is much more complicated *in vivo* so that the observed inhibition effect may be due to non-specific bindings between Au NP-DNA and biomolecules. Moreover, they claimed that there is not any inhibition effect from Au NP-nonsense DNA in cells; however, it is physically impossible for Au NP-DNA to avoid any non-specific bindings in real biological systems, therefore there must be some background level of inhibition.

We expect Au NP-DNA conjugates to bind better to mRNA when there are more DNA strands available on NP surface, and when each DNA strand has higher affinity to the target mRNA. Antisense DNA strands are designed to fully hybridize to mRNA so that Au NP-antisense DNA with higher coverage would be the best binder to the mRNA, specifically at the start codon zone, among different samples. One hypothesis can be made from the observation is that Au NP-antisense DNA may help recruiting biomolecules necessary for translations to the start codon area. There are many different types of molecules involved in translation (e.g. eukaryotic translation initiation factors), and each of them has a specific role

such as ribosome subunit association or dissociation, ribosome's binding to 5' terminus zone of mRNA, recognition of Kozak sequence and release of ribosome from mRNA, etc.[13, 14] Gene expression can be enhanced or inhibited if the activities of those enzymes and factors are regulated in some ways.[15, 16] For example, charged ions can be utilized to stabilize mRNA and enhance *in vitro* translation.[17] Using Au NP-DNA for translation enhancement is, however, proposed for the first time in this thesis.

It should be investigated what mechanism actually enhances the translation when Au NP-antisense DNA is used. Figure 4.12 shows that there are significant bindings between Au NP (or Au NP-DNA) with translation molecules in that those particles in translation mixture are retarded in gel electrophoresis. Since many of translation factors and enzymes are charged either positively or negatively, Au NP-DNA, which is highly negatively charged, must experience bindings or repulsions with the molecules. Bound molecules may be delivered better to near 5' terminus or start codon area of mRNA due to the affinity of antisense DNA on Au NP to the mRNA. However, it is still hard to identify which specific process benefits from the delivery in that charge interaction is more likely non-specific.

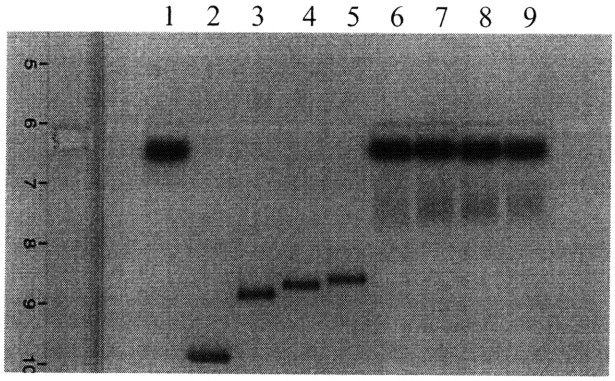

Figure 4.12 1% agarose gel electrophoresis in 0.5xTBE for 90min under E~3.8V/cm. 1: Retic Lysate Mix only, 2: Au NP (9.5nm), 3: Au NP-antisense DNA (coverage 65), 4: Au NP-nonsense DNA (coverage 59), 5: Au NP-25(T) DNA (coverage 54), 6: Au NP + Retic Lysate Mix, 7: Au NP-antisense DNA + Retic Lysate Mix, 8: Au NP-nonsense DNA + Retic Lysate Mix, 9: Au NP-25(T) DNA + Retic Lysate Mix. All samples were maintained at 30°C for 1hr, then cooled down to 4°C to mimic the translation process.

One concern specifically about eGFP is the fact that the translation process is very susceptible to charged ions and metal ions in solutions.[18, 19] Au NP solutions used in the experiments inevitably contain buffer ions and possibly Au ions, therefore Au NP-DNA solutions used for translation reaction must carry some unexpected ions. Buffer ions may be avoided in Au NP or Au NP-DNA solutions, but this diminishes the stability of the particles in the solutions, and hybridization of Antisense DNA to target position of mRNA is also inhibited. Figure 4.13 shows the effect of different TBE buffer concentration used in eGFP translation of fixed ratio between mRNA and DNA or Au NP-DNA. The buffer concentration is diluted by about one fifth in the actual translation. This means that eGFP expression is hurt even in very low TBE concentration.

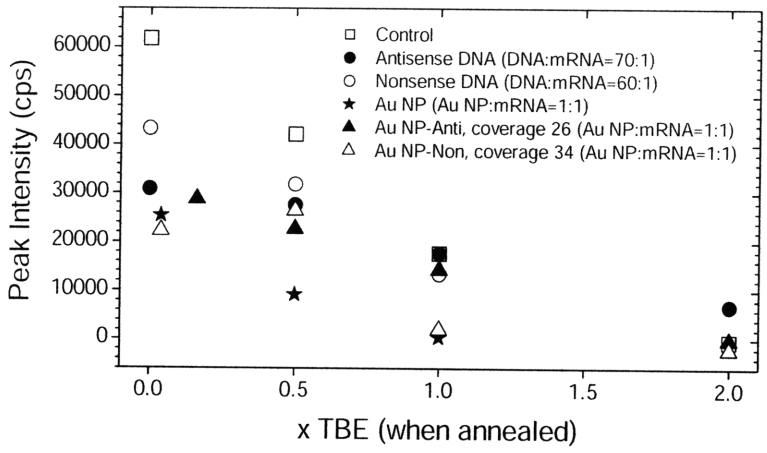

Figure 4.13 eGFP translation with fixed ratio of mRNA:DNA and mRNA:Au NP-DNA. TBE concentration on the horizontal axis is for the hybridization condition of mRNA and DNA or Au NP-DNA. TBE concentration in translation is 0.23 times that of the hybridization condition. Squares: control translation without DNA or Au NP-DNA. Filled circles: translation with antisense DNA with the DNA:mRNA ratio of 70:1. Open circles: with nonsense DNA, DNA:mRNA=60:1. Filled stars: with bare Au NP, Au NP:mRNA=1:1. Filled triangles: with Au NP-antisense DNA (coverage 26), with Au NP:mRNA=1:1. Open circles: with Au NP-nonsense DNA (coverage 34), with Au NP:mRNA=1:1.

In summary, the potential of Au NP-DNA as an *in vitro* translation enhancer has been shown in this chapter. Antisense DNA was designed to hybridize to start codon of mRNA and

Au NP conjugation to DNA was meant to inhibit ribosomal activity; however, actual translation result shows that Au NP-antisense DNA can enhance *in vitro* translation depending on sequence design and coverage. This strategy can be very beneficial to the existing industry and research groups who use *in vitro* translation technique for mass production of protein or assay of minimal amount of gene. It is proposed that affinity of DNA strands to start codon of mRNA is a key parameter that drives translation molecules to the mRNA. To confirm the idea, it is necessary to do more control experiments with different DNA sequences. For example, DNA strands which are the least sticky to mRNA and whose binding site to mRNA is away from start codon should have minimal translation effect when they are conjugated with Au NP. In addition, effect of charge is also important in this application so that it is necessary to understand charge status of Au NP / Au NP-DNA, and ionic condition of buffer as suggested in the previous chapters.

4.5 References

(1) Jason, T. L. H.; Koropatnick, J.; Berg, R. W. *Toxicol. Appl. Pharmacol.* 2004, 201, 66-83.
(2) Patil, S. D.; Rhodes, D. G.; Burgess, D. J. *AAPSJ* 2005, 7, Article 9.
(3) Rosi, N. L.; Giljohann, D. A.; Thaxton, C. S.; Lytton-Jean, A. K. R.; Han, M. S.; Mirkin, C. A. *Science* 2006, 312, 1027-1030.
(4) Jen, C.-P.; Chen, Y.-H.; Fan, C.-S.; Yeh, C.-S.; Lin, Y.-C.; Shieh, D.-B.; Wu, C.-L.; Chen, D.-H.; Chou, C.-H. *Langmuir* 2004, 20, 1369-1374.
(5) Thomas, M.; Klibanov, A. M. *Proc. Natl. Acad. Sci. USA* 2003, 100, 9138-9143.
(6) Tsien, R. Y. *Annu. Rev. Biochem.* 1998, 67, 509-544.
(7) Zimmer, M. *Chem. Rev.* 2002, 102, 759-781.
(8) Kimura-Suda, H.; Petrovykh, D. Y.; Tarlov, M. J.; Whitman, L. J. *J. Am. Chem. Soc.* 2003, 125, 9014-9015.
(9) Markham, N. R.; Zuker, M. *Nucleic Acids Res.* 2005, 33, W577-W581.
(10) Bertrand, J.-R.; Pottier, M.; Verkris, A.; Opolon, P.; Maksimenko, A.; Malvy, C. *Biochem. biophys. res. commun.* 2002, 296, 1000-1004.
(11) Parak, W. J.; Pellegrino, T.; Micheel, C. M.; Gerion, D.; Williams, S. C.; Alivisatos, A. P. *Nano Lett.* 2003, 3, 33-36.
(12) Zanchet, D.; Micheel, C. M.; Parak, W. J.; Gerion, D.; Alivisatos, A. P. *Nano Lett.* 2001, 1, 32-35.
(13) Fraser, C. S.; Doudna, J. A. *Nat. Rev. Microbiol.* 2007, 5, 29-38.
(14) Gingras, A.-C.; Raught, B.; Sonenberg, N. *Annu. Rev. Biochem.* 1999, 68, 913-963.
(15) Scheper, G. C.; Kollenburg, B. v.; Hu, J.; Luo, Y.; Goss, D. J.; Proud, C. G. *J. Biol. Chem.* 2002, 277, 3303-3309.
(16) Zuberek, J.; Jemielity, J.; Jablonowska, A.; Stepinski, J.; Dadlez, M.; Stolarski, R.; Darzynkiewicz, E. *Biochemistry* 2004, 43, 5370-5379.
(17) Kim, Y.-E.; Kim, D.-M.; Choi, C.-Y. *Biotechnol. Bioprocess Eng.* 2006, 11, 258-261.
(18) Mizuno, T.; Murao, K.; Tanabe, Y.; Oda, M.; Tanaka, T. *J. Am. Chem. Soc.* 2007, 129, 11378-11383.
(19) Richmond, T. A.; Takahashi, T. T.; Shimkhada, R.; Bernsdorf, J. *Biochem. biophys. res. commun.* 2000, 268, 462-465.

Chapter 5. Summary and future work

Nanoparticle-biomolecule conjugates have been one of the most popular and important research topics in recent years. Many noble ideas have been introduced and some of them have achieved a great success either academically or commercially. However, it must be pointed out that functionality of biomolecules attached to nanoparticles has rarely been maximized or optimized in most of the research. Especially in Au NP-DNA conjugates study, DNA's non-specific adsorption onto Au NP surface has been a common knowledge but also been ignored when Au NP-DNA conjugates are used in actual biological or nano-scientific applications. DNA's ability to hybridize with its complementary strand is the main power of Au NP-DNA conjugates system but this function is significantly limited unless non-specific adsorptions between Au NP and DNA strands are discarded. In addition, Au NP and DNA conjugates have very irregular charge distribution and conformation such that their behavior can be significantly different depending on NP size, type of ligand, length of DNA, etc. Knowing their charge status and conformation is very helpful to understand and predict their behaviors when being put into real bio/nano systems.

From the motivation it has been proposed in this thesis that Ferguson analysis is a reliable and repeatable method of measuring size and free mobility of not only nanoparticles but also nanoparticle-biomolecule conjugates. Ferguson plots are generated from repeated gel electrophoresis of samples at different polymer concentrations and varying running buffer concentrations. Actual Au NPs (5-20nm) were tested with Ferguson analysis and the superiority of the method over conventional dynamic light scattering devices was proven. In

addition, zeta-potential of particle can be calculated from Ferguson analysis data by use of Ohshima's equations which take into account buffer ions' lagging behind the particles.

The thesis research was not limited within just evaluating particle characteristics, but extended to active controlling of Au NP-DNA conformation via chemical modification of Au NP surface so that non-specific adsorption sites are removed and DNA strands become more radial on the particles. This improves hybridization ability of DNA therefore Au NP-DNA systems can be utilized at better efficiency.

As a real application of the proposed concepts, Au NP-antisense DNA was introduced and tested. Antisense DNA binds to Kozak sequence of mRNA and inhibits ribosomal activity. A concept originally proposed with antisense technique is that ribosome blocking efficiency can be improved by conjugating Au NP to DNA due to physical size of the particle. Au NP-antisense DNA in this thesis was designed to suppress enhanced green fluorescent protein (eGFP) expression. Measured fluorescence intensity directly tells the degree of gene regulations. However, the experimental results show that the conjugates actually enhance translation efficiency, and the trend is a function of DNA sequence and coverage in that those parameters affect the affinity of the conjugates to mRNA. Although negative result has been achieved from the original hypothesis it is considered even more beneficial if we can utilize the enhancement phenomena in a controlled way to achieve better efficiency in production of desired protein or assay of proteins expressed from minimal amount of gene.

The real mechanism that makes Au NP-antisense DNA enhance translation in vitro has not been elucidated in the thesis. It is proposed that Au NP-DNA recruits translation molecules such as ribosome and translation factors due to its affinity to both mRNA and the translation molecules, therefore broader research on Au NP-DNA's effect on translation

should be conducted. For example, different DNA sequences can be designed to have different affinity and binding position to mRNA, and then we can watch how the conjugates of the DNA and Au NP affect on translation. Also we may use Au NP with different size, different ligand on Au NP, etc. Since Au NP-DNA conjugate is suggested as an *in vitro* translation enhancer for the first time in this thesis, there must be a great room for improvement, optimization, and commercialization of the Au NP-DNA conjugate systems depending on the direction of further investigations.